HU ISSN 1785-6892

DESIGN OF MACHINES AND STRUCTURES

A Publication of the University of Miskolc

Volume 4, Number 1 (2014)

Miskolc University Press
2014

HU ISSN 1785-6892

DESIGN OF MACHINES AND STRUCTURES

A Publication of the University of Miskolc

Volume 4, Number 1 (2014)

Miskolc University Press
2014

EDITORIAL BORD

CONTENTS

Design of Machines and Structures, Vol. 4, No. 1 (2014), pp. 5–23.

PERCEPTION-ORIENTED PRODUCT DESIGN AS A DESIGN CHALLENGE

THOMAS GATZKY
Otto von Guericke University Magdeburg
Faculty of Mechanical Engineering
Research and Teaching Area Industrial Design
39106 Magdeburg, Universitätsplatz
thomas.gatzky@ovgu.de

1. Introduction

Product development focuses on creating a geometric-material entirety. Several engineering disciplines as well as industrial design contribute to reaching this objective. Depending on the specific profession and perspective, the term geometric-material entirety may refer to the form of a component, the form of an assembly or even the complex shape of a product.

Both engineers and industrial designers share the common goal of producing a product's geometric-material entirety. Common and interdisciplinary challenges clearly manifest themselves in form- and shape-finding processes which make up a large part of the product development process.

Designing means creating order.

If an engineer is aware of the aim of creating order as part of a form- and shape-finding process and if he or she understands how order in terms of design can be created, he or she will be open to the decisions made by a product designer. Principal findings and recommendations can even be derived for development work in engineering design which help reach and advance objectives pursued in product design. For this reason it is a key factor in the form- and shape-finding process to identify design problems from an aesthetic point of view in order to facilitate a cooperative and integrative approach followed by both engineers and industrial designers in product development.

Design aspects in terms of colour, material and surface aesthetics are indispensable to product design development as they are always associated with form- and shape-finding processes. This article focuses on the categories of form and shape because this is the area where most links to engineering disciplines exist. Furthermore, it is here where particular importance is attached to form and shape perception as an element of product perception.

1.1. Structure – form – shape

Drafting and designing are processes in the course of which an immaterial state turns into a geometric-material state after having gone through many development steps. Fresh ideas, initial sketches, abstract functional and use structures describe the product's future features, which however, cannot yet be experienced sensorially. They are the basis for initial form and shape concepts which in the further development process become more clearly defined, holistic and perceptible.

Technical, ergonomic and design objectives fuel the progressing form and shape-finding process.

In general, the development of a geometric-material product entirety follows the example shown in Figure 1.

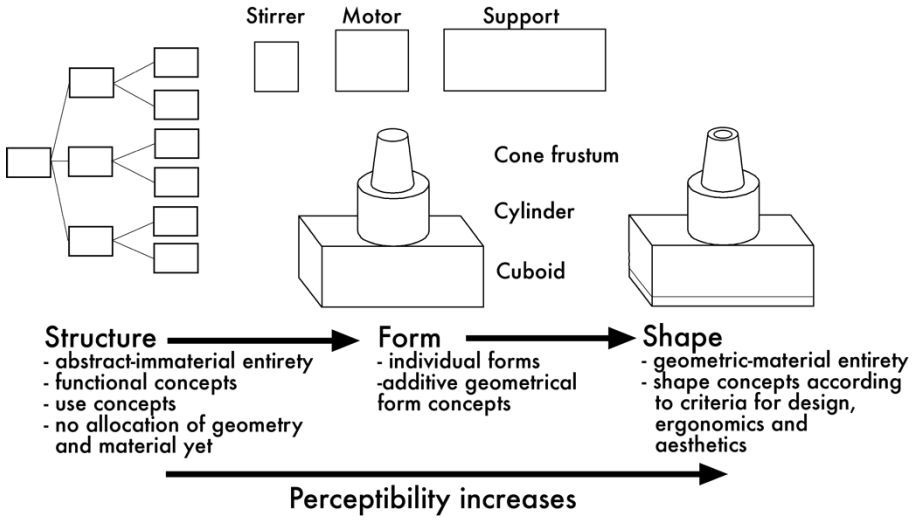

Figure 1: Transition from structure to shape [3]

Furthermore, the transition from immateriality to the geometric-material state of form and shape is also a transition from immaterial abstraction to perceptibility. From this stage on, concepts of form and shape can be sensorially experienced and are consequently subject to an aesthetical analysis and evaluation. Interestingly, it is not only the continuously changing product shape that can be experienced sensorially, but also its representation in the form of draft designs, engineering structural drawings and models. Various visualisation techniques applied in the early phases of product development aim at improving the perceptibility of design results.

2. Human-product interaction or the fundamental aesthetic problem

Until the 19th century, the word *aesthetics* (derived from the Greek *aisthetikos* meaning "aesthetic, sensitive, sentient") was often equated in traditional classical art with the doctrine of beauty. Works of painting, sculpture, music, theatre and literature were in the focus of aesthetics.

Traditionally, everyday products were not evaluated according to the criteria of classical aesthetics. However, various reform movements put the focus of aesthetic contemplation increasingly on normal life. The new unity of art and technology as propagated by the *Bauhaus Dessau* resulted in a new acceptance of industrially manufactured products.

The concept of beauty was extended to include industrially manufactured products, which, however, required a new approach to aesthetics. From this time on, aesthetics was defined as the theory and philosophy of sensory perception in arts, design, philosophy and science.

Hence the aesthetic value of a product is not determined by such terms as "beautiful" and "ugly", but by the product's sensory properties and/or meaningfulness. All questions of product perception, particularly the product's overall shape and all usage operations, are connected with this notion.

Humans perceive products through their sensory organs (receptors). On the product side this requires *perception stimuli* such as form, colour, material and surfaces. When processing such stimuli, humans respond by exhibiting *behavioural reactions* in the form of experiences, actions and evaluations.

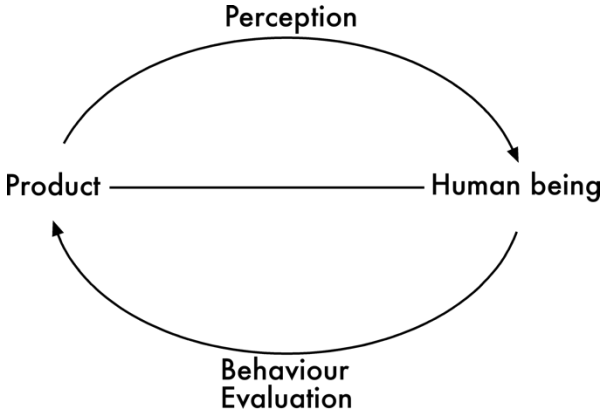

Figure 2: Human-product interaction as a basic aesthetic problem [3]

However, perception also means to understand content and meaning.

Behaviour can be described as a human being's response to what he or she has perceived. Observing or operating something are important actions which may be experienced in a special way. Experiences and actions prompt the user to make judgements and evaluations. Affirmation or rejection as well as verbal judgements such as "I like it" or "I don't like it" often complete a man-product interaction.

The degree of fulfilment of a human-product interaction always depends on the relationship between perception and behaviour. Therefore, it makes sense to postulate perception-oriented design as an objective of designing. With regard to the design process, satisfying this objective requires dealing with the stimuli of perception. The process of finding an overall product design (shape) that does not only meet technical but also aesthetic criteria should be highlighted in this context. Perception-oriented design also means to consider those requirements that result from the physiology and psychology of human perception as well as from an individual's experiences or as a result of his or her external environment. This also includes the elements used in designing products with regard to their appearance.

Perception-oriented design as a design objective and precondition means to design products so that a person can perceive such products in a way that suits his or her senses and intellectual perception.

2.1. Perception

Humans can perceive their environment in several ways.

Approximately 60–80% of all environmental stimuli are visually perceived. For this reason *visual perception* is of utmost importance for man-product interactions and it substantiates the dominance of visual design aspects in industrial design. Basic interrelations are shown in Figure 2.

Perception means seeing and understanding.

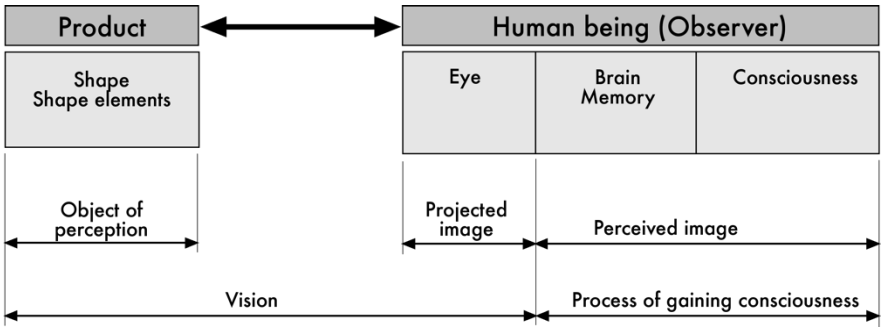

Figure 3: Human-product interaction as a process of visual perception [3]

A human being in his or her role as an observer recognises the product. The shape of the product and its design elements are prerequisites for perception. The shape of the product and its design elements are perceived visually and processed as a projected image in the eye, followed by a process of cognition which results in a perception image.

Therefore, we must distinguish between two phases of perception:

1st phase: The development of a projected image is an objective, physico-chemical process which is equally developed in almost all human beings.

2nd phase: The development of a perceived image is a subjective process that depends on the observer's individual memories, experiences and value concepts. Furthermore, the observer's subjectivity is also influenced by his or her sociocultural environment that particularly defines value concepts and norms.

The user perceives things in a subjective way and behaves accordingly.

Product design is part of a product development process focusing mainly on the manufacture of mass products that are to satisfy the needs of larger groups of buyers and users. However, large groups of buyers and users always consist of individuals. Consequently, it is a special challenge to develop mass products that are capable of satisfying individual needs. This is the reason why the product development process necessitates an intensive analysis of user requirements.

2.2. Perception, behaviour and use

Humans use products in order to organise their lives and satisfy their needs. It is evident that the design quality of products has a decisive influence on the quality of life and its meaningfulness. Use scenarios and/or use processes determine the active man-product

interaction. Therefore, it is obvious that drafting and designing take precedence in the process of planning a future object's use both intellectually and physically and of turning it into a model.

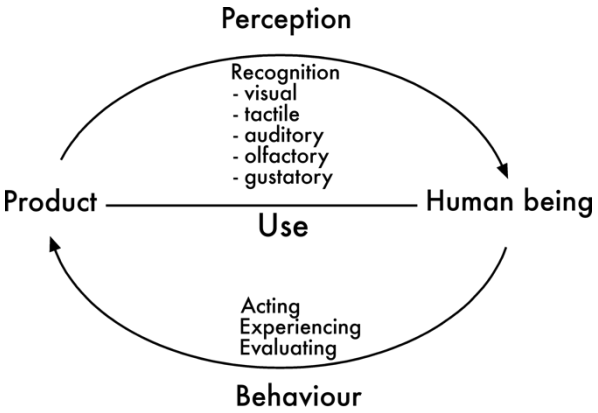

Figure 4: General interrelation between perception, behaviour and use [3]

The way a product is used illustrates the interrelation between perception, behaviour and use. The object transmits perception stimuli which are received and processed by a person who then acts upon them. Sometimes this may be a haptic response (pushing a pushbutton) or just an unconscious emotion (acceptance), often connected with an evaluation (verbal judgement).

3. Perception-oriented design as a design challenge

The primary objective of industrial design is to create a state that can be described as the quality of appropriate sense and intellectual perception *(Wahrnehmungsgerechtheit*).

Drafting and design processes help objectify immaterial concepts (ideas, thoughts) through drawings and physical models by making them a truly sensory experience. On this basis, the following basic statement with regard to designing can be made:

Designing products according to aesthetic criteria is about perceiving and experiencing harmony, a sense of well being and grace, but also contrasts and tensions. It is through the process of use that the user is sensorially stimulated and perceives it as a personal experience.

"Dimensioning" this sensory stimulation is a decisive problem in designing. It is determined by the relationship between perception and behaviour. Various creative measures are applied in the design process to develop and stimulate a user's future behaviour and experience of using a product.

3.1. The use scenario

Now the question arises of how the process of use can be described in greater detail. What does it mean to use a product? It is the aim of this section to identify various areas of

design and to analyse the requirements that make it possible to evaluate to what degree a product has the quality of being perception-oriented.

At the beginning of every design process, the designer faces the following questions:

- How should the product be used by a future user?
- What form/shape should the product have?
- What are the correct or appropriate sequences of handling and operation?

The above and similar questions result in designing tasks that determine future use scenarios. The use scenario is determined by the entirety of all operation and aesthetic requirements.

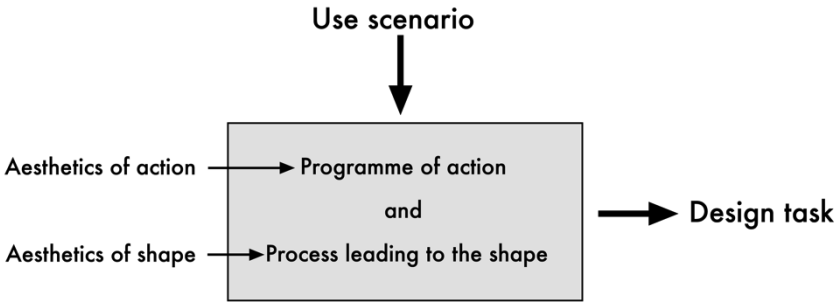

Figure 5: The use scenario as a design challenge [3]

3.1.1. Aesthetics of action

Operation and use determine product perception because the user experiences and evaluates specific operation processes. Frequently, the quality of these operations decides about a product's value.

Aesthetics of action is a sensory and meaningful element of design tailored to meet human needs. Where design is expected to be in line with a person's sense and intellectual perception it deals with performing, integrating and developing situations for concrete action. Criteria that can be designed and evaluated include, in particular, action competence and control.

Perception-oriented design is characterised by the following principles that reflect the relationship between perception and behaviour.

Simplicity: Appropriate cost/benefit ratio. One of the most important quality criteria is the appropriateness of the design (shape) in relation to the object's purpose, its use value and its value as such. Simplicity includes features such as honesty, authenticity, clarity and good organisation. Complexity (or overloading) is often experienced as confusing, disorienting and inappropriate.

Clarity: Quick and unambiguous recognition of a design situation facilitates controlled and reliable operation.

Visibility: Easily visible "signals" (information) are a prerequisite for safe use. For example, a coffee cup should have a reasonably sized handle to not only allow big fingers to grip it easily but above all to facilitate recognition of the cup's purpose. If these signals are not transmitted, irritation and inappropriate use may be the result.

Feedback: Both important signals for action but also the relevant feedback must be perceivable, preferably in a visible form. Any feedback should be given immediately after

the relevant action. If this feedback is not given or comes too late, the user does not know whether his or her action was correct and completed successfully.

Mapping: Mapping means that the functionality of acting and the result thereof are meaningful. When function, action and actual execution are made visible it is easier for the user to recognise and understand various relationships. Analogies and compatibilities with known experiences help the user to execute various operations. A typical example is the waste-paper basket or trashcan on the user interface ("desk top") of a computer. The design follows the artefacts and organisation of a real office. The image of a waste-paper basket on the desktop provides an abstraction of the "delete" function. The virtual processes of disposing, throwing something into a waste-paper basket and picking it up again are analogies to a waste-paper basket in the real world. Even though data on a computer are disposed of in a different way than normal garbage, the user is familiar with this process through the image of the waste-paper basket, though virtually.

In this connection the close interrelation of ergonomic and aesthetic design aspects in product design should be underlined.

Schürer referred to the reciprocity of ergonomics and design by stating:

"While ergonomics should be understood as a component of design, aesthetics should be seen as an element of ergonomics. However, aesthetics should not be understood as associative aesthetics, i.e., aesthetically pleasing, but as aesthetics related to the course of action, in other words as a function guiding action. On the one hand, it influences the process of how an object is experienced, on the other hand it has an influence on the response to these phenomena and finally on how actions are to be executed. Experiencing, behaving and acting are basic human dispositions. They cannot only be expressed by appropriately designed elements for executing an action, i.e., hardware-ergonomic design. On the contrary, they are essentially influenced by the meaningful design, i.e., the software-ergonomic design of elements related to the course of action." [6]

The progressive creative drafting of use scenarios is a real opportunity to overcome the divide between design and ergonomics.

3.1.2. Aesthetics of shape

Perception-oriented design always aims at finding a shape presenting a unity of form, colour, material and surface. As stated at the beginning, form is of prime importance with regard to product perception.

For this reason, the process of developing a form and shape in line with a person's sense and intellectual perception is key to the design process.

In the following section, the fundamentals of form and shape-aesthetical interrelations that support design and evaluation processes in line with sense and intellectual perception will be described.

3.2. Introduction to a theory of form and shape in line with human sense and intellectual perception

The term *theory of form and shape* should be understood as the recognition and application of objective criteria required to allow a person to create a form and shape and to evaluate them according to relevant criteria. As a rule, in engineering, mathematical/geometric descriptions are applicable as a result of technical requirements such as

load, functional performance, manufacture, etc. In product design, these are formal-aesthetic descriptions that are based on aesthetic requirements.

A perception-oriented theory of form and shape can aid the process of understanding and influencing effects on humans by considering how humans perceive features of form and shape.

3.2.1. Fundamentals of perception of form and shape

The most elementary type of perception is the figure-ground relationship.

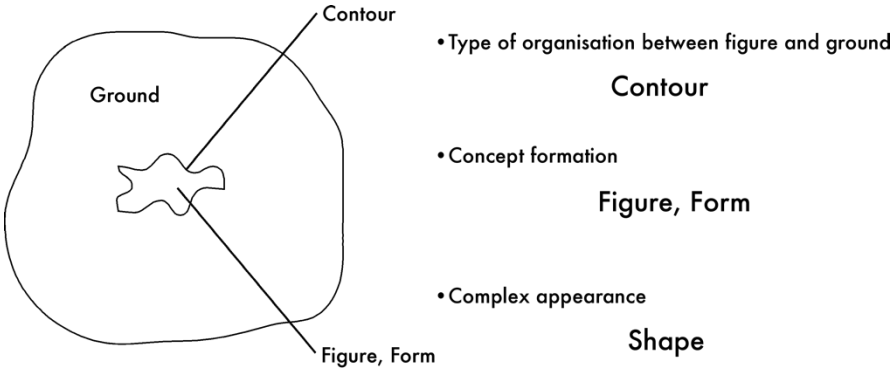

Figure 6: Figure-ground relationship [3]

An outline or contour creates a form, a perceptual grouping, which is in contrast to its surroundings or the background. This is a vital necessity for perceiving and recognising the form. The contour is decisive for identifying the form and determines its meaning/expression. The following example is typical of all contrast phenomena.

A circle has a typical outline whereas a triangle has one that differs from that of the circle. The observer assigns specific terms to these different shapes (here: circle and triangle) helping to distinguish and describe the relevant form. Both result in different perception images, i.e., the circle's effect on the observer differs from that of a triangle. This is the starting point of design knowledge to be applied in the design process.

3.2.2. Form and shape

The following section focuses on the difference between form and shape. This is important because this differentiation is vital to the design process as it facilitates analyses with regard to the results to be achieved in the process of perception.

Form is defined as a coherent single phenomenon. A contour creates an areal form, the shape of the surface creates a spatial form. Developing or creating a form means designing a contour or surface. The shape of the contour and surface determine perception.

The shape of the contour is a precondition for perceiving the areal form. The geometry of the contour determines the expression of the form.

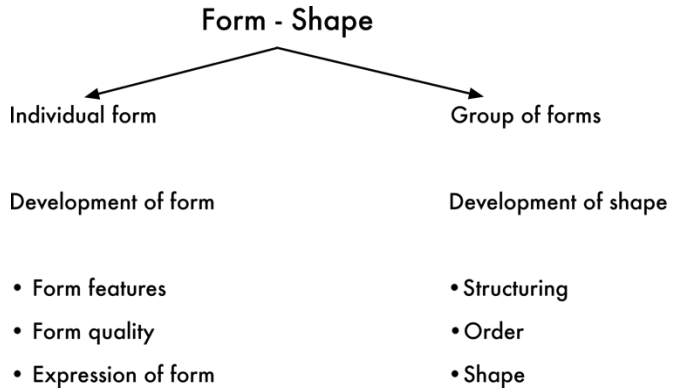

Figure 7: Terms used in the aesthetics of shape [3]

The shape of the surface is a precondition for perceiving the spatial form. The surface geometry determines the expression of the form.

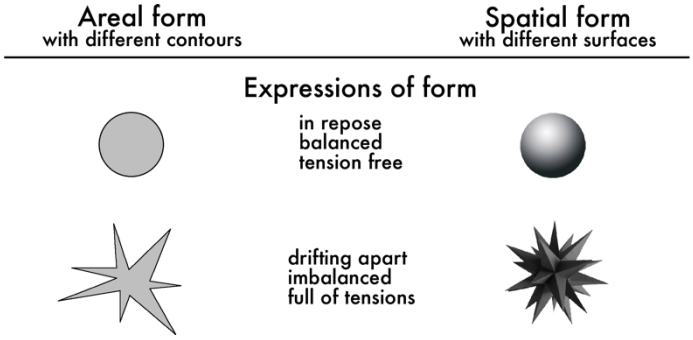

Figure 8: Examples of areal and spatial forms and their different forms of expression

The example given in Figure 8 shows the interrelation between contours and surfaces and their effect on the observer. These are the fundamentals of a perception-oriented theory of form which will be described in greater detail in Section 3.3.

From a design perspective, shape is defined as a group of forms. Developing a shape describes the way in which individual forms are combined to form a shape. The way an object is perceived can be consciously influenced by various design measures such as structuring and arranging.

In terms of their geometric-material characteristics, form and shape are the elements with the strongest impact on perception. Humans experience the most intensive and comprehensive perceptive impressions by perceiving forms and shapes. This is also the reason why creative work in design processes is particularly intense.

At this point the complexity of shape should be highlighted.

A shape is not only a geometric group of forms, but the entirety of the aesthetic elements of form, colour, material and surface and their individual characteristics such as the constellation of the shape elements vis-a-vis each other. It is only then that the shape emerges which is a precondition for complex product perception.

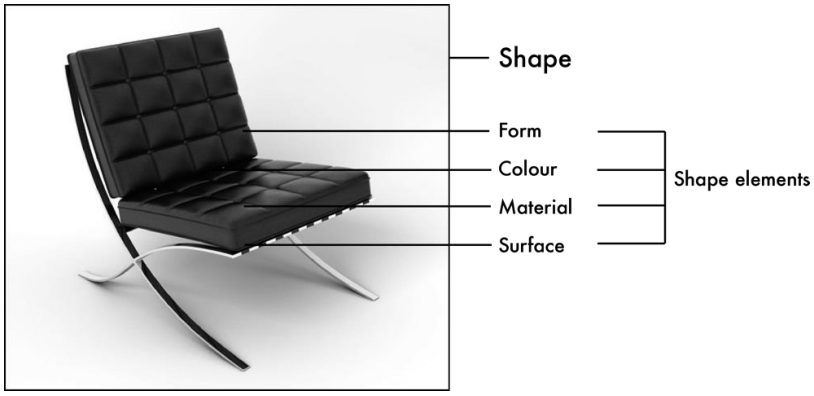

Figure 9: Overall shape
(as exemplified by Ludwig Mies van der Rohe's Barcelona chair, 1929) [3]

Developing a product shape requires dealing with its future situation of perception. The degree of interconnections between the aesthetic elements – described here as overall shape (design) – is of prime importance. This degree has a decisive influence on the perception of the design.

The overall design (shape) results from

- the nature of the shape elements used
- their quantitative use in the product and
- the relationship between the individual and the whole.

Depending on the proportions in the product, two ways of perception are possible: the impression of order or the impression of complexity. Figure 10 shows the impression of order and complexity as exemplified by two watches. This key differentiating factor alone causes different effects.

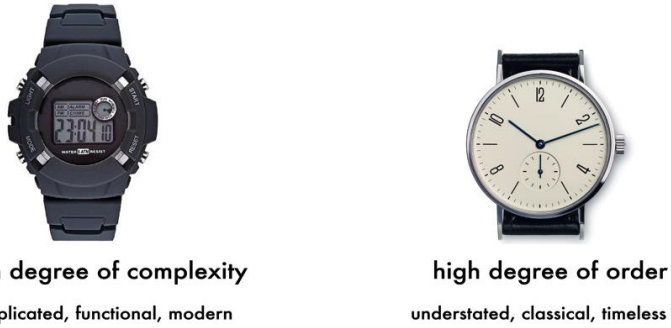

Figure 10: Example of different overall designs producing different effects [3]

Order means:

- low number of shape elements
- low number of arrangement features

Complexity means:

- large number of shape elements
- large number of arrangement features

Order and complexity are the result of a deliberate design process aiming at creating perceivable effects on the user.
Such effects can be, for example:

- simple – complex
- clearly arranged – confusingly complex to chaotic
- expensive – cheap
- old – new
- interesting (affirmation) - uninteresting (indifference)

The effect of order and complexity is also shown in Figure 11.

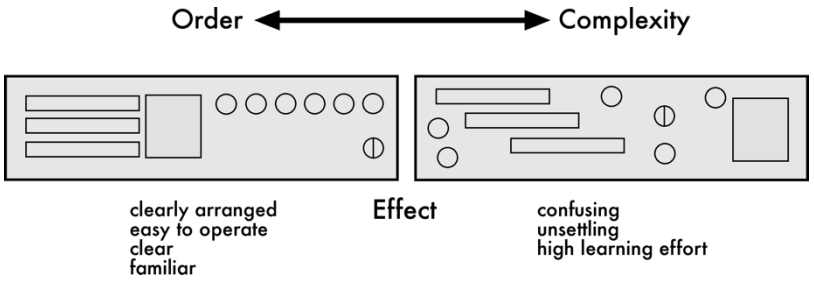

Figure 11: Different states as illustrated by a radio's user interface [3]

Figure 12: Example of the cockpit design of a middle-class car (top image: predecessor model, bottom image: 2013 model)

Figure 12 shows a recent example of a car cockpit design. The analysis focuses only on the design of the control elements. Other design features are not taken into consideration.

In summarising the following can be stated:

Only conscious design processes produce the desired effect.

Figure 13 shows a schematic drawing of two faces made up of identical design elements. Only one of these elements is arranged differently. However, this minor (design) difference causes a tremendous difference in effect.

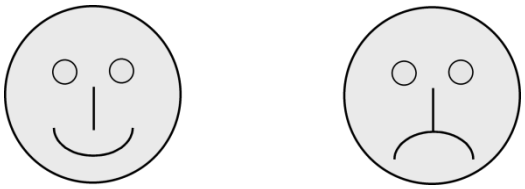

Figure 13: Schematic drawing of two design solutions consisting of identical design elements [3]

3.2.3. Rules of designing

The examples above confirm the interrelation between design and the effect caused in a user. This gives rise to the question of whether there are rules, recommendations and criteria for and examples of perception-oriented design processes. JAKOBY gives a good overview including practical examples of perception-oriented designing [1]. These recommendations are aimed at engineers and designers alike.

In contrast to mathematics, physics and technology, the application of rules does not inevitably lead to good results, i.e., well-designed products. In product design, it is important to continuously examine the resulting effect on the product and compare it with the desired objectives and correct them, if necessary. The rules of design are derived from the properties of the human visual perception system. They follow a set pattern that is almost identically experienced by all human beings. For this reason, these rules can help make designing processes more objective. In principle, all rules go back to the relationship between order and complexity.

For in-depth descriptions and examples see [1].

3.3. Methodical approach to a perception-oriented theory of form

A methodical approach to a perception-oriented theory of form rests on the assumption that human perception of forms is mainly shaped by our perception of forms in nature. Humans are permanently surrounded by archetypal forms in nature. They shape our geometric perception of form and attach relevant interpretations and meanings to them. Therefore, it is only natural to make use of these basic natural forms and apply them to “artificial” man-made forms.

The aim is to create effects on human beings while keeping in mind how we perceive forms.

From an evolutionary perspective, the perception of form can be derived from the perception of nature. To this end, it is evident that natural forms are always the result of processes in compliance with natural laws. The diversity of forms in nature is infinite and cannot be measured by human standards and needs. However, this does not apply to man-made forms because they reflect human needs and are based on human standards.

Natural and man-made forms shape the way how humans perceive their surroundings. For this reason, natural forms can also provide a basis for a perception-oriented methodology and theory of forms.

Human perception of forms is determined by areal contours and the shape of body surfaces. One method of systemising the large number of forms is to take the direction/orientation of the contour or surface as a distinctive feature and characteristic of order.

The principle of distinction can be illustrated by the example of a circle.

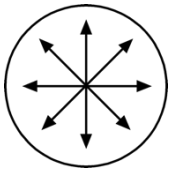

Figure 14: Form lacking direction [3]

The circle is perceived as a circle because its contour lacks a sense of direction. For purposes of typification, its form can be described as "lacking direction". Following this principle, other basic forms can be derived from nature.

Around the year 1970, Zitzmann developed a basic training course for designers at the Hochschule für Industrielle Formgestaltung, Halle-Burg Giebichenstein (Halle School of Art and Design). The systemisation of forms described in this paper is based on Zitzmann's work [2].

3.3.1. Methodology of forms – character of forms

In the following section, four characters of form are derived from forms in nature.

The aim is to present a design-oriented methodology for differentiating forms according to criteria of perception. This methodology helps analyse forms in terms of their visual effect on a user and to apply them purposefully to design tasks. Furthermore, this methodology offers a potential for overcoming the "lack of terminology" so frequently observed when forms are to be analysed and discussed.

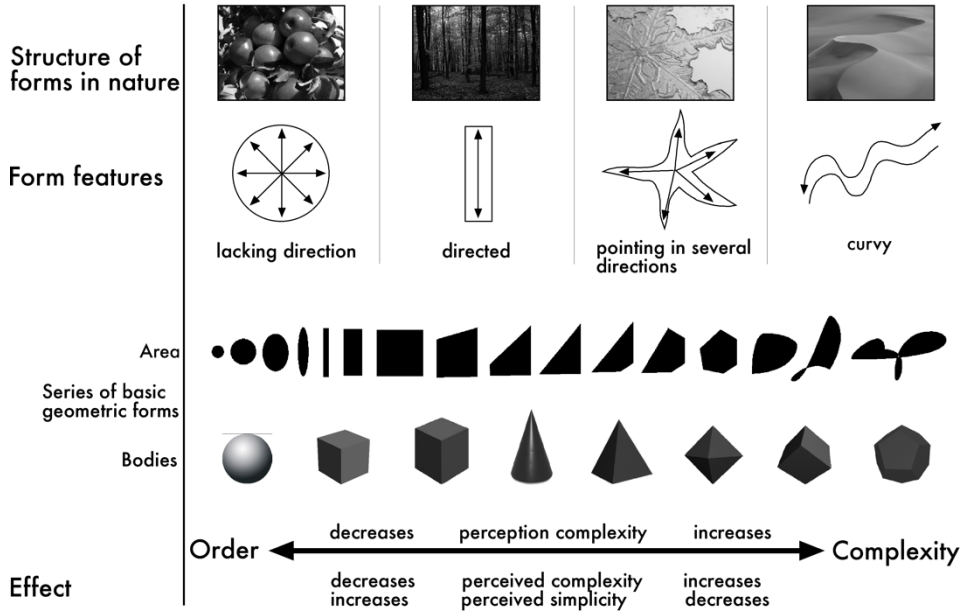

Figure 15: Systematics of forms [3]

3.3.2. Systematics of forms

As a result of analysing forms occurring in nature and reducing them to simple basic geometric shapes, it is possible to develop a system based on different perception efforts.

Let us assume that a circle is perceived quicker, more competently and accurately than a polygon or a complicated curvy/meandering form. However, not only the effort we have to make to perceive a particular shape or form is a differentiating or systemizing feature, but also the different effect the form has on an observer. A circle is perceived as a calmed form free of tensions while a triangle is perceived as aggressive and often as moving.

Based on these principles, a series of forms differentiated by perception effort and feelings triggered can be developed that is of great importance to practical design work. It is highly probable that a planned and desired feeling can be evoked in a person when adequate forms are used.

3.3.3 Form development – quality

A designer can derive fundamental know-how for designing certain effects from this system of forms.

The following three aesthetic qualities present another step towards creating forms in line with human sense and intellectual perception:

- purity of form,
- consistency of form and
- transitional forms and details.

If design processes aim at creating perception-oriented designs, these properties may also be connected with particular objectives. These can be high purity, consistency and compactness.

3.3.3.1. Purity of form

The relationships described in Section 3.3.1 and the series of forms presented in Figure 15 are now transferred to body shapes.

The perception effort and the effects caused in an observer are different for a sphere – for instance – a tetrahedron.

A high degree of purity, understood as a quality feature, is characterised by a lower number of type and form elements. Simple geometric lateral surfaces and a low number of faces and edges are design features to be achieved.

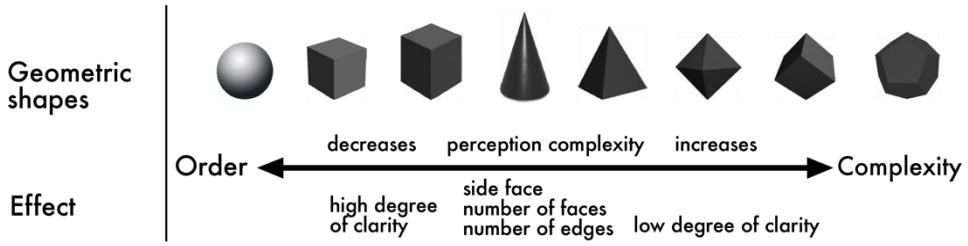

Figure 16: Differentiation between various geometric shapes according to the criterion of purity [3]

3.3.3.2. Consistency of form

The consistency of a form is often linked with the impression of harmony. In contrast, inconsistency conveys disharmony.

Therefore, the following holds: If the design objective is to create a "harmonious" form, the design has to have certain features:

- consistent contour or surface
- consistent direction/orientation and
- consistent curvature.

Consistency of contour and direction/orientation means that the form must not have any recess and sharp bend. Any inconsistency will spoil the harmonious impression and may dominate the design. In other words, the eye "gets stuck" at this point. However, it should also be mentioned that recesses or sharp bends may be created intentionally, for example, as a superior feature (to draw attention).

The third feature of consistency effecting perception is the curvature of a contour or surface. The more complex the curvature, the greater the perceived "disorder", the more disharmonious a form may be experienced.

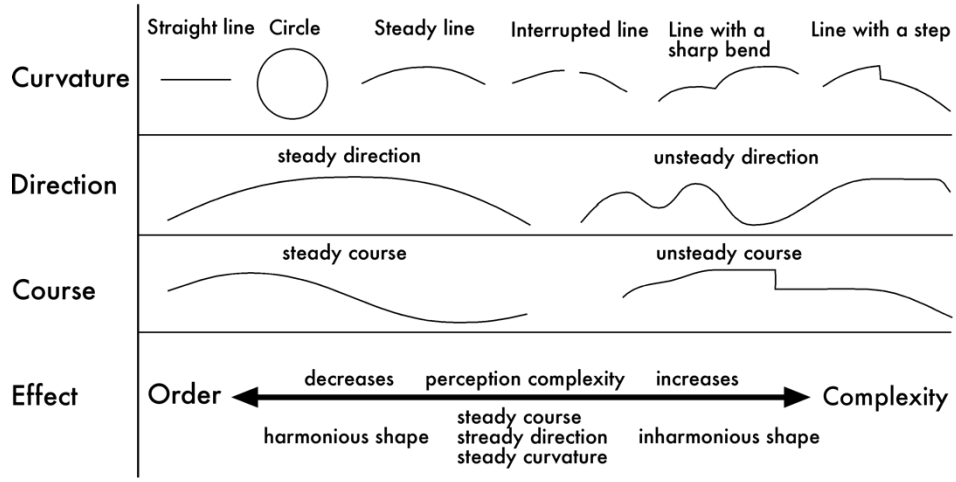

Figure 17: Differentiation according to the criteria of form development quality [3]

3.4. Design methods to create perception-oriented design solutions

The relationship between order and complexity determines the degree and distinctiveness of the shape or overall design. There are no established standards defining this relationship. Too many factors have an impact on the design process. Societal and cultural values, the zeitgeist, individual views and ideas, marketing aspects and design qualifications impact this design challenge.

And yet, it is possible to derive trends and recommendations for designing products. In the course of industrialisation and its concomitant cultural movements and changes, a clear tendency towards creating deliberately ordered forms can be observed. In 20th and 21st century design, attributes such as simple, organised, easy to understand, authentic and honest have been accepted as characteristics of quality.

Of course, the implementation of these characteristics requires complex professional design work. A designer can exert influence on the overall perception-oriented design (shape) during form- and shape-finding processes. Two methods are particularly well-suited to be applied to the engineering design process.

3.4.1. Combining forms to create a compact design and calming shapes

Combining forms to create a compact design and calming shapes are methods suitable to satisfy the need for visual order.

The term *combining forms to create a compact design* describes the combination of various individual forms to achieve a less complex general shape. If the criteria of perception-oriented design are taken as a yardstick, a high complexity of forms may create the impression of being chaotic, unbalanced, overloaded and overtaxing. The functional design shown in Figure 18 is an example of a design solution that is inappropriate from a perception perspective. Such a design may result when a designer works solely to meet

technical and functional requirements but does not take aesthetical aspects into consideration.

In other words, designing with the aim to simplify and harmonise forms is a step in the right direction, i.e., towards a meaningful and sensorially appropriate form.

In principle, there are two possible approaches:

- Developing a form from identical or related forms which are individually visible and appear in an open design (shape). This creates the impression of openness.
- Masking the diversity of forms by "enclosing" them (enclosure, housing). The diversity of forms is covered up and the enclosure fulfils the aesthetical function of the design. This creates the impression of coherence.

In practical designing processes, both methods are typically applied and are seen as methods suitable for calming forms/shapes.

Figure 18 shows the designing process from a functional form to a final perception-oriented shape.

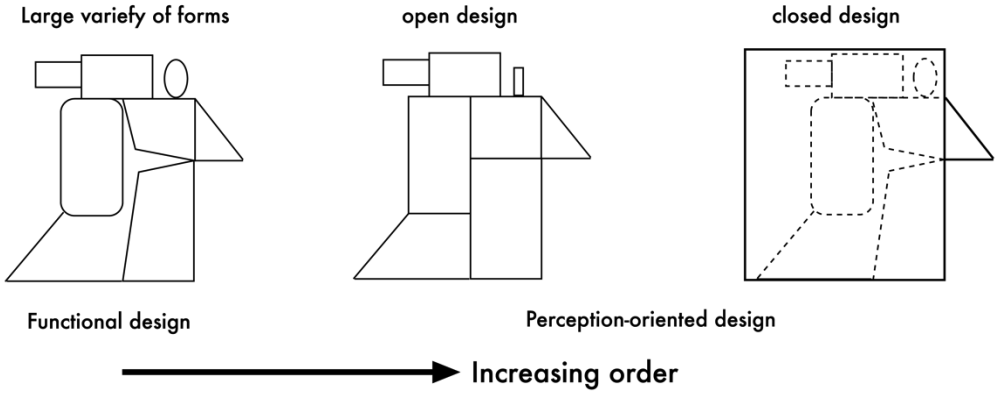

Figure 18: Two methods suitable for calming forms/shapes [3]

Calming a form is a designing method suitable to make a creative decision between order and complexity of the form to be perceived. The degree of order to be created decides about the intended effects.

A clear and orderly form and shape is considered an important and decisive design standard and quality criterion. A high degree of order creates feelings and effects such as

- clarity
- transparency
- security
- perfection
- tastefulness
- high quality, high value and
- long product life.

Evaluations made by both the individual and society always take place in a specific socio-cultural environment. Evaluation standards and concepts of value are always dependent on a particular epoch and culture. Values such as a high degree of order equalling high quality equalling high value equalling sustainability (long-lasting) are, for

example, conceptions of design that were accepted as standards at the end of the 19th century and have been valid to this day.

In product design, the method of combining forms to create a compact design and the method of calming forms take precedence provided the type of product and its intended use allow it. As a result, open, easy to understand and accessible overall designs can be created. While taking into consideration all functional and, in particular, safety requirements, designers should strive to disclose the principles of construction and use. By deliberately simplifying and calming forms, the diversity of construction features can be reduced to create a feeling of order. Using simple basic geometric forms is an important designing approach.

Technical and in particular safety-related reasons often require diverse form elements to be enclosed because such an enclosure also provides protection against external and internal threats. In this respect, an enclosure often also has a sheltering effect. The visual effect is based on the principle of concentration. The diversity created by many individual forms is no longer visible – only the overall design (shape).

This has a calming effect, but at the same time it is also somewhat confusing or even mysterious. At any rate, an enclosure has an ordering effect because the form of the enclosure can significantly reduce form diversity. Both methods are applied to product design. They are suitable for ordering shape features and for reducing or calming designs in terms of their visual complexity. These methods also help finding a product identity in the designing process.

Both methods are exemplified in Figure 19. As a rule, a bike is characterised by an open design. The form elements determining function and use create an open appearance based on the principle of construction and use (arrangement/assembly). The machine tool is accommodated in a housing. The design of the housing has an aesthetic function.

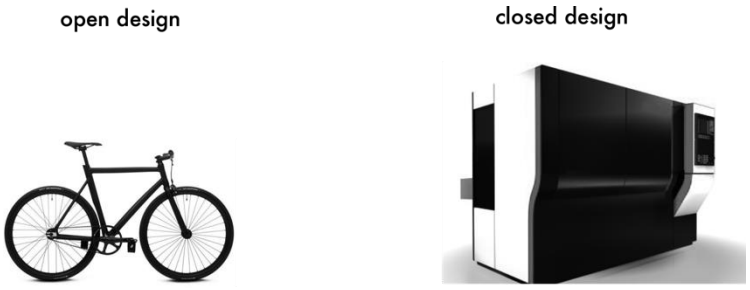

Figure 19: Open and closed design as exemplified in a bike and a machine tool [3]

4. Summary

Form and shape present the major functional and perception prerequisites for implementing technical and aesthetic product requirements in the process of product development. While the engineer follows the principle of form follows function, the industrial designer creates perception conditions that manifest themselves first and foremost in use processes. Both engineers and designers alike plan, visualise and create the geometric-material entirety of a product against the background of the specific objectives of their discipline.

Developing meaningful perception-oriented designs is a primary concern in product design. The approach to developing creative design solutions is based on the relationship between perception and behaviour. A user's or a user group's perception, emotions and behaviour can be purposefully influenced by product design.

A perception-oriented theory of form and shape introduces fundamental principles and interrelations, but it also illustrates the directions and ways to be taken in the design process. To this end, order and complexity are two possible design approaches suitable to develop the overall design (shape) in line with the effects desired. However, this does not mean that the entire range of potential design options available in a designing process will be exhausted. The professional industrial designer will make use of his or her expertise in composition and his or her skills acquired in practical design work. A high degree of sensitivity to form, colour, material and surface aesthetics are individual prerequisites for professional work.

Product development is an interdisciplinary process. Such an interdisciplinary and integrative approach is required if all qualities, expected today of a quality product, are to be achieved. New production development methods, shared drafting, design and construction tools as well as new forms of organisation enhance integrative working processes.

New design concepts such as the Masters Course in Integrated Design Engineering offered at the Otto von Guericke University Magdeburg have successfully taken up this challenge.

References

[1] Jakoby, J.: Ein Beitrag zum wahrnehmungsgerechten Gestalten, Reihe Konstruktionstechnik. Shaker Aachen, Verlag, 1993.

[2] Zitzmann, L.–Schulz, B.: Dokumente zur visuell-gestalterischen Grundlagenausbildung. Hochschule für Industrielle Formgestaltung, Halle-Burg Giebichenstein, 1990.

[3] Gatzky, Th.: Vorlesungs- und Übungsmaterialien zu den Lehrveranstaltungen Industriedesign/Produktdesign und Entwurf für Ingenieurstudenten der Fakultät Maschinenbau an der Otto-von-Guericke-Universität Magdeburg, 2012.

[4] Naumann, Th., Gatzky, Th., Vajna, S.: Integrierte Produktentwicklung als Ausbildungskonzept. In: CAD-CAM Report. Nr. 2, Jg. 23, 2004.

[5] Gatzky, Th.: Industriedesign in der Ingenieurausbildung: Über ein Ausbildungsmodell, das auf Integration setzt. In: Industriedesign und Ingenieurwissenschaften, TUDpress 2008, Verlag der Wissenschaften.

[6] Schürer, A.: Entwicklungstendenzen im Investitionsgüterdesign in Design aktuell 1. Schriftenreihe des Design Center Stuttgart, 1988.

[7] Ehrenstein, W.: Probleme der ganzheitspsychologischen Wahrnehmungslehre. Johann Ambrosius Barth Verlag, Leipzig, 1954.

Design of Machines and Structures, Vol. 4, No. 1 (2014), pp. 25–32.

DESIGNING A PORTABLE FORGE

DÁNIEL HERBST–ÁGNES TAKÁCS
University of Miskolc, Institute of Machine and Product Design
3515, Miskolc-Egyetemváros
herbstdaniel12@gmail.com; takacs.agnes@uni-miskolc.hu

The open die forging like ancient profession accompanied the path of humanity to both technical and aesthetic aspects. So this way it will be industrial technology and art of fancy metalwork at the same time that has forges as a chief assistant.

1. Open die forging is technology and art

Since ancient times people were stimulated towards development by their complex minds. Tools and weapons initially were made of non-metallic materials, than later more durable metals. Application of iron meant one of the significant, if not the most significant step in the evolution of mankind. *„In the human history the iron production achievements within the acquis, a kind of discovery, which has no parallel in, a performance equivalent to not know, and besides that, everything else was insignificant inventions and discoveries, or at least seems subordinate significance. We owe the discovery of iron smelting the metal hammer and the anvil, the forged iron sword, axe and chisel, the iron slippers plow, briefly the basic tools of civilization. The lack of iron tools hampered the development of humanity." [1]*

Production and processing of iron has become increasingly sophisticated in the storms of ages. The forging from the unique hand-made pieces reached die forging that is economical in large quantity.

However considering any ages of forging open die forging has not been lost because some aesthetic surplus belonged to it. This surplus enabled the development of artistic forging, the raison d'etre of fancy smiths. Their work is flanked our history with ages spanning, lasting creations. There is no age style in which artistic fancy metalwork-pieces would not have made. As the opposite of the impermanence of human life and the fragility of human being objects, which was made of metals express the longing for eternity and the invulnerability. Thus, for example, may witness a forged rose of eternal love, even if we are aware of the impermanence of metals. So the target audience of the designed machine are those users, who wish to deal with fancy forging.

2. The motivation of designing a portable forge

A smithery for the large majority of people is highly rooted at regional level with a conventional fire brick oven fanned by leather bellows. Experienced may have come across portable forges, or whole portable workshops, or even recognize their right to exist. You cannot even find a fair, in which would not be at least one ornamental blacksmith, who proclaims the beauty of his profession in a noble way, with his portable workshop, whose heart and soul is a portable forge.

Today, the need of the deviation from the average is formulated by many, social norms refract their creativity, but confronting with the grey twilight of averageness, they begin to create their own. The branch of ornamental metalwork art is not obvious to the average, since the above-mentioned image of a stationary workshop is really alive for them. One of the main aims is to make the heating device for the forgeable feedstock portable. The installation process is easy to carry out it takes just a few seconds. After a short fixing capture process, the user can start working.

3. The energy needs of forging

The most important sector of forging is hot forging, which is based on heating the work piece to a more favourable temperature for forming. Required heat energy can provide on several different ways. Nowadays three main possibilities can be recovered on the basis of the available technologies for heat transfer medium or physical interactions.

- With burning or heating of solid fuels work pieces can be heated with low efficiency by continuous supplementation of its favourable carbon content. Such solid fuels could be black coal, brown coal, coke, charcoal.
- In case of aero form fuel, the fuel is injected through focused burners into the heating chamber, where during combustion it heats the work piece to optimal temperature. However, in this case carbon loss occurs, thus the use of additives proposed.
- The most energy intensive process that is mainly applied in the industry is heating by induction coils. Fast and effective process with good efficiency but high electricity and safety claim.

In terms of the forging pieces the best of these three methods is to use solid fuel. Its advantages include simplicity resulting of traditional sophistication and its safer and more economical operation.

4. The most important considerations in combustion technology

In combustion technology approach the quantity of required air for combustion of the fuel used in the heating has to be known, which from the required amount of air to annealing follows. The professional literature, which deals with forging does not provide specific calculations for heating with solid fuels, it only recommend air intake limits for industrial furnace chamber design. The air necessity values of a small portable forge are determined in speculative way and can be refined with preparation of subsequent iteration prototypes.

Considering the raw materials of the work pieces and the dimensions of the blanks a base volume is assumed, in which the heating will be carried out. Taking the perfect combustion of fuel as a basis and taking the possible contamination of fuels, the efficiency of combustion and that the aim is only annealing into account the approximate value of the required air volume arisen. So the suitable fan unit can be selected that will provide the airflow.

Depending on the fuel the amount of combustion products has to be considered this will appear as ash and fuel gas in case of the selected form. Calculations carried out on the ash content it can be concluded that how big amount of ash will be generated during the operation of the equipment, so what specifications (recommendations) can be made to the users for smooth operation due to the removal of combustion products.

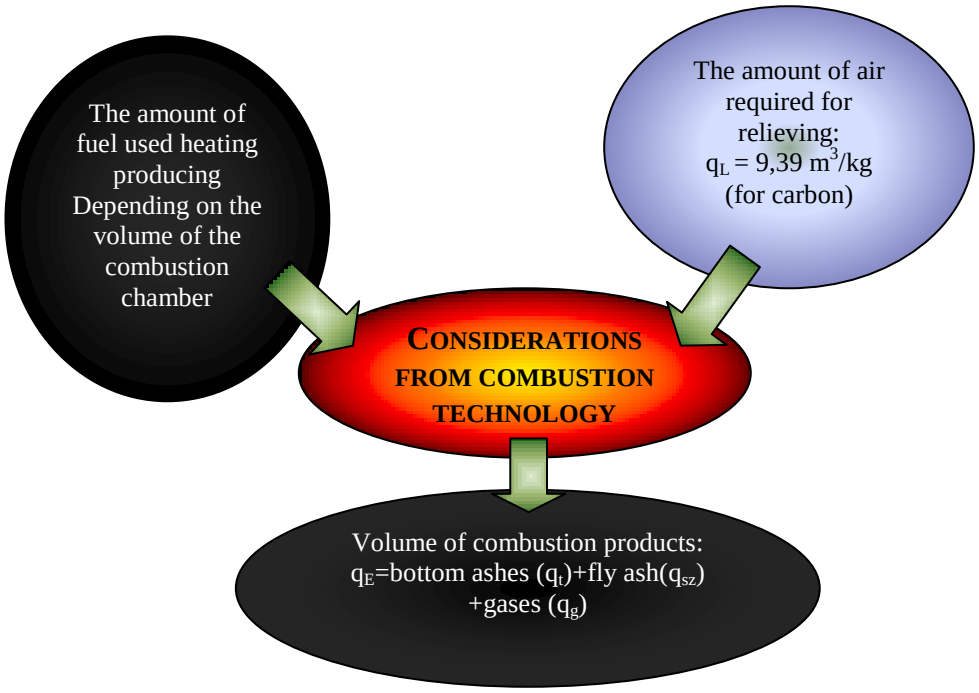

Figure 1: Combustion considerations

5. The design process broadly in line

The first step of the whole design process is the conceptual design phase, when the opportunities in patents and potential rivals in the market, and the resulting operational features are discussed. Solution variants can be built up from the simplest level to create a portable forge. Analysing the variants the optimal solution can be defined that can be carried out in the construction design phase.

The construction design relies on the functions identified during the conceptual design. The application of a countervailing space for ensuring constant pressure of the air stream before the furnace can be mentioned as an example.

When creating the construction, it is important to take the statutory provisions and specifications into consideration in order to let the product be merchandized. These provisions mainly defined for preserving the user's safety and comfort during the use of the product. The currently in force regulation in our country has been published in the 127th issue of the Hungarian Bulletin (Magyar Közlöny), which is the regulation of the National Development and Economy Ministry 16/2008 (VIII. 30.) that is about the certification of machines safety requirements and conformity. Another aspect is the compliance of the

human body's anthropometric parameters, which helps the long-lasting, comfortable and thereby pleasant work, the adequacy of comfort [4]. Ultimately during design of a unique product it is worth taking the command of specific engineering ideas and guidelines into account.

The design of the construction can happen in accordance with the foregoing written, and bearing in mind the logical edification of the parts on each other, their hierarchy. The selected equipment for air flow and the sum of the heating- and the necessary control components enter the final dimensions of the workspace. On this basis the construction of the structure can be continued, the position and construction of mechanisms for movement and for security.

Embedded in the design process every opportunity can be captured to improve the structure from the mechanical model all the way in the conduct of finite element investigations. Using finite element software the distribution of the heat load resulting from the furnace and the analysis of its effects had been recorded. (For example: the furnace must be fixed flexible, otherwise it is arousing large deformation in the basic structure).

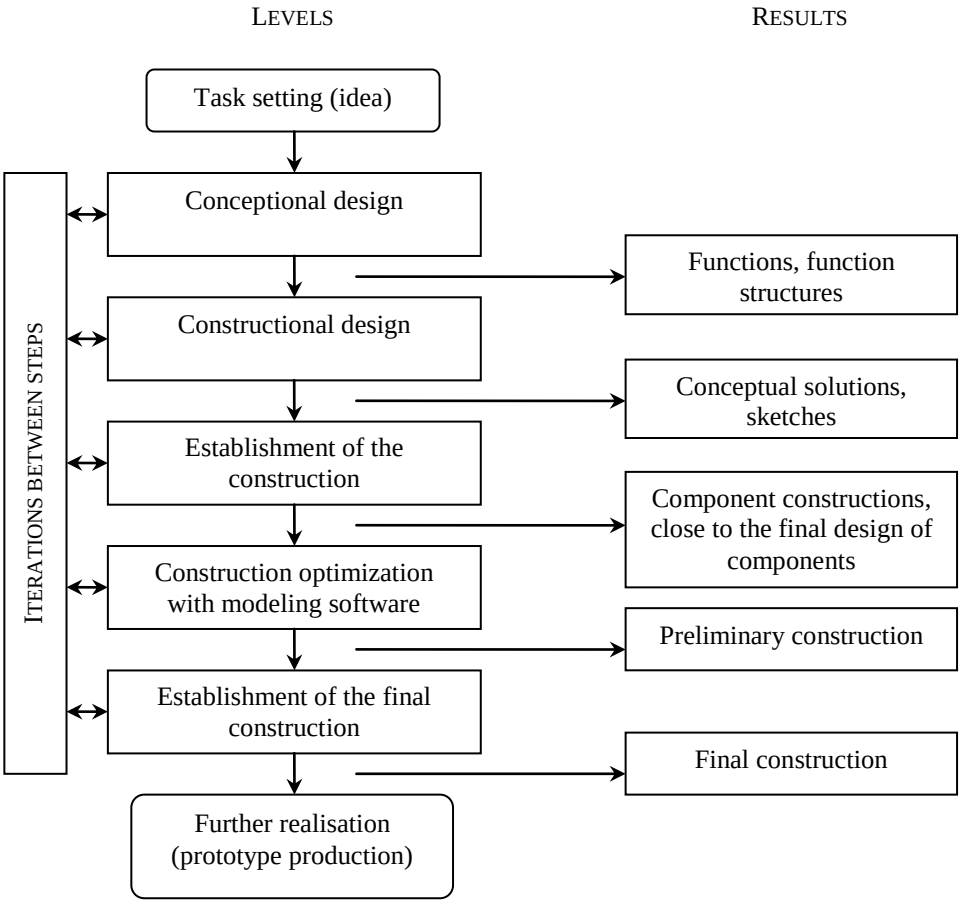

Figure 2: Design process in case of individual design

The portable machine received by the end of the design process, although it pulls through in principle, it is strongly recommended to implement an iterative repair on a prototype and to improve the cost efficiency before putting on the market, consequence of which it can be further improved, personalized.

6. Introducing the construction

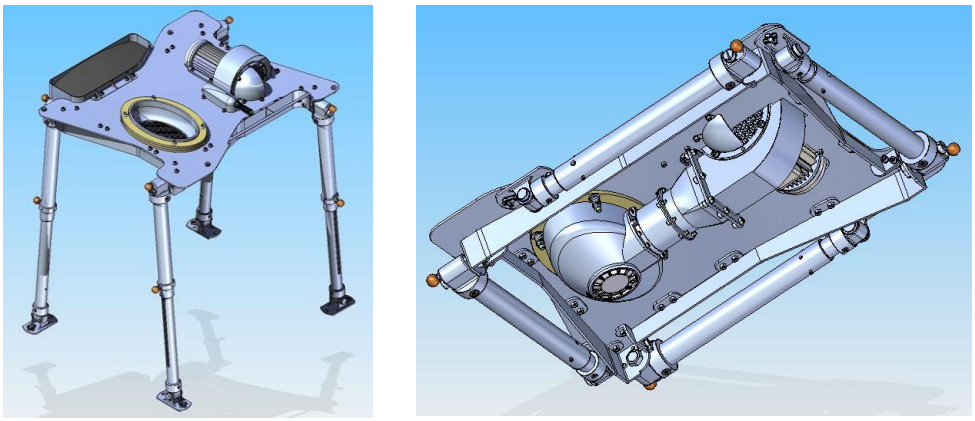

Figure 3: Completed construction in 3D

The in principle finished construction can be seen in the pictures of Figure 3. The image on the left shows standing condition, while on the right the packed base condition of the fully assembled construction can be seen.

7. FEM analysis of the equipment

During the presentation of the construction it is important to take the hierarchical relations among the components into account. It was already mentioned that the heating assisting elements are the primary components. The furnace is a heat-resistant cast steel, which is embedded a socket framed of aluminium-silicate ceramic insulator rings and it has dimensions that make it suitable for full heating of smaller work pieces or partial heating for larger work pieces.

Using FEM software the propagation of heat and the appearance of adverse effects of heat stress in the structure may be assessed. It is important to know how much heat the isolation of the furnace loads it's surrounding, possibly in contact parts.

In the left picture of Figure 4 the heat propagation in the contact zone at the furnace, the insulator rings and the table top can be seen. It can be observed that the insulator rings absorb much of the heat protecting the nearest elements of the structure from the 1100 °C heat loading. In the picture the hottest area (I) is shown in red, while the coldest (III) is signed by dark blue. The second darkest blue shades zone (II) start from that part of the table top, where it is contacted with the insulator rings. The local temperature is about 110 °C.

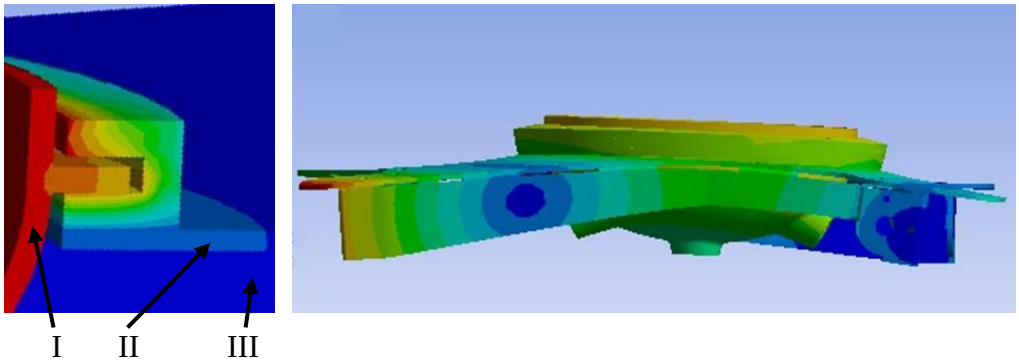

Figure 4: Heat loading and deformation

Components with different materials produce different thermal expansion due to the heat loading, which would result in case of solid anchoring of the components impermissible deformations and inherent fatal tensions.

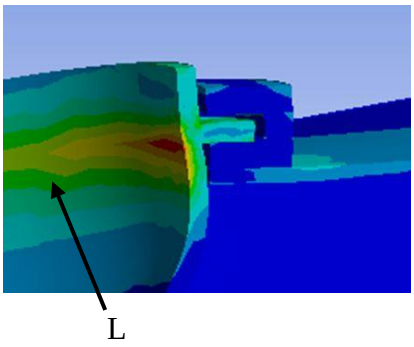

Figure 5: Equivalent stress

According to the above written in Figure 5 an emphasized detail the deformation caused by the stress distribution can be seen. Green zone (L) shown in the figure already exceeds the allowable stress of the furnace material, thus leads to immediate failure. Cross the yellow all the way to the red zone the model shows even higher stress, so it can be said that, the combustion chamber and it's insulation should be flexibly fixed to the other elements of the structure to minimize stresses and deformations caused by heat.

8. The structure of the device

From below the combustion chamber is closed by a pressure countervailing chamber its bottom is possible to open by a bayonet type lid to remove combustion products. The countervailing chamber and the insulator rings are flexible fixed to the table top.

The air gets access to the combustion chamber through three holes, while to the countervailing chamber cross in a larger inlet. Between the countervailing chamber and the fan a dilations-yielding pipe section and the air flow control laminar gate valve are located. The air flow control can be provided by an interrupt can crank, which is derecognised from the gate valve to the user interface. The scrolling transfer mechanisms are protected from the heat and soiling by a sheet formed part.

The fan unit is selected on the basis of combustion calculations and it is a commercially available item, which is applied with some minor modifications. It will be underpinned fixed with half rings by the drive motor. On the suction side a grind and a split quarter spherical baffle plate protect users from potential damage and the ingress of impurities to the impeller.

After the previous outlined steps arises the ‘heart’ of the structure, which determines the additional dimensions. The next step is the development of a table frame, which consists of general-purpose structural steel curved plate parts. It is composed exactly four pieces, endeavouring a flexible yet strong construction. The table frame is made up table top perpendicular sections, thus increasing the resistance to bending stress. In its four corners suitable pins for receiving the foot wrists will be placed.

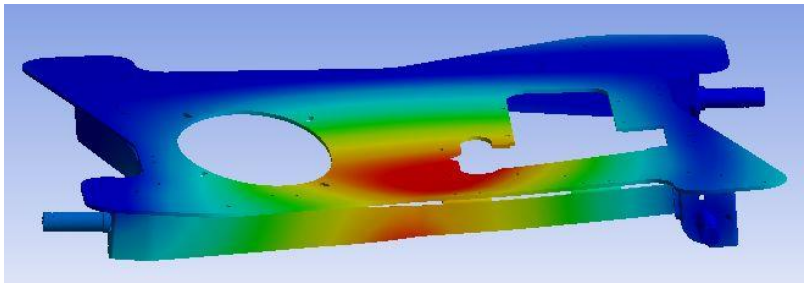

Figure 6: Table frame deformation

The sizes of the table frame sections are determined by calculation. Figure 6 shows an example for the examination of overload and the case of inappropriate use, assuming a mass of 100 kg user sitting on the edge of the table structure and exerts on a differentiated load. The maximum displacement in this case is 0.7 mm, which is not a permanent deformation, so the structure suffers no damage.

Four spiral-opening, two-stage, double-secured telescopic legs intended to perform the holding task of the table work space. In closed state legs are recorded to the lower surface of the table top and the frame. At the junction of the articulated foot and the table top works a mechanism for ensuring a kingpin associated with a sliding, while at the frame a single spring-pin ensuring mechanism.

To open a third mechanism also have to be released, which is a pin-type spring mechanism, located between the two pipe sections of the legs. When the legs are completely set free, grabbing the table top and lifting the equipment the legs because of their own weight swinging and the spring-loaded safety-pinned mechanisms click into their position. On the wrists and on the frame formed abutment surfaces meeting subdue the momentum of the legs.

Once the legs have been extended position, it is possible to rotate the soles into required position, around their pivot axis and around the axis of the leg up to ninety degrees. The

fixing of the table can be enhanced with nails placed through the holes of soles slider mechanism into the ground.

Finally got the table top its shape and it is fixed to the so far listed items with screws as the rest of the structure. It is designed to follow the spiral motion of the legs. As well as providing an optimum location, when the legs are closed to gripping them for the easier transport.

Acknowledgement

The research work presented in this study based on the results achieved within the TÁMOP-4.2.1.B-10/2/KONV-2010-0001 project and carried out as part of the TÁMOP-4.1.1.C-12/1/KONV-2012-0002 „Cooperation between higher education, research institutes and automotive industry" project in the framework of the New Széchenyi Plan. The realization of this project is supported by the Hungarian Government, by the European Union, and co-financed by the European Social Fund.

References

[1] Morgan, L. H.: The ancient society, Transaction Publishers, 1877.
[2] Kamondi L.–Sarka F.–Takács, Á.: Fejlesztés-módszertani ismeretek. Elektronikus jegyzet. Készült: „Korszerű anyag-, nano- és gépészeti technológiákhoz kapcsolódó műszaki képzési területeken kompetencia alapú, komplex digitális tananyag modulok létrehozása és online hozzáférésük megvalósítása" TÁMOP-4.1.2-08/1/a-2009-0001, http://web.alt.uni-miskolc.hu/tananyag/index.html, Miskolc, 2011.
[3] Kamondi L.–Takács Á.: Környezettudatos tervezés. Útmutató és segédlet az előadáshoz és a gyakorlathoz BSc. szakos Ipari termék- és Formatervező hallgatók részére. Elektronikus jegyzet. Készült a TÁMOP-4.2.1.B-10/2/KONV-2010-0001 jelű projekt részeként az Európai Unió támogatásával, az Európai Szociális Alap társfinanszírozásával, Miskolc, 2012.
[4] Woodson, W. E.–Conover, D. W.: Human Engineering Guide for Equipment Designers. University of California Press, 1964.

Design of Machines and Structures, Vol. 4, No. 1 (2014), pp. 33–43.

DEVELOPMENT OF A DESIGN AND OPTIMIZATION METHOD FOR HIGH PRESSURE COMPONENTS

ALEXANDER MÜTHER[1]–BERND MAIER[1]–ISTVÁN GÓDOR[1]–
THOMAS CHRISTINER[2]–RENÉ STÜHLINGER[2]–FRANZ TRIEB[2]
[1] Montanuniversität Leoben, Chair of Mechanical Engineering
Franz- Josef- Strasse 18, A-8700 Leoben–Austria
[2] BHDT GmbH, Industriepark 24, A-8692 Hönigsberg–Austria

In this paper the development of an automated design and optimization method for high pressure cylinders is explained. To reduce the total stress in the structure during the operating state different manufacturing processes are used. By implementing standard design rules into MS EXCEL® the automated calculation of the significant stress conditions is possible. The automated calculation sequences allow a coupling with an optimization software and the investigation of computed calculated optimized parameter combinations.

Nomenclature

symbols for the calculaution of the load induced stress

σ_t = tangential load induced stress, MPa
σ_r = radial load induced stress, MPa
σ_{ax} = axial load induced stress, MPa
p_i = inside pressure, bar
r = random point in the structure, mm
r_i = inside radius, mm
r_a = outside radius, mm

symbols for the calculation of the residual stress due to autofrettage

σ_{tRA} = tangential residual stress in the plastic part of the structure, MPa
σ_{rRA} = radial residual stress in the plastic part of the structure, MPa
σ_{tR} = tangential residual stress in the elastic part of the structure, MPa
σ_{rR} = radial residual stress in the elastic part of the structure, MPa
σ_F = yield stress, MPa
D = random point in the structure, mm
D_O = outside diameter, mm
D_I = inside diameter, mm
D_p = diameter of the plastic elastic boundary fibre, mm

symbols for the calculation of the shrinkage strain in the layered structure

P_{if} = pressure in the interface between inside and outside cylinder, MPa
δ = interference between inside and outside cylinder, mm
D_{if} = shrinkage diameter, mm
E_i = elasticity modulus inside cylinder, MPa
E_o = elasticity modulus outside cylinder, MPa
υ_i = Poisson's ratio inside cylinder
υ_o = Poisson's ratio outside cylinder
σ_{tri} = tangential shrinkage strain inside cylinder, MPa
σ_{rri} = radial shrinkage strain inside cylinder, MPa
σ_{tra} = tangential shrinkage strain outside cylinder, MPa
σ_{rra} = radial shrinkage strain outside cylinder, MPa
Y_i = ratio of the shrinkage diameter and the inside diameter
Y_o = ratio of the outside diameter and the shrinkage diameter

1. Introduction

In highly stressed cylinders residual stresses are generated due to the manufacturing processes autofrettage and shrinking, which leads to a reduction of the total stress in the operating state. Thereby autofrettage is used to create compression stress at the inside diameter by plastifying a certain part of the structure. The design of layered wall cylinders causes a related effect due to an interference at the interface between the single walls [1]. In this paper the structure and application of a design and optimization tool for determination and reduction of the stress conditions in highly stressed components is explained. The tool can be used for the efficient preliminary design of the coponents. The calculation of the residual and operating stress conditions after autofrettage and shrinking of the components are implemented to the design tool. The calculations are based on standard design rules and the ASME Boiler and Pressure Vessel Code [2], that further considers the Bauschinger effect. This effect leads to a reduction of the compression strength of the material and decreases the residual stress after autofrettage. If the quotient of the tangential residual stress at the inside bore and the yield stress is more negative than –0,4 the effect is considered in the calculation and the stress is corrected [2]. Moreover the tool provides the opportunity to estimate the approximate durability based on Miner's rule. By coupling the developed calculation sheets with the free available optimization software DAKOTA® it is possible to optimize several stress conditions considering different geometric and process input parameters. For the validation of the developed calculation and optimization method the tool is applied on highly stressed components. Extensive tests have been performed in which different optima were identified. Thereby stress is reduced up to 44% and the load capacity is increased up to 30% at the same level of damage. The final design of the components is based on a finite element analysis whose results are copmpared with the analytic calculations.

2. Theory

The inside pressure in thick walled cylinders causes a triaxial state of stress in the structure in which the tangential stress has the highest tensile stress value. Thereby the tangential stress at the inside bore is higher than the one at the outside bore. The inside bore of the structure is identified as a critical point for damage due to the mentioned tangential stress. The operating stress condition is shown in Figure 1. The analytic equations 1, 2 and 3 given below enable the calculation of the operating stress conditions [1].

$$\sigma_t = p_i * \left(\frac{r_i}{r_a^2 - r_i^2} + \frac{r_a^2 * r_i^2}{r_a^2 - r_i^2} * \frac{1}{r^2} \right) \tag{1}$$

$$\sigma_r = p_i * \left(\frac{r_i}{r_a^2 - r_i^2} - \frac{r_a^2 * r_i^2}{r_a^2 - r2_i} * \frac{1}{r^2} \right) \tag{2}$$

$$\sigma_{ax} = p_i * \left(\frac{r_i^2}{r_a^2 - r_i^2} \right) \tag{3}$$

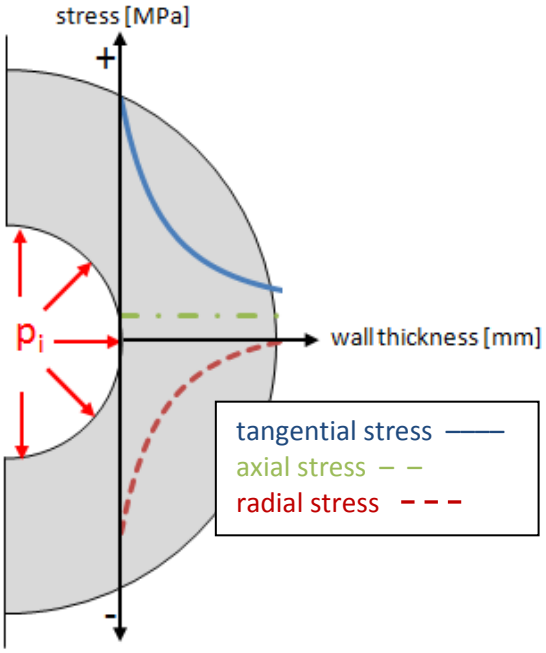

Figure 1: Operating stress condition due to inside pressure

By using autofrettage the cylinder is charged with a high pressure that plastifies a certain part of the wall from the inside bore to a certain fibre in the structure. The plastified percentage of the wall depends on the autofrettage pressure, the cylinder wall thickness and the yield stress of the material. Due to its resilient property the outside part presses on the plastic part which acts like and inside pressure on the outside part [1]. These conditions lead to a stress state shown in Figure 2.

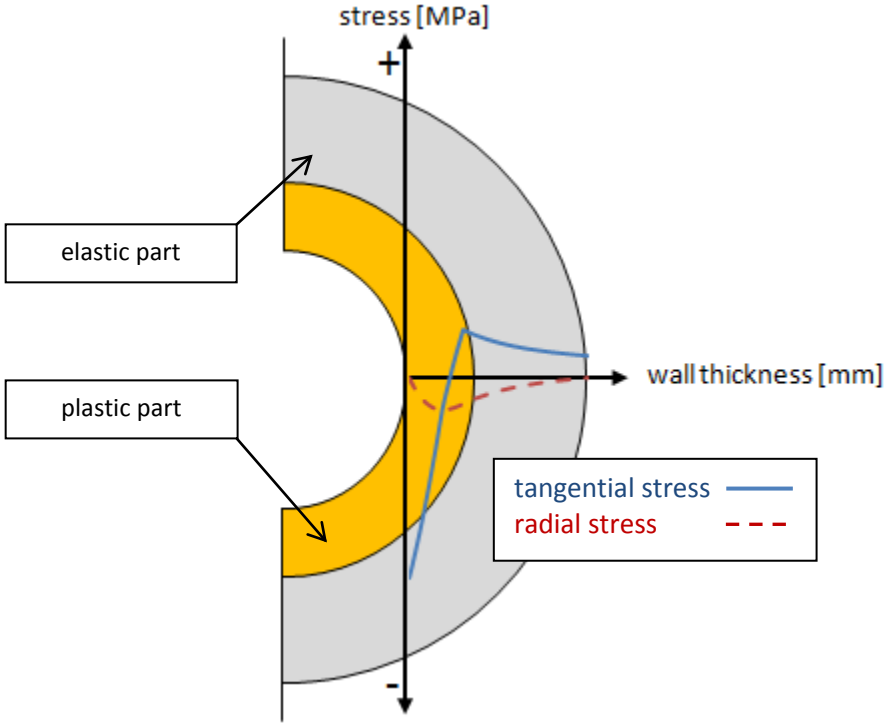

Figure 2: Residual stress conditions after autofrettage

At this point only the calculation without the consideration of the Bauschinger effect is explained. The ASME Boiler and Pressure Vessel Code [2] considers only the tangential and radial stress conditions. The calculation of the residual stress is realized separately for the elastic and plastic part of the wall. The equations 4 and 5 for the calculation of the plastic part are given below [2]:

$$\sigma_{tRA} = 1{,}15\sigma_F \left[\left(\frac{D_p^2 + D_o^2}{2D_o^2} \right) + \ln\left(\frac{D}{D_p} \right) - \left[\frac{D_t^2}{D_o^2 - D_t^2} \right] \left[\frac{D_o^2 - D_p^2}{2D_o^2} + \ln\left(\frac{D_p}{D_t} \right) \right] \left(1 + \frac{D_o^2}{D^2} \right) \right] \quad (4)$$

$$\sigma_{tRA} = 1{,}15\sigma_F \left[\left(\frac{D_p^2 - D_o^2}{2D_o^2} \right) + \ln\left(\frac{D}{D_p} \right) - \left[\frac{D_t^2}{D_o^2 - D_t^2} \right] \left[\frac{D_o^2 - D_p^2}{2D_o^2} + \ln\left(\frac{D_p}{D_t} \right) \right] \left(1 - \frac{D_o^2}{D^2} \right) \right] \quad (5)$$

The equations 6 and 7 for the calculation of the elastic part are given below [2]:

$$\sigma_{tR} = 1{,}15\sigma_F \left[\left(1 - \frac{D_o^2}{D^2} \right) \left\{ \frac{D_p^2}{2D_o^2} + \frac{D_t^2}{D_o^2 - D_t^2} * \left(\frac{D_p^2 - D_o^2}{2D_o^2} - \ln\left(\frac{D_p}{D_t} \right) \right) \right\} \right] \quad (6)$$

$$\sigma_{tR} = 1{,}15\sigma_F \left[\left(1 - \frac{D_o^2}{D^2} \right) \left\{ \frac{D_p^2}{2D_o^2} + \frac{D_t^2}{D_o^2 - D_t^2} * \left(\frac{D_p^2 - D_o^2}{2D_o^2} - \ln\left(\frac{D_p}{D_t} \right) \right) \right\} \left(1 - \frac{D_o^2}{D^2} \right) \right] \quad (7)$$

Another manufacturing process to generate stress conditions reducing the stress in the operating state is the shrinking of layered cylinders. An interference between the inside and outside cylinder in a two layer cylinder wall causes a pressure in the interface between the two layers. This pressure acts like an outside pressure on the inside cylinder and like an inside pressure on the outside cylinder. The generated stress conditions are shown in Figure 3. The pressure causes a compression stress in the inside cylinder that gets superimposed with the operating stress. The following equations 8 and 9 allow the calculation of the pressure P_{if} in the interface between the two layers [2]:

$$P_{if} = \frac{\delta}{D_{if} * A} \quad (8)$$

$$A = \frac{1}{E_i} * \left(\frac{D_t^2 + D_{if}^2}{D_{if}^2} - \nu_i \right) + \frac{1}{E_o} * \left(\frac{D_{if}^2 + D_o^2}{D_o^2 - D_{if}^2} + \nu_o \right) \quad (9)$$

The calculation of the stress conditions in the inside cylinder can be performed by the following equations 10 and 11 [2]:

$$\sigma_{tri} = -\frac{P_{if} * Y_i^2}{Y_i^2 - 1} * \left(1 + \frac{D_t^2}{D^2} \right) \quad (10)$$

$$\sigma_{rri} = -\frac{P_{if} * Y_i^2}{Y_i^2 - 1} * \left(1 - \frac{D_t^2}{D^2} \right) \quad (11)$$

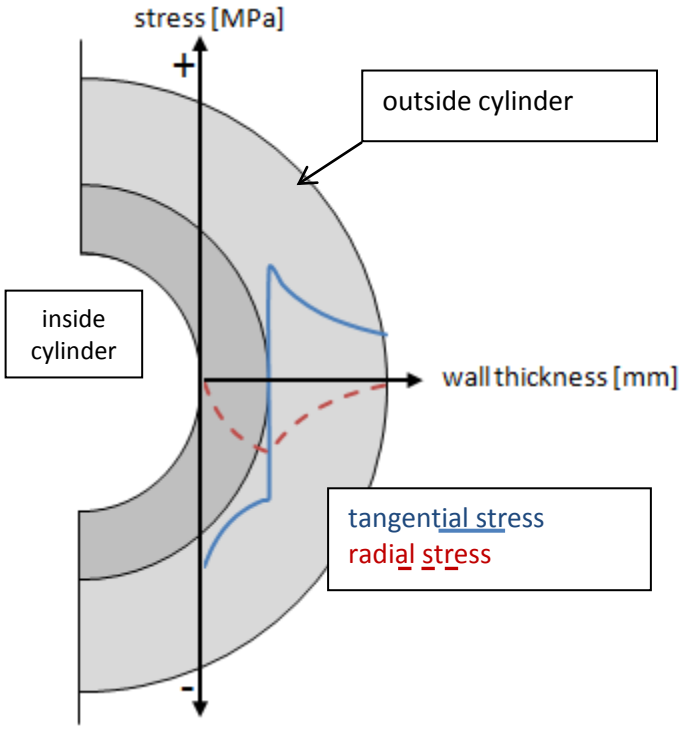

Figure 3: Stress conditions in an a two layer cylinder

The calculation of the stress conditions in the outside cylinder can be performed by the following equations 12 and 13 [2]:

$$\sigma_{tro} = -\frac{P_{if}}{Y_o^2 - 1} * \left(1 + \frac{D_o^2}{D^2}\right) \tag{12}$$

$$\sigma_{rro} = -\frac{P_{if}}{Y_o^2 - 1} * \left(1 - \frac{D_o^2}{D^2}\right) \tag{13}$$

For assembling the two cylinders the outside cylinder needs to be expanded due to the interference between the inside and outside cylinder. For manufacturing the outside cylinder is heated up to a certain temperature that expands the cylinder and enables the assembling of the two cylinders. By cooling the shrink fit down to room temperature the outside cylinder is shrinked on the inside cylinder which creates the pressure in the interface. By combining the two processes of autofrettage and shrinking it is possible two create residual stress conditions up to the value of the yield stress of the material which is the limit for residual stresses. Thereby the necessary autofrettage pressure is reduced compared with the autofrettage pressure that is used to create the same level of residual

stress in a solid wall cylinder. The calculation of the effective stress conditions after interference of the residual and operating stresses is done by simple addition of the single stress conditions.

2.1. Analytic calculation tool

By implementing the analytic equations into a calculation tool using MS EXCEL® the automated calculation of the several stress conditions is possible. For coupling the MS EXCEL® calculation sheets with the optimization software DAKOTA® and applying optimization algorithms it is necessary to have automated calculation sequences capable to edit the results after the input of different parameters [3]. The structure of the tool is shown in Figure 4. Dimensions of the cylinders or process parameters like the autofrettage depth are given to the input data sheet. On the following sheets of the tool the stress conditions are calculated and edited automatically. Furthermore the approximate durability can be estimated provided that the data from the Wöhler fatigue test is available.

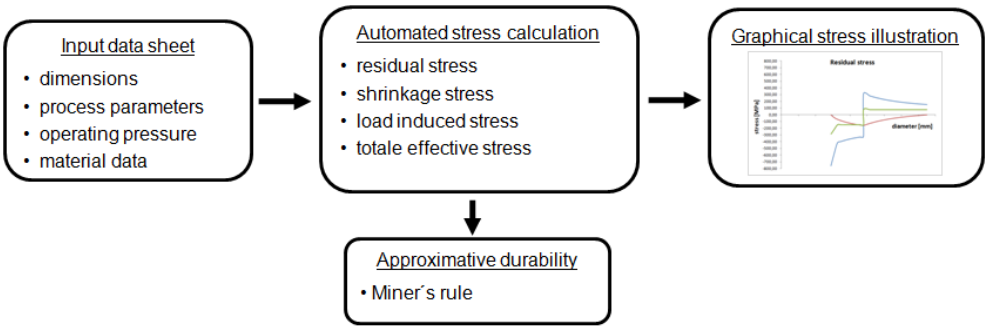

Figure 4: Structure of the calculation tool

2.2. Optimization with DAKOTA®

DAKOTA® is a free available optimization software from the Sandia National Laboratories. DAKOTA® provides several optimization algorithms and interfaces with software tools like MS EXCEL®. The optimization process runs a loop in which the settings from the DAKOTA® input file are processed into a parameter file. Certain parameter combinations are imported to the MS EXCEL® sheets and the results are automatically given to a result file. If the predetermined number of calculation sequences has been performed the break condition is fulfilled and the optimization is stopped. The parameters and results are given to an output-file in which the best parameters are listed separately. The input file contains the settings for the predetermined parameters like the lower and upper bounds of the parameter values or the number of optimization sequences. The structure of the optimization loop is shown in the following Figure 5.

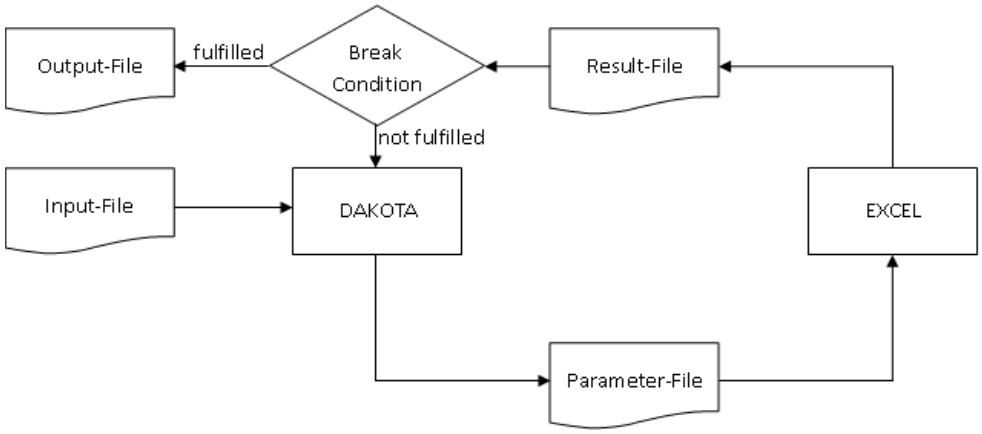

Figure 5: Optimization loop

For the optimization of the cylinders a multi-objective genetic algorithm is chosen which provides the opportunity of the optimization of two or more objective functions. The user is able to weight the single objective functions before running the optimization. Another reason to use genetic algorithms is their ability for searching reliably for a global optimum [4]. The algorithm copies an evolutionary process in which the first generation of parameters is chosen randomly in the defined parameter space. In the following generations only the "best" parameters that minimize the objective function are allowed to reproduce [3].

2.3. Optimization of high pressure cylinders

Reducing the stress conditions in the structure of high pressure cylinders is the aim of the optimization. Different input parameters like the operating pressure, the geometry of the cylinder or process parameters of autofrettage and shrinking influence the stress conditions. At this point an optimized combination of the autofrettage depth of the inside cylinder, the shrinking diameter and the interference between the two cylinder layers is searched. The inside and outside diameter of the cylinder and the material properties are supposed to be constant.

Parameter analysis can help to find a reasonable parameter space of the single input parameters defined by a lower and upper limit for the values. The optimization algorithm is performed for 20000 sequences to optimize the tangential stress at the inside bore of the inside and outside cylinder of two different versions of high pressure cylinders. By plotting the stress values of the initial situation the district of the optimized result points can be identified. The comparison of the two objective functions of version 1 is shown in Figure 6.

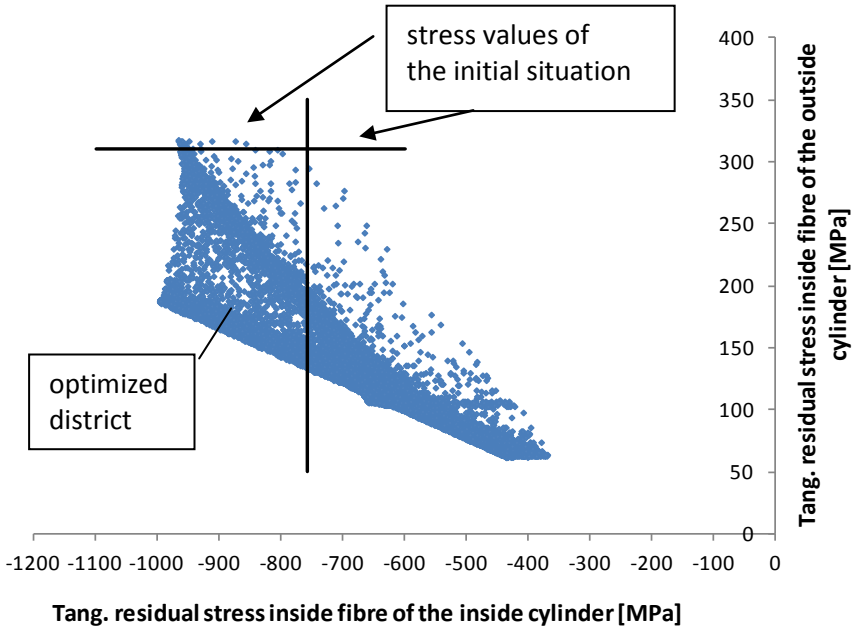

Figure 6: Results of the optimization of an autofrettaged layered cylinder version 1

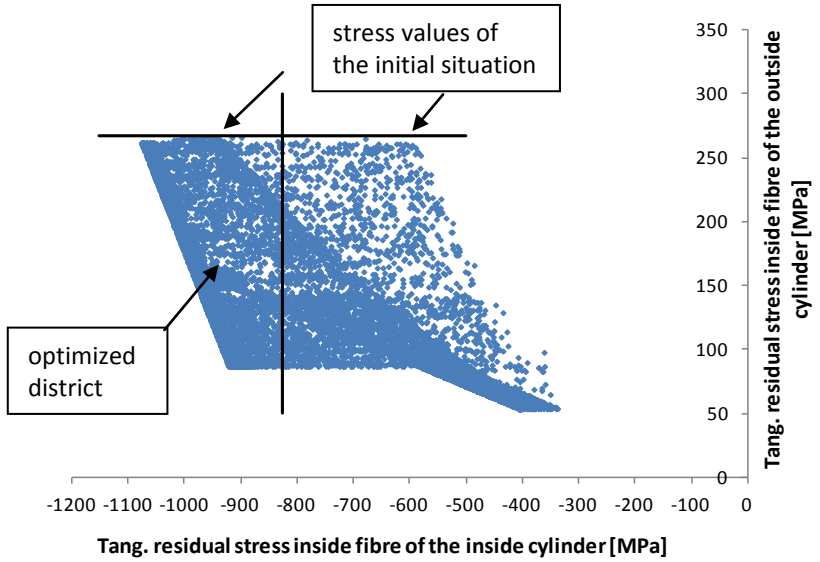

Figure 7: Results of the optimization of an autofrettaged layered cylinder version 2

Version 1 of the cylinder is designed for a lower operating pressure than version 2 and has according to this a lower wall thickness. The results after 20000 optimization sequences of version 2 designed for a higher operating pressure and wall thickness is shown in Figure 7.

By interpreting the results an optimized combination of the varied input parameters can be found. The optimized values were edited to the output-file that is created by DAKOTA®.

The combination of optimized input parameters under consideration of the defined parameter space for the two different versions is listed in table 1.

Table 1

Optimized input parameters and stress values of the objective functions

cylinders	input parameters	objective functions	
version 1	autofrettage depth inside cylinder	tang. stress inside fibre of the inside cylinder	-425 MPa
	shrinking diameter		
	interference of the cylinder layers	tang. stress inside fibre of the outside cylinder	538 MPa
version 2	autofrettage depth inside cylinder	tang. stress inside fibre of the inside cylinder	-213 MPa
	shrinking diameter		
	interference of the cylinder layers	tang. stress inside fibre of the outside cylinder	377 MPa

2.4. Compare of analytically and numerically investigated stress

For the final design of the high pressure cylinders a finite element analysis is used to detemine the stress conditions and investigate the best geometry. By comparing the results of the numerically and analytically investigated stress conditions differences are detectable. The numerically calculated compression stress in the inside cylinder is higher than the analytically calculated stress. In the outside cylinder the numerically calculated tensile stress is higher than the numerically calculated stress conditions. At the outside section of the two layers and the inside section of the outside cylinder the results deviate from each other on a lower level than in the structure. The highest deviance exists at the inside section of the inside cylinder and the transition of the plastic and elastic part of the wall. One reason for the deviation is the approval of a linear elastic material behaviour during the analytically calculation. The finite element analysis is based on an elastic plastic constitutive equation. Furthermore the analytically calculation does not consider the variation of the geometry that exists after the manufacturing process. For the design of the cylinders the analytically calculation shows conservative results for the stress conditions in the inside cylinder [5].

3. Summary

By developing automated analytic calculation sequences it is possible to determine the stress conditions in the analyzed components in a very short time. The process of finding a preliminary design of the components is accelerated and initial data for a following finite element analysis can be generated. Furthermore it is possible to couple the automated tool with an optimization software to investigate the best combination of the input parameters and minimize the stress conditions at the critical points for damage. Thereby the durability can be increased and the damage can be decreased just by varying geometrical and process parameters without changing the material or the inside and outside geometry of the components. Due to the optimization of two objective functions the chosen optimizer could help to consider a goal conflict. The conflict appears if the improvement of one objective function induces the degradation of the second function which was the case in this work. By weighting the objective functions before running the optimization sequences an optimized result under consideration of the improvement of both functions compared with the initial situation was figured out.

References

[1] Buchter, H. H.: Apparate und Armaturen der Chemischen Hochdrucktechnik. Konstruktion, Berechnung und Herstellung. Springer-Verlag, Berlin–Heidelberg–New York, 1967.

[2] ASME: Boiler and Pressure Vessel Code. Section 8, Division 3, 2013.

[3] Sandia National Laboratories: DAKOTA User's Manual, Version 5.3.1, Livermore, CA, 2013.

[4] Schumacher, A.: Optimierung mechanischer Strukturen. Grundlagen und industrielle Anwendung. 2. Auflage, Springer-Verlag, Berlin–Heidelberg, 2013.

[5] Müther, A.: Entwicklung einer Auslegungs- und Optimierungsmethode für Hochdruckbauteile. Diplomarbeit. Montanuniversität, Leoben, 2014.

Design of Machines and Structures, Vol. 4, No. 1 (2014), pp. 45–49.

KINEMATIC TEST OF MECHANISMS

[1]MÁRIA NÁNDORI-TÓTH–[2]BÉLA KOVÁCS
[1]Associated professor, Department of Descriptive Geometry,
Faculty of Mechanical Engineering and Informatics, University of Miskolc
3515 Miskolc-Egyetemváros, e-mail: nnetm@abrg.uni-miskolc.hu
[2]Associated professor, Department of Analysis,
Faculty of Mechanical Engineering and Informatics, University of Miskolc
3515 Miskolc-Egyetemváros, e-mail: matmn@uni-miskolc.hu

In this paper, some single and multiple mechanisms having pivots and slides in the plain are analyzed. It has been demonstrated that using a computer program we can describe trajectories and velocity curves of any point of the mechanism, which are suitable for further investigations.

1. Introduction

One of the basic tasks of designing mechanisms is description of the actual position of a mechanism link with the help of driving parameters (displacement of the driven link and/or angle of rotation). Another basic task – the inverse kinematic one – is the opposite of the above, i.e. determination of possible values of the driving parameters (displacement and angle of rotation) for the given position of a point of the mechanism. The latter task has been reported on at the 27th Seminar of Machine Designers and Product Developers [6]. In this paper, some results from the background of this work will be presented, i.e. computer program related to the first task.

2. Basic terms related to mechanisms

Mechanisms contain kinematic chains [1], while these chains consist of links and joints. Links are rigid bodies. They are denoted by straight lines which connect joints on them. For example, if the links are connected by two joints, they are denoted by a straight line, if by three joints, they are denoted by a triangle. A joint can be a pivot, which allows for rotation of the connected links against each other around the pivot axis; or it can be a slide, which allows for displacement (slip) along the given line. Depending on the number of links, there are single-linked, double-linked, triple-linked, etc. kinematic chains.

3. The analytical method

The test of motion of mechanisms consisting of links connected by pivots and slides is carried out knowing some initial parameters. In the case of mechanism with one degree of freedom, the motion of the driven link is described as function of time t or of a geometric parameter proportional to time. The motion of the mechanism is studied in the

$$t_1 \le t \le t_2$$

range.

By equidistant division of the above range, the actual position and velocity are determined at discrete time instances. The test precision can be increased by decreasing the scale division, i.e. by dividing the above range into more sections.

The positions of other links of the mechanism are determined for the position of the driven link at a given time instance. Knowing the two successive positions, the vector of displacement of an arbitrary point can be determined, out of which the average velocity can also be calculated. The instantaneous center curve and velocity curve are drawn in a similar way.

The determination of trajectory and instantaneous center curve leads towards elementary geometric constructions [2], [3]. The cross-points of circle and circle, circle and line, line and line should be determined; in other words, the desired points are determined by the ruler-and-compass construction. If the geometric task has several solutions, then, in order to determine the mechanism position for the given displacement of the driven link, further testing is required. It should be taken into consideration that the mechanism cannot be disassembled. For this reason, when determining a new position the previous state should be taken into account and a close to that solution should be chosen; if required, the scale division should be decreased.

In the case of mechanisms with several degrees of freedom the law of motion of all the driven links should be given.

Three-dimensional cases have also been considered, specifically, those pivot and slide mechanisms whose first kinematic chain consists of three links and its second and third joints must move within a plane. Other two-linked kinematic chains may connect to this. The importance of studying such type of mechanisms is discussed in [4].

4. The computer program

In order to carry out the above calculations and drawings, computer programs in **FORTRAN** and **C** programming languages were developed. In the former case the type of driving should be given as Function segments. The **FK(I)** segment gives displacement of the driven link in the case of rotation, while the **FE(I)** segment gives that in the case of linear motion; in our case in the

$$\boldsymbol{1} \leq \boldsymbol{I} \leq 50$$

range. In the case of mechanisms with two degrees of freedom, the motion of the other driven link is determined by segments **FK2 (I)** and **FE2 (I)**.

If interruption occurs when drawing the instantaneous center curve, and in case the curve falls outside the drawing area, the drawing is interrupted and resumed at the next point. Naturally, the scaling is set so that the whole mechanism fall within the diagram, only the points of the instantaneous center curve being too far from the mechanism are not drawn in order to facilitate evaluation of the diagram.

The program in **C** language creates data files, based on which the **KEYCREATOR** 3D mechanical design system carries out drawing. The ***mech0.cdl*** file in **CADL** programming language draws the mechanism using the ***mech1.dat*** and the ***mech2.dat*** data files. It denotes the tested points and their trajectories as well as draws the instantaneous center curve of bars containing those points, and creates a separate velocity curve.

This way one has numerical data and diagrams for an easier further analysis of the mechanism.

5. Example

Chosen different points of a triple-linked mechanism, the program draws trajectory of the point and, in another figure, its velocity curve or the hodograph. In this example, the instantaneous center curve is not denoted. Figures 1–4 present the analysis of two different points of the given mechanism. In the first case, the motion of the endpoint of a bar is studied (Figures 1–2); in the second case (Figures 3–4) the center of the bar connected to another bar is chosen.

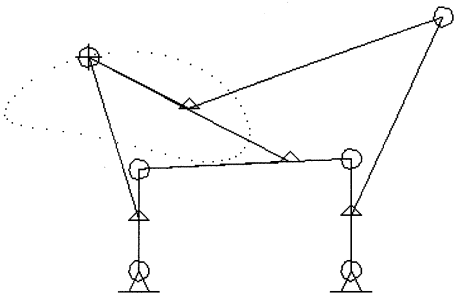

Figure 1: Trajectory of a point of the mechanism

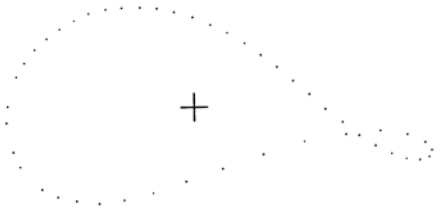

Figure 2: Velocity curve of a point of the mechanism

The pivots are denoted by empty circles. The joint between intermediate point of the bar and a pivot is denoted by triangles. The velocity curve of the given point is shown next to the mechanism. A plus sign shows the point whose trajectory is calculated and positions corresponding to the discrete displacement of the driven link are denoted. The distance measured between the positions shows the value of velocity. The farther the two successive positions are from each other, the higher is the velocity of the point. The velocity curve shows the variation of velocity more illustratively.

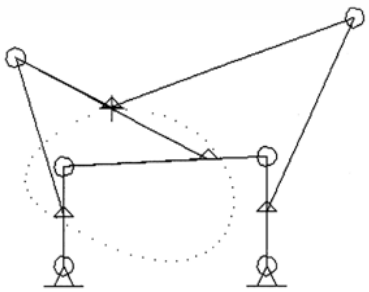

Figure 3: Trajectory of another point of the mechanism

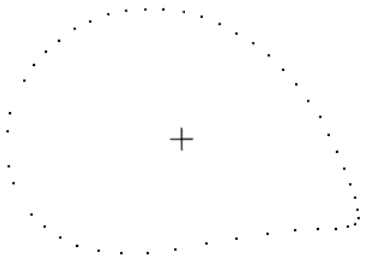

Figure 4: Velocity curve of another point of the mechanism

6. The inverse kinematic task

The other task is to determine possible values of the driving parameters (displacement and angle of rotation) for the given position of a point of the mechanism, for example, by methods of algebraic geometry. Such a task was solved in [5, 6] for open chained mechanisms, in other words, robots (Figure 5).

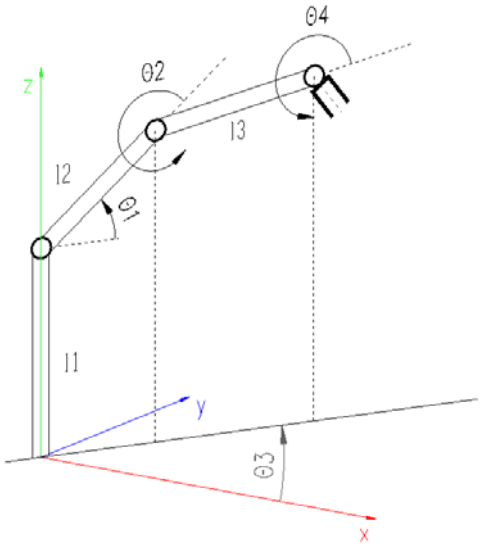

Figure 5: Spatial location of the robot [5]

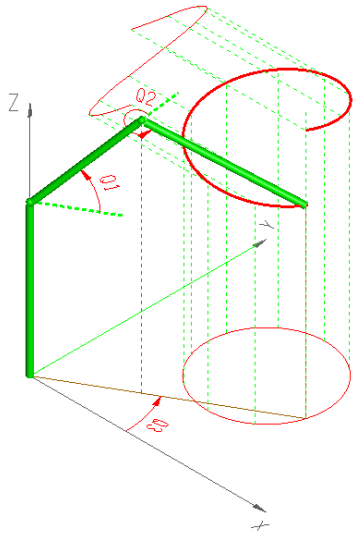

Figure 6: Structure moving along trajectory prescribed by its endpoint [5]

In the following task, the motion of the robot along a specific trajectory was studied; the calculations were performed with the help of MAPLE16 software, while the actual positions were drawn by KEYCREATOR software (Figure 6, 7).

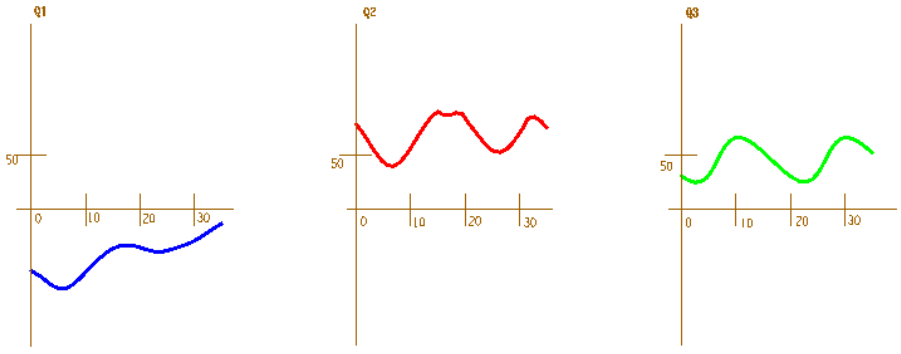

Figure 7: The variation of the angles of structure

7. Summary

A computer program has been developed for the case of planar pivot and slide mechanisms, which is suitable for the determination of position and velocity state on the basis of kinematic analysis of the law of motion of the driven link. More specifically, the program determines the position of an arbitrary point, that of the instantaneous center of velocity of an arbitrary link and then draws trajectories, instantaneous center curves and velocity curves as function of a geometric parameter proportional to time. In the case of rotation, the program examines whether the driven link is rotatable or not.

Another program solves the opposite task, i.e. determines the driving parameters of motion along a pre-defined trajectory.

References

[1] Ifj. Sályi I.: Mechanizmusok. Tankönyvkiadó, Budapest, 1975.
[2] Nándoriné Tóth M.*:* Síkbeli mechanizmusok kinematikai analízise. Borsodi Műszaki Hetek, 1982. jún. 4.
[3] Nándoriné Tóth M.: Síkbeli csuklós mechanizmusok kinematikai analízise. Gépszerkezettani Akadémiai Bizottság Mechanizmusok Munkabizottságának ülése, 1982. november 25.
[4] Kozák I.né: Egyszabadságfokú térbeli mechanizmus sebességállapotának vizsgálata geometriai úton. NME Közleményei, X. Kötet, 1964, pp. 235–242.
[5] Kovács B., Nándoriné Tóth M.: *Robotok inverz feladatának megoldása*, Géptervezők és termékfejlesztők XXVII. szemináriuma, Gép, LXII. évf., 2011/7–8., pp. 79–82.
[6] Nándoriné Tóth M.–Kovács B.: Mechanizmusok kinematikai vizsgálata. Multidiszciplináris tudományok: a Miskolci Egyetem Közleménye, 2013, 3:(1) pp. 21–26.

Design of Machines and Structures, Vol. 4, No. 1 (2014), pp. 51–56.

DESIGNING THE NEW LOCAL DEFECT DIGITAL FILTER FOR THE SURFACE ROUGHNESS MEASUREMENT SYSTEMS

[1]VALERY POROSHIN–[2]DMITRY BOGOMOLOV
Moscow State Industrial University of, Science Department
115280, Avtozavodskaya st. 16, Moscow, Russia
+7(916) 507 50 98
[1]vporoshin@mail.ru; [2] bogom-ov@mail.ru

Paper describes the new adaptive digital filtration algorithm for removing the local defects on the measured surface roughness profiles. The benefits of the proposed filtration algorithm in comparison with traditional Gaussian filter are shown.

1. Introduction

Surface geometry analysis is widely used in modern mechanical engineering and design for the assessment of the operational characteristics of the machine components and structures such as wear resistance, contact stiffness, corrosion resistance, impermeability etc. When analyzing the surface layer processes, which is comparative to initial surface roughness, it is strictly necessary to understand the processes of asperity forming, strengthening, and interacting taking into account all the complex surface geometry.

One of the major problems that arise during the surface geometry analysis is the separation of roughness, waviness and form from the measured surface profile [1]. The urgent need of reliable separation procedure is caused by the overlapped ranges of modern surface geometry measuring devices. For example, typical stylus profilometer is capable of measuring surface roughness, waviness and form, modern roundness machines are capable of measuring both surface form and waviness.

The Gaussian digital filter is the most common and recommended by international and many national surface geometry standards include ISO 11562:1996. High-pass Gaussian filter is used for the separation of surface roughness. Low pass Gaussian filter is used for the separation of surface waviness. But it has several well-known disadvantages.

First of all Gaussian filter produces significant surface distortion near the surface profile begin and end (boundary effects). For the boundary effect compensation the significant portions of the surface profile (about half of surface roughness base length) should be eliminated from analysis after the Gaussian filtration.

The second well known disadvantage of Gaussian filter is inability to filter relatively large surface form effects (for example surface cylindricity). That is why the additional form filters should be used in combination with Gaussian filter.

The third well known disadvantage is the poor efficiency dealing with local defects on the surface profile. For example the single surface scratch does not reflect the common surface characteristics. But it's significant relic still remains in the surface profile after Gaussian filtering.

The Gaussian regression filter allows to minimize first two disadvantages [2]. Well known double filtration method [3] do not remove local defect and only corrects the mean line position. Morphological filters [4] can deal with local anomalies on the measured

surface profile. But they are very complicated and slow and can hardly be used in built-in electronic modules.

Present article introduces the new digital filtration algorithm for removing the local defects on the measured surface profiles. The benefits of the proposed filtration algorithm in comparison with traditional Gaussian filter are shown. The proposed digital filter can be easily combined with Gaussian filter for removing both local defects and surface waviness.

2. Filtration algorithm

The proposed new algorithm for filtration of the local defects on the measured surface profile has two adjustable parameters shown in Figure 1. First adjustable parameter is the filter sensitivity *Ara* to the *Ra* surface roughness parameter (arithmetically average profile roughness height within the base length). Filter recognizes the local defect if it produces the local *Ra* deviation exceeding the *Ara* value. The valid *Ara* values are 1.5 and more. Second adjustable parameter is the filter sensitivity *Asm* to the *Rsm* surface roughness parameter (arithmetically average horizontal profile roughness step within the base length). According to *Asm* value the critical local defect width is specified. The valid *Asm* values are 0.5 and less.

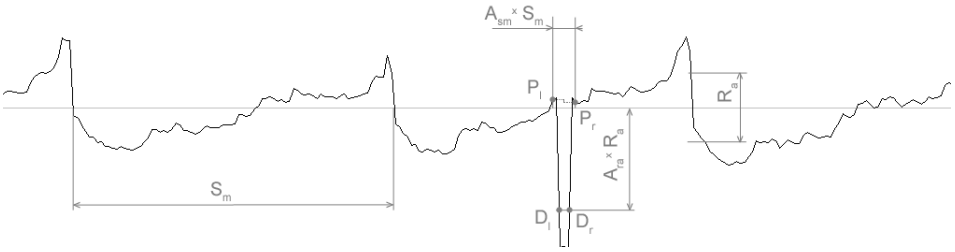

Figure 1: Profile parameters involved in the local defect filtering algorithm

Filtration algorithm includes four main steps. The first step of algorithm is the local defect detection. The line for detecting the local defects is constructed according to local *Ra* parameter value and *Ara* value specified. The Y_i profile nodes are marked belonging to the local defect if:

$$|Y_i| \geq A_{ra} \cdot R_a . \tag{1}$$

The second step of algorithm is the local defect boundary definition. The boundary nodes of local defect D_l and D_r are determined on this algorithm step. The third step of the algorithm is the profile smoothing zone definition. At this step the boundary nodes of the profile smoothing zone are determined according to following procedure:

$$P_l = D_l - N_{ld}\,, \quad P_r = D_r + N_{ld}\,, \quad N_{ld} = \frac{1}{2}\left(A_{sm} \cdot S_m - \left(D_r - D_l\right)\right). \tag{2}$$

The last fourth step of algorithm is the profile smoothing. At this step the measured profile values in the determined profile smoothing zone $(P_l ; P_r)$ are substituted by the

smooth linear distribution values. The smooth line is drawing from the left boundary node Y_{P_l} to the right boundary node Y_{P_r} of the removed local defect.

3. Analysis of the filter capabilities

Two different surface roughness profiles were used to investigate the main advantages of the proposed local defect filter. The first is profile is a simulated surface roughness profile which is combined of 5equal size half-ellipsoid roughness elements (Figure 2). The second profile is the real technological surface roughness profile for the surface after polishing (Figure 3).

The single local scratch of significant height and very small width was added to the source surface roughness profiles as shown in Figure 2. b), Figure 3. b). This local defect significantly changes the resulting values of the roughness parameters as shown in Table 1 and Table 2. For example the Ra parameter value was changed by 2.6% for smooth simulated profile and by 12.7% for polished profile. An extremal surface roughness parameter Rmax was changed even more significantly. It's value was changed by 74% for simulated surface profile and 103% for polished surface profile.

Table 1

Comparison of Gaussian filter and Local defect filter for ellipsoid profile

Roughness parameter	**Parameter value**				
	Source profile	**Local defect added**	**Difference from source profile**	**Local defect-filtered**	**Difference from source profile**
	Without gauss filtering				
Ra (um)	0.8057	0.8263	2.56%	0.8057	0
Rmax (um)	2.0000	3.4876	74.4%	2.0000	0
	Combined with gauss filtering				
Ra (um)	0.8018	0.8222	2.54%	0.8017	0,01%
Rmax (um)	1.996	2.6332	31.92%	1.996	0

Table 2

Comparison of Gaussian filter and Local defect filter for polished profile

Roughness parameter	**Parameter value**				
	Source profile	**Local defect added**	**Difference from source profile**	**Local defect-filtered**	**Difference from source profile**
	Without gauss filtering				
Ra (um)	0.1288	0.1452	12.73%	0.1285	0.23%
Rmax (um)	0.9187	1.8640	102.9%	0.9187	0
	Combined with gauss filtering				
Ra (um)	0.1242	0.1352	8,86%	0.1239	0.24%
Rmax (um)	0.9040	1.8030	99,45%	0.9040	0

Only part of local defect was removed after implying the traditional Gaussian filter and the significant trail of the scratch remained as shown in Figure 2. c) and Figure 3. c). Roughness parameter Ra still changed by 2.5% and 8.9% respectively. Roughness parameter Rmax changed by 31.9% and 99.5% respectively. Local defect was almost fully removed by implying the proposed local defect filter as shown in Figure 2. d) and Figure 3. d).

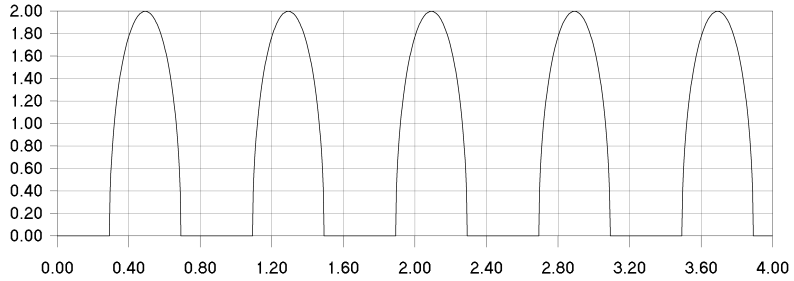

a) source profile

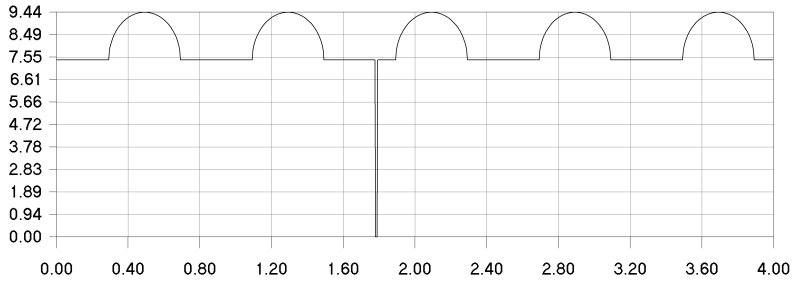

b) single scratch on source profile

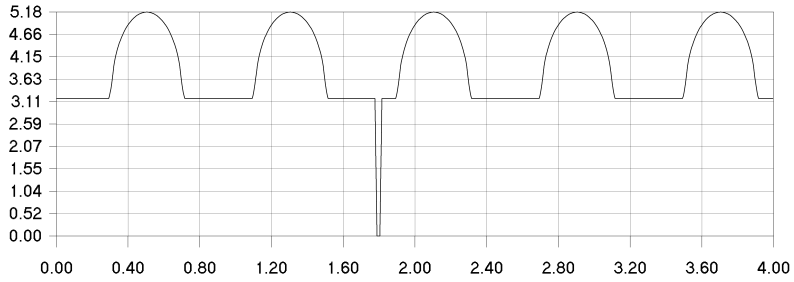

c) local defect remnants after Gaussian filtering

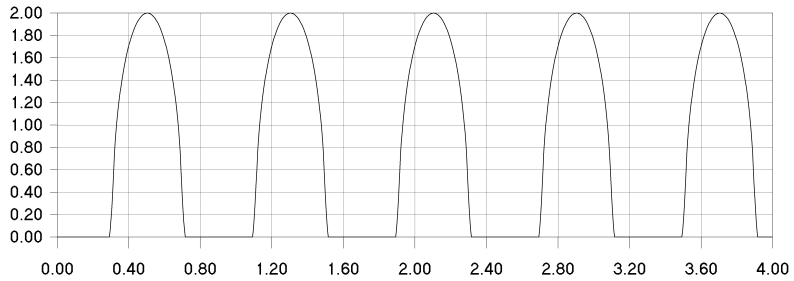

d) local defect removed by proposed filter

Figure 2: Filtration of single scratch on ellipsoid surface

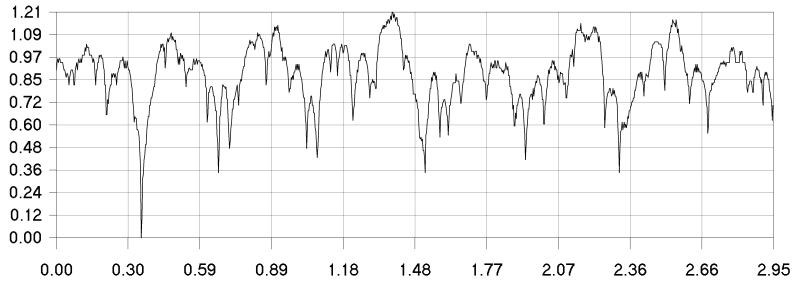

a) source profile

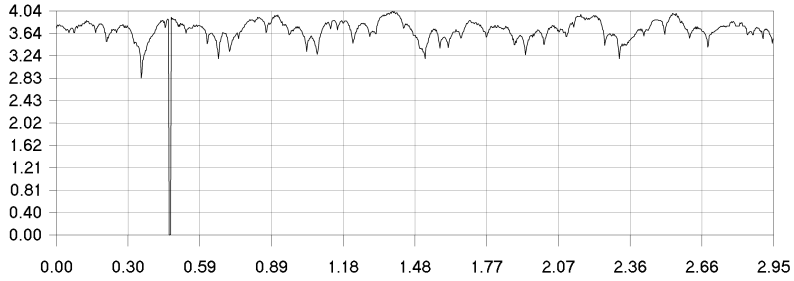

b) single scratch on source profile

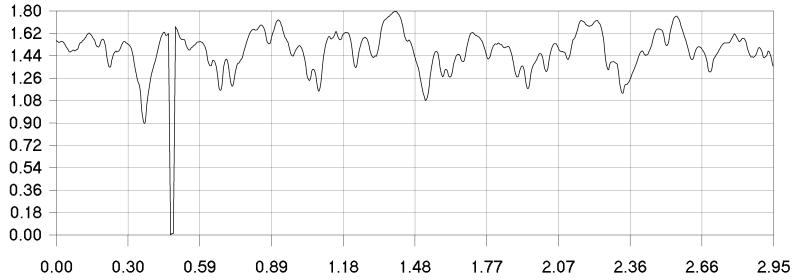

c) local defect remnants after Gaussian filtering

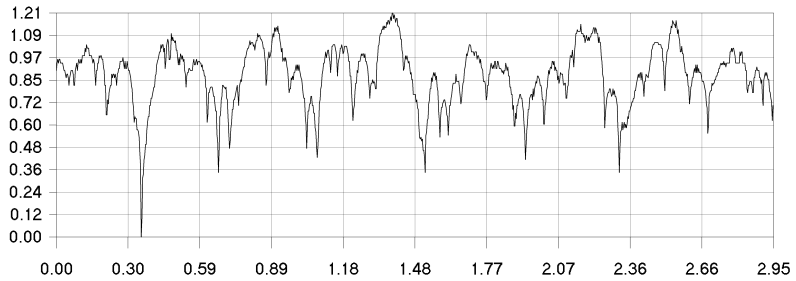

d) local defect removed by proposed filter

Figure 3: Filtration of single scratch on polished surface

4. Conclusion

Proposed digital filter has the advantage over the traditional digital Gaussian filter in processing surface profiles having local defects that does not characterize the surface roughness geometry. But the implementation of local defect filter does not discard the necessity of using Gaussian filter. The Gaussian filter is still needed for removing some surface slope and nano-roughness effects. The proposed filter should be used in combination with traditional Gaussian filter. Combination of the proposed digital filter with Gaussian filter can ensure the adequacy of the resulting surface roughness parameters.

Acknowledgement

The research was performed with the financial support of the Ministry of Education and Science of the Russian Federation for higher education institutions within the basic part of the state job service (Project 2080).

References

[1] Whitehouse, D. J.: Handbook of surface metrology. Institute of Physics Pub., 1994, p. 988.
[2] Muralikrishnan, B.–Raja, J.: Computational Surface and Roundness Metrology. London: Springer. 2009, p. 263.
[3] International Organization for Standardization, ISO 13565:1996. Geometrical Product Specification (GPS) – Surface texture: Profile method; Surfaces having stratified functional properties.
[4] International Organization for Standardization, ISO/TS 16610-40:2006. Geometrical Product Specifications (GPS), Filtration, Part 40: Morphological Profile Filters: Basic Concepts, ISO, Geneva, Switzerland.

Design of Machines and Structures, Vol. 4, No. 1 (2014), pp. 57–64.

ANALYSIS OF GEAR-DRIVES AND SEARCHING OF NOISE REDUCTION POSSIBILITIES WITH THE HELP OF GRAPHS

FERENC SARKA–ÁDÁM DÖBRÖCZÖNI
University of Miskolc, Institute of Machine and Product Design
3515, Miskolc-Egyetemváros
machsf@uni-miskolc.hu, machda@uni-miskolc.hu

This paper shows a new approach of gear-drive analysis. The aim of the new approach is that through the description of gear-drives with graphs ensuring an opportunity for parts and machine elements having new properties. The reason for creating parts with new properties is to reduce noise in gear-drives.

1. Introduction

Gear-drives are often used in industry, to make connection between the engine and the machine. Because using them widely, extensive researches were made in the past as in abroad and in Hungary too. In the 18th century the noise is generated by coupling of gears was discovered, but researchers seriously dealing with this problem only in the past 30 years. Load-bearing ability, which is used to be considered as a primary aspect, has been overshadowed by the acoustic attitude and the low noise emission in the designing process of wheel-gears. The significance of strength as an inevitable condition has still not been reduced.

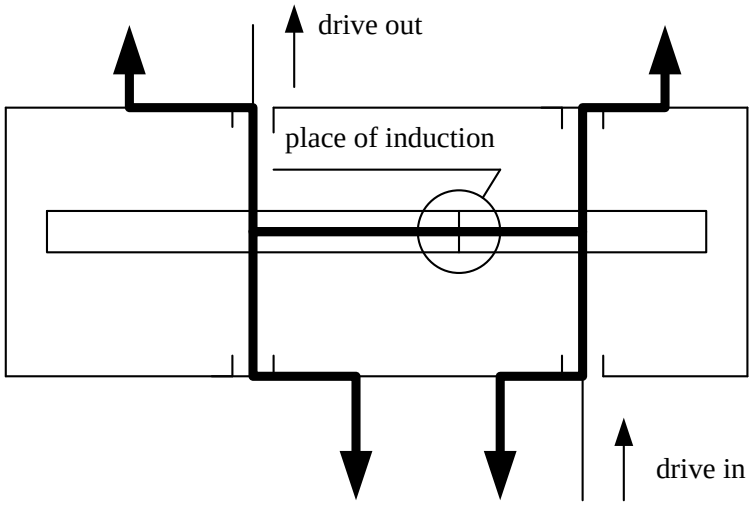

Figure 1: Scheme of single speed gear-box, with primary transmission routes [5]

This paper presents a theoretical method, which introduces how to find opportunities to reduce the noise in gear-drives.

Figure 1 shows the sketch of a one speed gear-drive. In the Figure the main vibration transmission route can be seen with black arrows, which is called *primary transmission route*. The vibration gets from the place of induction to the environment on this route.

2. Transformation of the gear-drive to a graph

With the help of the graph theory an important field of the mathematics the single speed gear-drive, which is shown in Figure 1, can be described shove off from the conventional engineering approach. Handling gear-drive as a graph can help creating new constructional recommendations or parts with new or modified properties. The parts of the drive corresponds to the nodes of the graph, the acoustical connection between the parts corresponds to the edges of the graph. With this kind of correspondence the acoustical behaviour of the gear-drive can be defined as a graph (Figure 2).

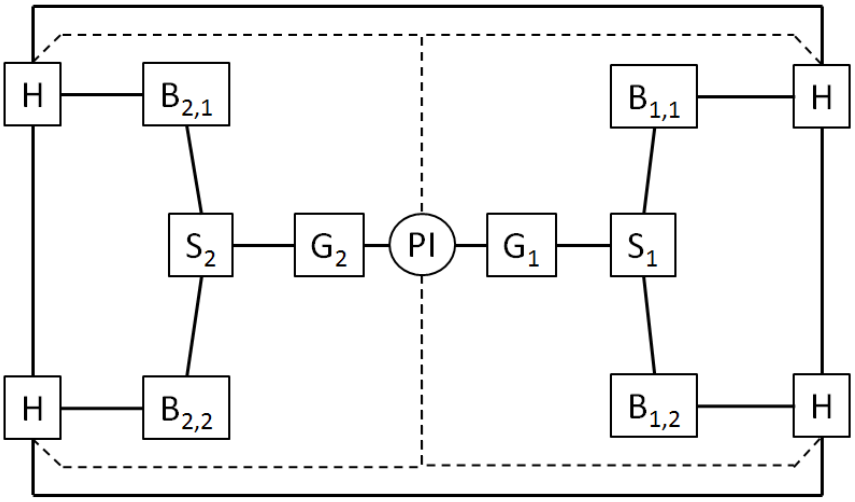

Figure 2: Acoustical connection graph of a single speed gear-drive

The meaning of the signs used in Figure 2:

- G_1: drive gear,
- G_2: driven gear
- S_1: drive shaft,
- S_2: driven shaft,
- $B_{1,1}$; $B_{1,2}$: bearings of the drive shaft,
- $B_{2,1}$; $B_{2,2}$: bearings of the driven shaft,
- H: house,
- PI: the place of induction.

Dashed line in Figure 1 demonstrates the secondary transmission route of the gear-drive. The secondary transmission route is irrelevant on the basis of the practice [3]. The secondary transmission route does not appear in the further discussion. The name of the created graph should be the acoustical connection graph (Figure 2).

3. Describe the graph with matrix

Graphs can be described with the help of matrixes. With the matrix of the acoustical behaviour of a gear-drive the connection between the parts of the drive can be shown with the proper value of logical connection functions. The connection function ($f_{i,i}$) has two values. If the connection is exist the value is 1, if the connection does not exist, the value of the connection function is 0.

A=

	F_1	F_2	…	F_{n-1}	F_n
F_1		$f_{1,2}$	…	$f_{1,n-1}$	$f_{1,n}$
F_2	$f_{2,1}$		…	$f_{2,n-1}$	$f_{2,n}$
…	..	…		…	…
F_{n-1}	$f_{n-1,1}$	$f_{n-1,2}$	…		$f_{n-1,n}$
F_n	$f_{n,1}$	$f_{n,2}$	…	$f_{n,n-1}$	

Figure 3: The acoustical connection matrix of a gear drive in common form

The basis of the creation of the matrix **A** is Figure 2. This figure shows the part of the gear drive and the connection functions between them. F_n means the parts of the gear-drive. All of them embody a sort of function too. It can be registered into the proper places of the matrix if there is, or there is no connection between the parts of the gear-drive. This way defined matrix, should be the acoustical connection matrix (**A**) (Figure 4).

A=

	H	G_1	S_1	$B_{1,1}$	$B_{1,2}$	G_2	S_2	$B_{2,1}$	$B_{2,2}$
H	0	0	0	1	1	0	0	1	1
G_1	0	0	1	0	0	1	0	0	0
S_1	0	1	0	1	1	0	0	0	0
$B_{1,1}$	1	0	1	0	0	0	0	0	0
$B_{,2}$	1	0	1	0	0	0	0	0	0
G_2	0	1	0	0	0	0	1	0	0
S_2	0	0	0	0	0	1	0	1	1
$B_{2,1}$	1	0	0	0	0	0	1	0	0
$B_{2,2}$	1	0	0	0	0	0	1	0	0

Figure 4: The acoustical connection matrix of a single speed gear-drive with helical gears

4. Description of a graph with formula

On the basis of the acoustical connection graph, gear-drives can be described by formulas introducing a new notation. Establishing the formula is implemented by alphanumeric characters and connection signs. This has to be conformist with the acoustical connection graph and the acoustical connection matrix. Observing the acoustical connection graph there are parts that are parallel and there are parts with lined up connection. The sign

of the parallel connection is //. The sign of the lined up connection is. The sign of graph segment: ( ). The acoustical spreading formula can be created after giving the creation rules (1).

$$[(H\text{-}B_{2,2})//(H\text{-}B_{2,1})]\text{-}S_2\text{-}G_2\text{-}G_1\text{-}S_1\text{-}[(B_{1,1}\text{-}H)//(B_{1,2}\text{-}H)] \quad (1)$$

5. Create a modified graph, described with matrix and formula

On the basis of literature dealing with the acoustical behaviour of gear-drives it is declared that the most effective constructional modification place of the gear-drives is to reduce the emitted noise between the source and emission in the primary transmission route. The statement above can be built into the acoustical connection matrix of the acoustical connection graph of a gear-drive introduced in Figure 2. To reduce the emitted noise of the gear-drive such a connection has to be created between each part, which prevents the spread of the vibration and has a good vibration absorbing properties.

The acoustical connection matrix has to be supplemented with new columns and rows. The new supplementation contains the parts between the original parts of the drive. New parts symbolize the obstacle of the vibration spreading. I_i (Isolator) is the sign of a new part. In this case the acoustical connection graph of the drive looks like the one in Figure 5. Uniting the parts of the modified graph on the basis of function merging principle new and acoustically better machine elements can be created. In this case the new property of the part is the vibration isolation. Of course new property not only the vibration isolation can be. In Figure 5 circles show examples for the function merging principle.

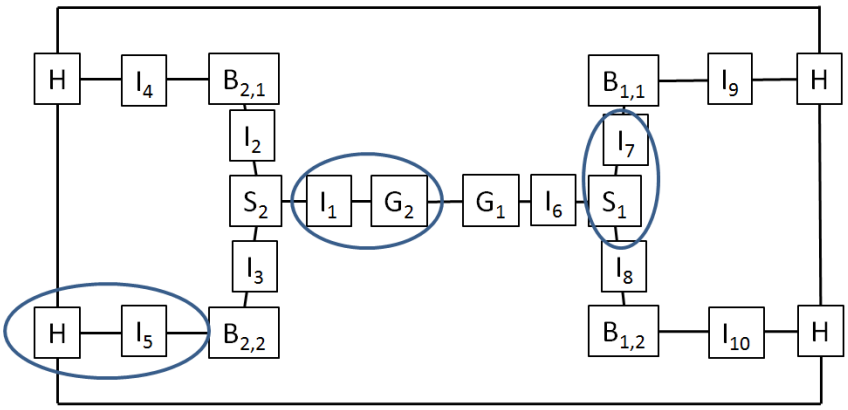

Figure 5: The supplemented acoustical connection graph of the gear-drive, supplemented by vibration isolator parts

Sorting by type the parts of the gear-drive is another way to create the **A** matrix of the graph shown in Figure 5. Gears, shafts, bearings are side by side. With this type of matrix creation can be generated the acoustical connection matrix **A** of Figure 6.

A=

	H	G_1	G_2	S_1	S_2	$B_{1,1}$	$B_{1,2}$	$B_{2,1}$	$B_{2,2}$
H	0	0	0	0	0	1	1	1	1
G_1	0	0	1	1	0	0	0	0	0
G_2	0	1	0	0	1	0	0	0	0
S_1	0	1	0	0	0	1	1	0	0
S_2	0	0	1	0	0	0	0	1	1
$B_{1,1}$	1	0	0	1	0	0	0	0	0
$B_{1,2}$	1	0	0	1	0	0	0	0	0
$B_{2,1}$	1	0	0	0	1	0	0	0	0
$B_{2,2}$	1	0	0	0	1	0	0	0	0

Figure 6: Acoustical connection matrix of a single speed gear-drive operated with helical gears, parts lined up side by side

Supplementing the matrix of Figure 6 with the new parts of Figure 5 a modified acoustical connection matrix of Figure 7 arises. The upper left part of the matrix is the original base matrix (Figure 6), the other three segments of the matrix are the supplementation. If there is connection between the parts of graph in Figure 5 there will be 1 in the matrix of Figure 7. If there is no connection between parts, there will be 0 in the matrix of Figure7. The supplemented acoustical spreading formula can be also created to the modified/supplemented gear-drive (2).

$$\{[(H\text{-}I_5)\text{-}(B_{2,2}\text{-}I_3)]//[(H\text{-}I_4)\text{-}(B_{2,1}\text{-}I_2)]\}\text{-}S_2\text{-}(I_1\text{-}G_2)\text{-}(G_1\text{-}I_6)\text{-}S_1\text{-}\{[(I_7\text{-}B_{1,1})\text{-}(B_9\text{-}H)]//[(I_8\text{-}B_{1,2})\text{-}(I_{10}\text{-}H)]\} \quad (2)$$

With the examination of the upper right or lower left part of the matrix of Figure 7 it is declarable that each ones ("1") in the matrix signs a new machine element with the help of the function merging principle. New constructional recommendations can be given on the basis of supplemented acoustical connection matrix **A'** by selecting a cell, that contains one (Figure 7).

A' =

	H	G_1	G_2	S_1	S_2	$B_{1,1}$	$B_{1,2}$	$B_{2,1}$	$B_{2,2}$	I1	I2	I3	I4	I5	I6	I7	I8	I9	I10
H	0	0	0	0	0	1	1	1	1	0	0	0	1	1	0	0	0	1	1
G_1	0	0	1	1	0	0	0	0	0	0	0	0	0	0	1	0	0	0	0
G_2	0	1	0	0	1	0	0	0	0	1	0	0	0	0	0	0	0	0	0
S_1	0	1	0	0	0	1	1	0	0	0	0	0	0	0	1	1	1	0	0
S_2	0	0	1	0	0	0	0	1	1	1	1	1	0	0	0	0	0	0	0
$B_{1,1}$	1	0	0	1	0	0	0	0	0	0	0	0	0	0	0	1	0	1	0
$B_{1,2}$	1	0	0	1	0	0	0	0	0	0	0	0	0	0	0	0	1	0	1
$B_{2,1}$	1	0	0	0	1	0	0	0	0	0	1	0	1	0	0	0	0	0	0
$B_{2,2}$	1	0	0	0	1	0	0	0	0	0	0	1	0	1	0	0	0	0	0
I1	0	0	1	0	1	0	0	0	0	0	0	0	0	0	0	0	0	0	0
I2	0	0	0	0	1	0	0	1	0	0	0	0	0	0	0	0	0	0	0
I3	0	0	0	0	1	0	0	0	1	0	0	0	0	0	0	0	0	0	0
I4	1	0	0	0	0	0	0	1	0	0	0	0	0	0	0	0	0	0	0
I5	1	0	0	0	0	0	0	0	1	0	0	0	0	0	0	0	0	0	0
I6	0	1	0	1	0	0	0	0	0	0	0	0	0	0	0	0	0	0	0
I7	0	0	0	1	0	1	0	0	0	0	0	0	0	0	0	0	0	0	0
I8	0	0	0	1	0	0	1	0	0	0	0	0	0	0	0	0	0	0	0
I9	1	0	0	0	0	1	0	0	0	0	0	0	0	0	0	0	0	0	0
I10	1	0	0	0	0	0	1	0	0	0	0	0	0	0	0	0	0	0	0

Figure 7: Supplemented acoustical connection matrix of a single speed gear-drive

6. Creating the isomorph version of the acoustical connection graph

Creating the isomorph version of the single speed gear-box shown in Figure 1 described by the acoustical connection graph introduced in Figure 2 and 5 the graph in Figure 8 arises, where the starting point is the place of induction (PI) and the end point is the house (H).

This kind of graph is a directional, circle-free graph. The name of this graph should be isomorph acoustical connection graph. Of course this kind of isomorph graph can be modified by new parts, as shown in the graph of Figure 5 (Figure 8).

The new parts of the graph in Figure 9 may not only be noise reduction parts, but there should be parts with other properties too. The sign of the newly build in parts is I_i again. In this case of graphs there is an opportunity to weight each connection, namely taking account of the proper importance of each connection.

In Figure 8 the starting point of the graph is the PI (place of induction) node, and the end node is the H (House) node. The place of the induction is the coupling/meshing of the gears. In the graph of Figure 8 and Figure 9 there are four different admittance ways to get from the start (PI) to the finish (H).

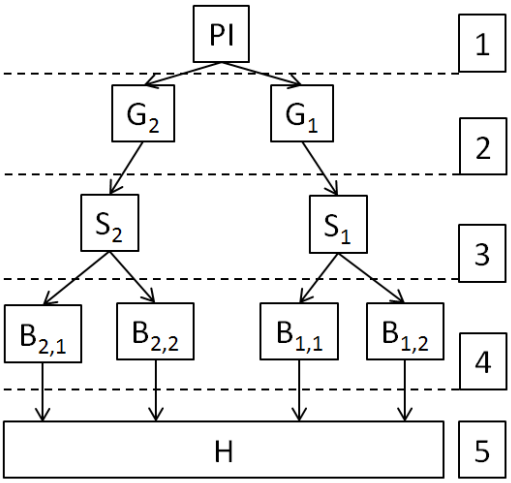

Figure 8: Realigned acoustic connection graph of a single speed gear-drive

The number of the admittance ways of the graph on Figure 8 is the same as the primary transmission routes of the original gear-drive. Multi-level can be distinguished in the graph. The higher level of the graph is examined the closer is the starting point of the graph that is the place of induction.

Results can be reached in noise reduction (adding I_i nodes) in the whole gear-drive only then when the reduction hits every connections of a single level in the isomorph graph. In that case when the modification happens only in the right side admittance way of level 2 several expectations are not realised, because on the left hand side admittance way the

property that should be modified can go through without any changes. It is declarable too, that the modification touches more levels it has more effect to the whole gear-drive.

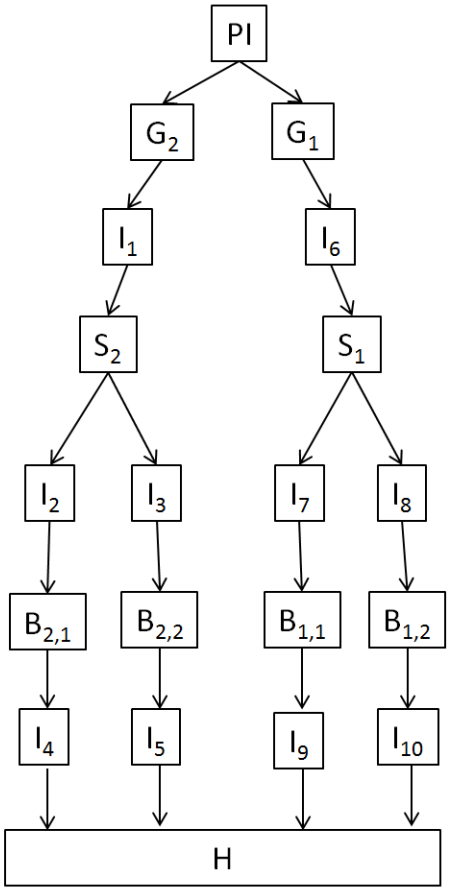

Figure 9: Supplemented realigned acoustic connection graph of a single speed gear-drive

The position of the round brackets in formula (2) can be varied; it depends on which part is the modified one. There is an example of the round brackets translocation in formula (3).

$$\{[H\text{-}(I_5\text{-}B_{2,2})\text{-}I_3]\|[(H\text{-}I_4)\text{-}(B_{2,1}\text{-}I_2)]\}\text{-}S_2\text{-}(I_1\text{-}G_2)\text{-}(G_1\text{-}I_6)\text{-}S_1\text{-}\{[(I_7\text{-}B_{1,1})\text{-}(I_9\text{-}H)\|(I_8\text{-}B_{1,2})\text{-}(I_{10}\text{-}H)]\} \quad (3)$$

The examination method of acoustical connection graph that has a purpose to create parts with new properties can be broaden to other type of gear-drives beyond the single speed gear-drive.

7. Summary

The method that was shown in this paper can gives an opportunity to the designer to reveal new constructional modification that evaluate noise reduction in gear-drives with new properties of the modified parts. Partly giving up traditional mechanical engineering design aspects this is a possibility for modifying gear-drives not only referring to the acoustics.

Acknowledgement

The research work presented in this study based on the results achieved within the TÁMOP-4.2.1.B-10/2/KONV-2010-0001 project and carried out as part of the TÁMOP-4.1.1.C-12/1/KONV-2012-0002 "Cooperation between higher education, research institutes and automotive industry" project in the framework of the New Széchenyi Plan. The realization of this project is supported by the Hungarian Government, by the European Union, and co-financed by the European Social Fund.

References

[1] Åkerblom, M.: Gear Noise and Vibration – A Literature Survey. Trita-MMK, 2001.
[2] Andrásfai B.: Ismerkedés a gráfelmélettel. Tankönyvkiadó, Budapest, 1985.
[3] Dömötör F.: Rezgésdiagnosztika II. kötet. Dunaújvárosi Főiskola Kiadói Hivatala, Dunaújváros, 2010.
[4] Kováts A.: Gépszerkezettan (Műszaki akusztika). Tankönyvkiadó, Budapest. 1988.
[5] Sarka, F.–Döbröczöni, Á.: Directives of Designing Machines with Low Noise Emission. Advanced Engineering, Vol. 5, No. 2, 2011.
[6] Takács Á.: Számítógéppel segített koncepcionális tervezési módszer. PhD-értekezés, Miskolc, 2009.
[7] Åkerblom, M.: Gear Geometry for Reduce and Robust Transmission Error and Gearbox Noise. Trita-MMK, 2008.

Design of Machines and Structures, Vol. 4, No. 1 (2014), pp. 65–75.

USING METAL FOAMS IN GEAR-DRIVES TO REDUCE THE EMMITED NOISE

FERENC SARKA–ÁDÁM DÖBRÖCZÖNI
University of Miskolc, Institute of Machine and Product Design
3515, Miskolc-Egyetemváros
machsf@uni-miskolc.hu, machda@uni-miskolc.hu

This paper shows a new approach of gear body design, with the use of a new generation technological materials, the metal foams. This paper introduces analytically the possibilities of use. The basis of this paper is the paper with the title 'Analysis of gear drives and searching of noise reduction possibilities with the help of graphs'.

1. Introduction

In the literature there are detailed descriptions about important gear body shape modifications that are important in acoustical point of view. The acoustical behaviour of gear can achieve not only by gear profile shape modification, but such changes of the gear body that modifying the emitted noise of the gear.

The generated vibration in coupling of the drive's gears, get to the walls of the drive on the primary transmission route. From this viewpoint the vibration is emitted to the environment as air noise or solid noise. If we can establish barrier against the vibration spreading on this primary transmission route, then we can reach result in environmental view.

Examples to this type of barrier can be found at KOVÁTS [1], respectively in [4] and [10]. With the use and improve of the examples in [1] and the technological development since then, a new construction solution is shown in this paper. Technological development allows the industrial usage of the metallic foams in quantity production [2], [3].

2. About metallic foams

The name metallic foam indicates such a solid metallic material, which has more than 90% porosity (some manufacturer produces 'metal foams' less than 90% porosity). The density of this kind of materials is less by one order of magnitude. Metallic foam has more properties that make its use desirable in engineering. These properties are energy-absorbing, heat conduction, damping, sound-absorbing and filtering abilities. Metallic foams have two types; the open-cell and closed-cell. Most of the cases the material of the metallic foam is aluminium-alloy but metallic foam also can be created from other materials (steel, copper, silver and titan) [2], [3].

Many researches were done to determine physical, chemical and mechanical properties of metallic foams. The properties of the metallic foams depend on the size of the cells, the thickness of the walls (bridges) between the cells and the shape of the cells if the material is the same. With the use of the modified ratio between the solid metal density and the foam metal density, we can determine approximately the foam material properties. The computational equation is the equation (1).

$$\frac{P}{P_0} = k \cdot \left(\frac{\rho}{\rho_0} \right) \tag{1}$$

where,

P: a kind of property,
ρ: density,
0: index for metals, without index 0 is for metal foams,
n, k: can be chosen according to Table 1, parameters from measurements.

Table 1

k and n factors to determine the parameters of metal foams

Property	**k**	**n**
R (Ωm)	1	–1,6 … –1,85
λ (W/mK)	1	1,6 … 1,85
E (GPa)	0,1 … 4	1,8 … 2,2
σ (MPa)	0, … 1,0	1,5 … 2

3. Designing the gear body

Figure 1 shows gear body for general application. In the figure the parts of the gear were signed for the later references.

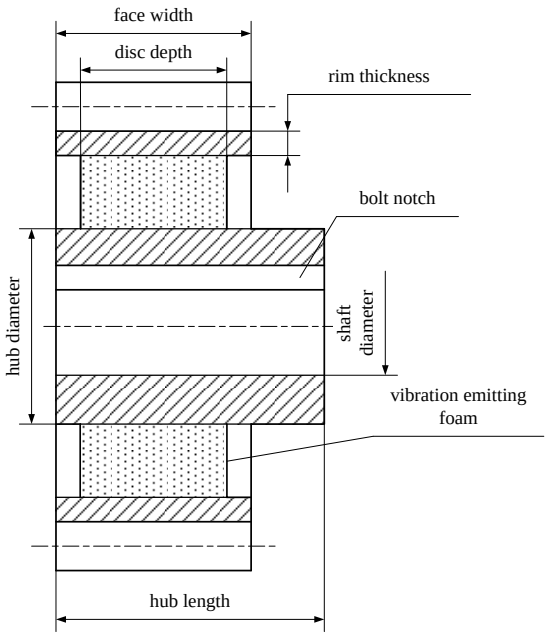

Figure 1: General shape of a gear with denominations

Radial position of the emitting material in the gear body is influenced by two factors. From the teeth of the gear to the direction of the shaft-line the first factor is the rim thickness. According to the strength calculations of gears a modify factor appears labelled with Y_B that takes the size of the gear ring into account. Y_B can be determined according to Figure 2 for external gears.

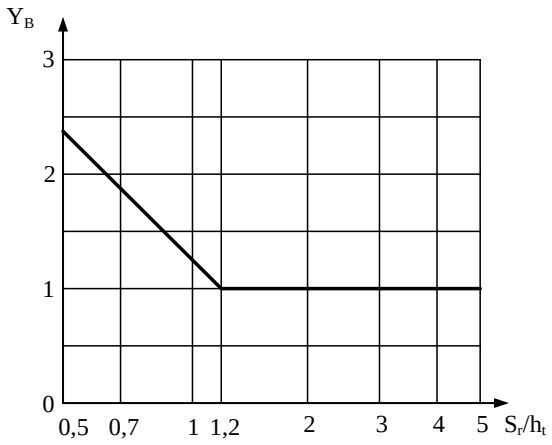

Figure 2: Rim thickness factor

For the determination the ratio between the tooth thickness and the rim thickness is needed. As a function of this ratio the value of Y_B can be chosen. In the diagram it can be very well seen when the ration reaches the value 1.2 Y_B is equal to 1 and has no effect on the root stress. Under the ratio value 1.2 Y_B has increasing effect on the root strength.

It can be determined that for the size of the vibration emitting foam in case of the input (small) gear is quite limited. So if it is possible it is strongly recommended to fill in the whole space between the hub and the rim with the metallic foam.

The lubrication of gear-drives is realised by oil in many cases. As the foam has a percolative structure it should be supervised no oil can get into the cells of the foam. In case of closed cell structure it does not mean a problem, because the surface cells are opened according to the producing. In case of open cell foams those cells that are on the outer surface should be sealed to avoid the oil getting into the gear body.

In case of the output gear a little bit different situation is given. The structure of the output gear is usually the same as the input gear. The only difference is in the radial sizes, because output gears generally have larger sizes. In case of output gear designer has the possibility to determine free the radial size of the emitting foam. As for the recommendations of the foam width a simple mechanical model and calculation is introduced in the following.

4. Mechanical model

The most important task of the vibration emitting foam to stop the vibration is realised during the connection of the gears. The cause of the vibration is the deflection that occurs

under loading the tooth of the gear and later flexion that happens when the tooth quits the connection and unloaded again. As in case of the strength calculation the tooth can be modelled as a one end walled-up rod with constant intersection in this case too. At the end of the rod (top land) the deflecting tangential force is working (Figure 3).

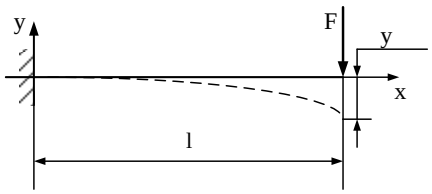

Figure 3: The model of a tooth to calculate the deflection

Deflection can be determined according to Figure 3 and equation (2).

$$y(x = l) = \frac{F \cdot l^3}{3 \cdot I \cdot E} \tag{2}$$

where:

F: deflecting force working at the end of the rod,
l: length of the rod,
I: second moment of the rod,
E: modulus of elasticity of the rod material.

Vibration arises during tooth connection is a damped vibration. As the starter amplitude of this damped vibration displacement counted by the equation (2) can be used. The frequency of the arisen vibration is the connecting vibration that can be determined according to the equation (3) when the number of teeth and revolution is known.

$$f_k = z \cdot \left(\frac{n}{60} \right). \tag{3}$$

Vibration springs while tooth connection moves on the gear body and damps, its amplitude slightly decreases. In case of solid material the decrease of the amplitude is not considerable, because of the relatively low damping factor of the average used steel material. The damping factor of the metal foam that is between the hub and the rim is much higher than the damping factor of the solid metal, so a more significant damping characterises this section. Unfortunately literature is quite reticent due to the damping factor of materials. MAKHULT [5] gives LEHR damping factors and logarithmical decrements for traditional structure materials. Literature [6] gives for damping factor of metal foams about 10 times higher values than for solid metals. On the basis of the literature [3] introduced conversion equation and the vales of the Table 1, an approximate value for the damping factor of the metal foam can be counted. Of course it cannot be forget reliable data can only be derived from measurements. Measuring of damping factors for different materials is not only complicated but expensive as well. It might be the reason for few data for the damping factor of metal foams. If the necessary data of the damped vibration managed to collect equation (1) can be written, and counted that describes the vibration [7]. Nominations of equation (4) are explained by Figure 4.

$$x = A \cdot e^{-\beta \cdot t} \sin(\omega \cdot t + \alpha), \tag{4}$$

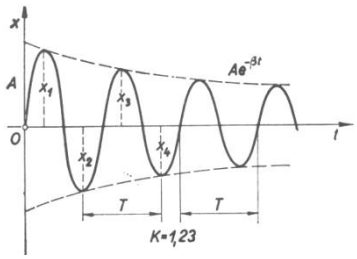

Figure 4: Figure of a damped vibration in case of K = 1.23 damping ratio [7]

where:

A: starting amplitude,
β: damping factor,
e: 2.718 the basic number of natural logarithm,
ω: pulsatance. $\omega = 2 \cdot \pi \cdot f = (2 \cdot \pi)/T$, where, f is the frequency, T is period time,
α: starting phase.

As all parameters are known in equation (4) amplitude belonging to an optional t can be counted. Damping ratio signed by K (5) and its natural basic logarithm, the logarithmical decrement signed by Λ (6) that characterises damping are introduced.

$$K = \frac{x_1}{x_3} = \frac{e^{-\beta t_1}}{e^{-\beta(t_1+T)}} = e^{\beta T}, \tag{5}$$

$$\Lambda = \ln K = \beta T. \tag{6}$$

Knowing the logarithmical decrement and the frequency of the vibration damping factor (8) can be counted, using equation (6):

$$\omega = 2 \cdot \Pi \cdot f = \frac{2 \cdot \Pi}{T}, \tag{7}$$

$$\beta = \frac{\Lambda}{T} = \frac{\Lambda}{\frac{1}{f}} = \Lambda \cdot f. \tag{8}$$

Counting equation (8) the frequency and the starting amplitude of the damped vibration and the size of damping is known. After these it should be determined what kind of effect the thickness of the selected metal foam has for the amplitude of the vibration. Finding the answer easier the damping in solid material and the reflection in the border of the two media are eliminated only the amplitude reduction happens in emitting metal foam is noted.

In solid metals (c) spreading speed of longitudinal and transversal waves is different. In Table 2 wave spreading speeds for solid steel and aluminium can be seen in m/s. Spreading speed of the longitudinal wave in solid body can be counted according to equation (9).

$$c = \sqrt{\frac{E}{\rho}} \tag{9}$$

where:

E: modulus of elasticity of the material,

ρ: density.

For transversal waves there is no equation like equation (9). So the approximate spreading speed in metal foam material is determined on the basis of the longitudinal and transversal spreading speed of solid metals.

Table 2

Spreading speed of vibration in different materials

	Speed of the longitudinal wave in m/s	**Speed of the transversal wave in m/s**
steel	5100	3100
aluminium	5200	3100

Literature [8] gives a relative density range of 0.04÷0.65 for the density of metal foams that corresponds to 315÷5100 kg/m^3 'real' density. According to the introduced table the 0.3÷0.4 relative density range is the most frequent, so the average of this range (0.35) will be used in the following. In the calculations the density of the metal foam is 2750 kg/m^3. Estimating the spreading speed of the wave spreading in the metal foam elasticity modulus of the foam is also necessary. Literature [8] also shows data for modulus of elasticity with similarly wide ranges as in case of density. In case of 0.35 relative density, modulus of elasticity should be E = 5600 MPa. The spreading speed (for longitudinal waves) in metal foams can be calculated according to equation (10) following from the above mentioned.

$$c_{metalfoam,long.} = \sqrt{\frac{E}{\rho}} = \sqrt{\frac{5600 \cdot 10^6 Pa}{2750 \frac{kg}{m^3}}} = 1427 \frac{m}{s} \cdot \tag{10}$$

Assuming that the ratio between spreading speed of longitudinal and transversal waves for metal foams is the same as for solid metals the spreading speed of transversal wave in metal foam is 60% (856 m/s) of the value determined in equation (10). In view of spreading speed and frequency the wavelength can be determined according to equation (11).

$$\mathrm{c} = \lambda \cdot \mathrm{f} \Rightarrow \lambda = \frac{\mathrm{c}}{\mathrm{f}} \tag{11}$$

Λ value of metal foams can be forecast using equation (6) and values introduced in literature [8] of 'n' and 'k' presented in Table 1. During forecast k can be chosen from the range and for 'n' 2 is suggested by literature [8]. Knowing Λ logarithmic decrement and T period time β can be determined. Contexture introduced above could be right for the emitting factor, but unfortunately it is not. Because this way the emitting factor of the metal foam is less than the emitting factor of the solid metal. This contradicts the uncountable amount of literature that celebrates the excellent vibration emitting feature of metal foams. Modifying equation (1) equation (12) arisen.

$$\beta_{foam} = k \cdot \left(\frac{\rho_{foam}}{\rho_{solid}} \right)^{n} \cdot \beta_{solid} \cdot \tag{12}$$

In the characteristic curve k multiply factor changes in range of 0.1÷4 till other factors are constant. Counting the value of emitting factor for metal foams with equation (12) the

$$k \cdot \left(\frac{\rho_{foam}}{\rho_{solid}} \right)^{n} \tag{13}$$

multiplier is still 0.5 at the highest value (that is equal to 4) of k, so enlargement does not happen. Conclusion can be defined: for the emitting factor of metal foams equation (1) is not suitable.

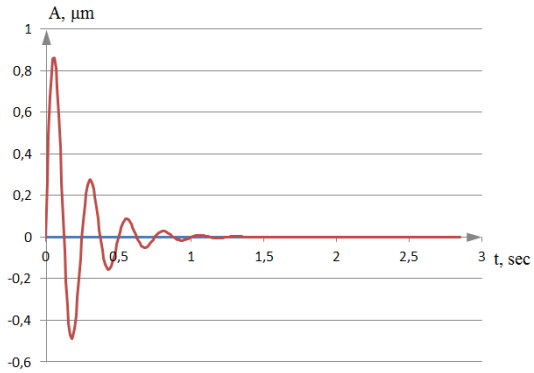

Figure 5: Damped vibration in case of high strength steel

Literature is quite reticent referring to the emitting factor of metal foams. The only source [9] for logarithmical decrement suggested a range 0.22÷0.62 for it. In Figure 5 an image of a damped vibration in case of high stress steel shows the changes of the vibration amplitude.

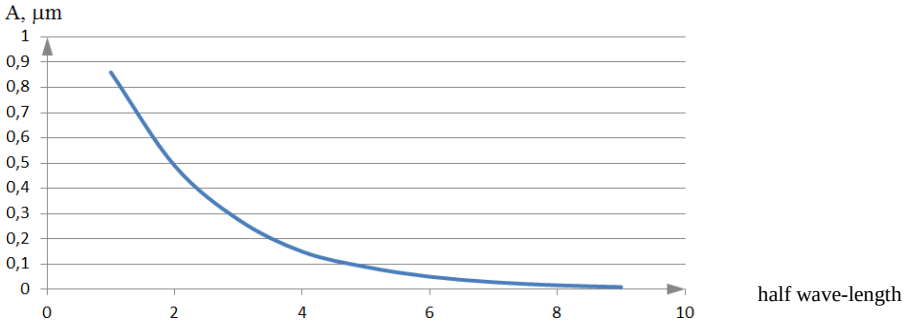

Figure 6: Characteristic of amplitude reduction depending on half wave-length

It can be seen quite well that after four wave-lengths there is almost no amplitude. In case of solid metals depending on the frequency of the vibration wave-length is in the range of 10 m [according to equation (11) and Table 2]. On the basis of the four wave-lengths the

total disappear of the vibration amplitude can be learned in distance of 40 m. In Figure 6 reduction of positive-negative vibration amplitudes coming subalternating can be seen depending on the half wave-length that shows the above written amplitude reduction in a little bit more expressive way.

In case of steel metal foams taking the average (that is 0.4) of the logarithmical decrement range given by literature [9] Figure 7 introduces the image of the damped vibration.

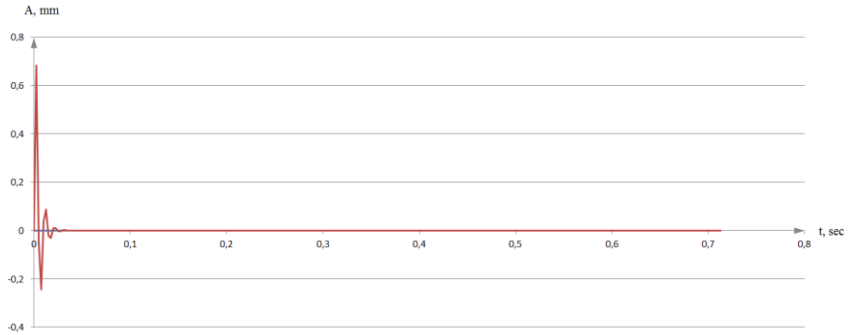

Figure 7: The image of the damped vibration in steel foam

In case of vibration can be seen in Figure 7 it can be determined that after two wave-lengths amplitude can hardly be measured. Estimated spreading speed in metal foam can be calculated according to equation (11). In this case quite smaller wave-length appears. Wave-length is in the range of metre. This is favourable in the point of view of vibration decreasing. If it is possible to use metal foam that is twice thick as the wave-length of the emerged emitted vibration in a gear-body, the amplitude of the vibration eliminates. It means still at least a 2 meter range. Changes of the amplitudes depending on the half wave-length can be seen in Figure 8. In practice there is no need for such a drastic vibration decreasing in many cases of gear-drives. There is only need for a couple of per cents, maximum 10% vibration amplitude reduction. With this kind of reduction expectations usually can be hold. On the basis of the characteristics of Figure 8 it can be seen that during one wave-length about 70% of amplitude reduction realises. Of course in the output gears of gear-drives there is not enough space for emitting material to reach the above mentioned 70% amplitude reduction.

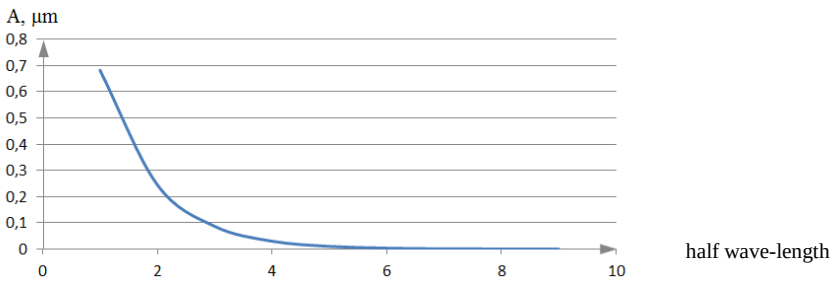

Figure 8: Changes of the amplitudes for metal foams depending on the half wave-length

However it is possible to build in metal foam with the thickness of 100 mm (that is the tenth of the wave-length from the meter range), we can calculate with a 7% reduction in the meaning of the vibration amplitude. Generally there is a space about 100 mm in output gears of gear-drives. According to the above mentioned equations suggestions can be defined for vibration emitting effect of steel metal foam as an inset, and for the foam thickness for given amplitude reduction. Of course it cannot be forget that the above mentioned are conclusions on the basis of clearly theoretical correlation that had the aim to improve if it is useful to apply this kind of material in the gear-body, in the primary transmission route. The result is absolutely positive.

For locating real processes it is necessary to experimentally determine vibration emitting values.

5. Strength analysis of gear with metal foam in it

For the strength analysis of gear body and metal foam built in it is indispensable to know the stresses work on them and strength indexes for the metal foam. In case of spur gears basic stress of gear-body is torsion that derives from the torque on the shaft. According to Figure 1 the volume between hub diameter and the rim of the gear ring can be replaced by metal foam. This volume is cylinder with a ring intersection (tube). Applying equation (14) for metal foams the emerging shearing stress can be calculated.

$$\tau = \frac{T}{K_P}, \tag{14}$$

where:

τ: shearing stress deriving from clean torque,

T: torque in the given intersection,

K_P: polar section modulus.

Polar section modulus in case of ring intersection can be calculated according to (15).

$$K_P = \frac{D^4 - d^4}{16 \cdot D}, \tag{15}$$

where:

D: the larger diameter of the ring intersection,

d: the smaller diameter of the ring intersection.

The smallest value of the inner diameter for the metal foam inset cylinder can be calculated from the stressing of the hub part of the gear. The hub part of the gear made from solid metal has also a ring intersection, so shearing stress generating here can be determined also by equation (14) and (15). Imagine that the diameter of the hub increases and the bore of the gear does not changes the stress emerging in the gear-body shows a sheer falling character on the basis of equation (16).

$$\tau_{hub} = \frac{T \cdot 16 \cdot D_{hub}}{D_{hub}^4 - d_{hub}^4}, \tag{16}$$

where:

D_{hub}: outer diameter of ring intersection hub,

d_{hub}: inner diameter of ring intersection hub.

In ring intersection that is given by the distance from the shaft, where stress emerges in the hub of the gear decreases a level where it can transmit torque, the size of the solid metal hub is determined. This value can be calculated by equation (17) solving for D_{hub}.

$$D_{hub}^4 \cdot \tau_{hub} - T \cdot 16 \cdot D_{hub} - d_{hub}^4 \cdot \tau_{hub} = 0 \cdot \tag{17}$$

Determining the size of gear ring and rim Figure 2 should be followed, as the value of the tooth root stress should not increase because of the factor Y_B. During the determination of the size of gear ring and rim the larger diameter of metal foam cylinder is given. Knowing the allowed shearing stress for metal foam (τ_{foam}) the inner diameter of the metal foam cylinder can be calculated with the help of equation (18).

$$d_{foam} = \sqrt[4]{\frac{D_{foam}^4 \cdot \tau_{foam} - T \cdot 16 \cdot D_{foam}}{\tau_{foam}}} \cdot \tag{18}$$

If the value of d_{foam} coming from the equation (18) is greater than, or equal to D_{foam} coming from the equation (17) the metal foam can be used and can transmit the torque. In other case it cannot be applied.

When building the metal foam in the gear body an other condition also has to be realised ensuring the operation. On the border of the metal foam and solid metal a connection should be established that can transmit the drive.

6. Connecting the elements of the gear-body

Connecting the elements of the gear-body is a very important stress viewpoint. It seems to be obvious to use some kind of shaft-hub connection. There are several kinds of shaft-hub connections. Choosing the applied type it should be analysed what characters and effects the different types have for solid metal and for metal foam. In case of frictional connections friction force emerges between surfaces transmits torque. Friction force is generated by pressing the surfaces of the hub and the shaft to each other. Generating the necessary friction force generally quite a large pressing force is needed. This expects strength requirements that cannot be realised in case of metal foam.

Connecting the foam and solid metal parts an other opportunity is to create shape locking connections. These kind of shaft-hub connections are widely spread. From the existing solutions the one should be chosen that is suitable for metal foam. Keeping this viewpoint in front of the eye there are only two solutions for the task. One of them is the spline drive shaft, the other one is the polygon connection. There are pros and contras in both cases.

As spline drive shafts are quite frequent, it is easy and cheap to produce. The connecting surface sizes of the shaft splines can be determined only then when the allowed surface stress for metal foam is known. Its symmetrical shape does not cause unbalance. The edges of splines are stress concentration points is the only disadvantage of this connection.

Technical application of polygon connection is quite rare in proportion to spline drive shafts. The reason for this is the expensive production. It does not consist of sharp edges, so there are no stress concentration points. Despite of its small size it can transmit large moment.

The use of metallic glue is the third opportunity to fasten the parts of the gear-body, besides the above mentioned. The shear strength of metallic glues reaches the 175MPa, while they are stable until 80 °C. [11]. There are glues that are still stable at higher temperature, but these have shear strength that is lower one order of magnitude. Advantage of the bonding is that the glue material can easily take up between the parts of the gear. The

parts of the gear-body have to be placed into a device during the hardening process of the glue. Glues are usually not expensive. Disadvantage is that many times additional operations have to be done during bonding, for example pressing the parts to each other, or using heating. The time of glue hardening changes in the function of the applied temperature and the type of the used glue. The engineer has to count with these parameters when choosing the technological process.

The combination of the above mentioned three types of connection between the parts of gear-body also can be adapted. For example frictional connection between the outer surface of inner part of gear-body (hub) and the inner surface of metallic foam and a bonded connection between metallic foam and gear rim can be used. The task of the engineer is to choose the proper connection type for the elements of the gear-body.

7. Summary

According to the above mentioned it can be determined that there is an opportunity to use metal foams in the gear-body to take advantage of the good vibration emitting properties of the metal foams. Specific constructional suggestions will be established in a further publication.

Acknowledgement

The research work presented in this study based on the results achieved within the TÁMOP-4.2.1.B-10/2/KONV-2010-0001 project and carried out as part of the TÁMOP-4.1.1.C-12/1/KONV-2012-0002 „Cooperation between higher education, research institutes and automotive industry" project in the framework of the New Széchenyi Plan. The realization of this project is supported by the Hungarian Government, by the European Union, and co-financed by the European Social Fund.

References

[1] Kováts A.: Gépszerkezettan (Műszaki akusztika). Budapest, Tankönyvkiadó, 1988.
[2] Orbulov I. N.: Szintaktikus fémhabok. PhD-értékezés, 2009.
[3] Korposné Kelemen K.–Kaptay Gy.–Borsik Á.: Fémhabok – A géptervezés potenciális szerkezeti anyagai.
[4] Sosa Mario, J.–Björklund, S.–Sellgren, U.–Flodin, A.–Andersson, M.: Gear Web Design with Focus on Powder Metal. VDI Berichte, Nr. 2199, 2013, pp. 1199–1208.
[5] Makhult, M.: Gépágyazások rezgéstani méretezése. Akadémiai Kiadó, Budapest.
[6] Ashby, Michael, F. A.–Tianjian, L.: Metal foams: A survey. Science In China, Vol. 46, No. 6, 2003.
[7] Budó Á.: Kísérleti fizika I. Nemzeti Tankönyvkiadó, Budapest, 1997.
[8] Smith, B. H.–Szyniszewski, S.–Hajjar, J. F.–Schafer, B. W.–Arwade, R.: Steel Foam for Structures: A review of applications, manufacturing and material properties. Journal of Constructional Steel Research, 2011.
[9] Neugebauer–Leopold–Schmidt: Gerauschminderung an Werkzeugen für die Hochleistung-bearbeitung. METAV, 2004.
[10] Handschuh, R. F.–Roberts, G. D.–Sinnamon, R. R.–Stringer, D. B.–Dykas, B. D.– Kohlman, L. W.: Hybrid Gear Preliminary Result – Application of Composites. 2012.
[11] Zsáry Á.: Gépelemek 1. Nemzeti Tankönyvkiadó, Budapest, 1999.

Design of Machines and Structures, Vol. 4, No. 1 (2014), pp. 77–85.

ONLINE MONITORING SYSTEM FOR STRUCTURES AT ELEVATED TEMPERATURE

SZABOLCS SZÁVAI–SZABOLCS JÓNÁS–
BALÁZS BAPTISZTA–ZOLTÁN BÉZI
Bay Zoltán Nonprofit Ltd., Department of Structural Integrity
3519, Miskolctapolca, Iglói str. 2.
szabolcs.szavai@bayzoltan.hu

OLMOST-HT project aimed to develop an integrated hardware and software system for on-line and on-site measurement of structure displacements in most critical regions in order to prevent failure due to flaw or fatigue occurred by degradation mechanism as creep, thermal ageing, and hydrogen embitterment on high temperature. Due to the unknown condition and the high consequences of any failure means that the operational risk can be extraordinary high. To prevent failure, maintenance in time requires special dedicated monitoring techniques. Having proper online global and local displacement and deformation data comparison can be done between the estimated and real data and decision can be. In this paper the previous experience of the OLMOST-HT monitoring system is presented. This study describes the main laboratory test, the trial of the monitoring system and a finite element case study of a catalytic reactor.

1. Online monitoring

Thermal power and chemical plants are highly capital intensive and hence it is necessary to ensure not only their safe operation, but also their economic viability in the long run. Integrity of important components is essential for operational safety, reliability and low cost operation. Normally, a plant is designed with a life expectancy of 30 to 40 years to produce continuous operation economically. However, because of conservatism in the design, the actual lives of these plants are expected to be much more than the estimated value. The sustained interest in the area of remaining life prediction arises from the need to avoid costly outages and to ensure safe operations, and the necessity to extend the component operation life beyond the original design life. In power generation systems, many structural components, such as steam pipes, superheater headers, and turbine rotors operate at elevated temperatures. At the same time, they are also subjected to cyclic loading due to fluctuation of process parameters. Hence, these components are exposed to a damage mechanism caused by fatigue, creep and creep-fatigue interaction. It is neither possible nor necessary to monitor the degradation effects for all the components of a plant. An in-depth understanding of the possible damage mechanism and the plant process dynamics is essential for the selection of an optimum number of components [2].

OLMOST-HT system is an on-line monitoring system for structures that operates at elevated temperatures. The system has a modular structure, which means it is possible to expand it with different additional modules (Figure 1). Sensors are equipped on the chosen components of the in-situ structure. The number of modules is determined by the number of probable failures. The different modules can be built into the system in accordance with the requirements of the structure. The measured data are constantly stored on a server. The

system has decision support software which contains a material database, several cases of hypothetic failures examined by FEA and an engineering assessment method.

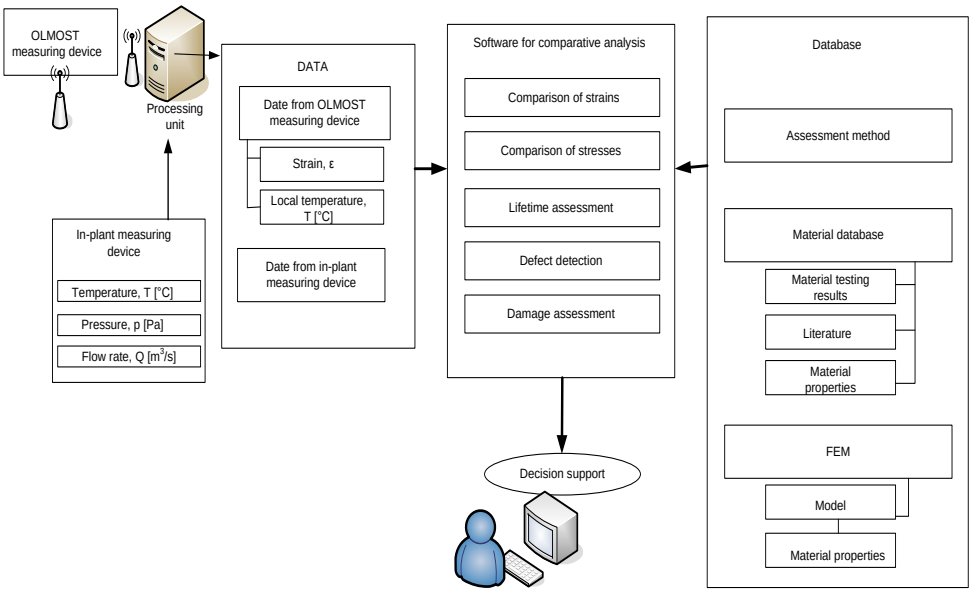

Figure 1: Block diagram of the OLMOST-HT system

The procedure described for advanced numerical analysis to calculate the expected structure response due to creep for design stage and based upon real operating temperature history. There are different creep models available:

- Combining Creep Material Models
  - This model illustrates how to combine different creep models to accurately represent the material behaviour.
- Combining Elastoplastic and Creep Material Models
  - This model shows how to combine different types of material nonlinearity, such as creep and elastoplasticity.
- Thermally Induced Creep
  - This model computes the stress history over a very long time for a material that exhibits creep behaviour.
- Primary Creep Under Nonconstant Load
  - primary creep using a Norton-Bailey law.

The monitoring system is online, so the measured values are accessible on the internet through an application called FieldLogger. The software has a pre-determined security level system. If the measured values at a component reach critical level, the system automatically sends an SMS or an e-mail to the appropriate people. Due to this function the intervention could be quick. OLMOST-HT was installed to an elbow of a steam pipeline as a test for the pilot system. Strain and temperature gauges were spot welded to the outer surface of the

elbow. The temperature of environment was also measured as a control value. In 2013 the online measurement system was installed to an elbow in BorsodChem Zrt. The Figure 2 shows the device.

Figure 2: OLMOST-HT measurement device

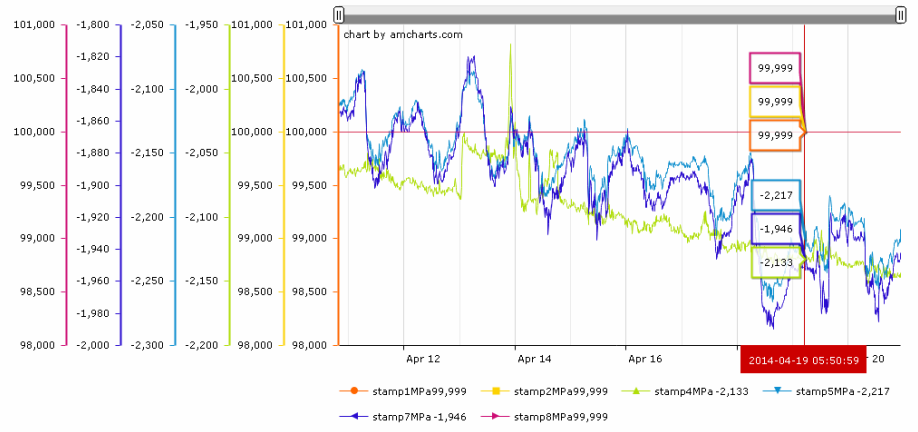

Figure 3: Measured stress values at different gauges

From the software the data can be able to export and comparable with FEA data. In the future we would like solve to connect the database with the software. Now the comparison is only works by manually, but the software development to come to an end soon. The measured values as a function of time are shown in Figure 3–4 as some results from the software. Each gauge can be examined independently. Development and testing of the pilot system was aided by laboratory tensile test results from an elbow specimen. Strain gauge layout identical to the pilot system was used during testing.The results of the test and the FEA (Figure 5) of the elbow were compared as it is shown in Figure 6. Strain 3 and strain 5 measured the same stress component, but at the opposite side of the elbow. The results are in good agreement.

Figure 4: Measured temperature values at different gauges

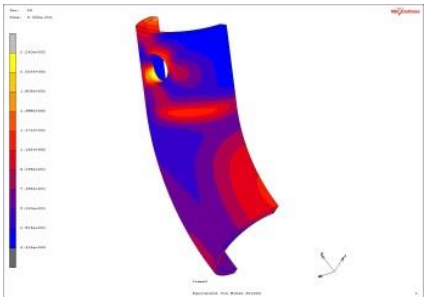

Figure 5: FEA of the laboratory test specimen

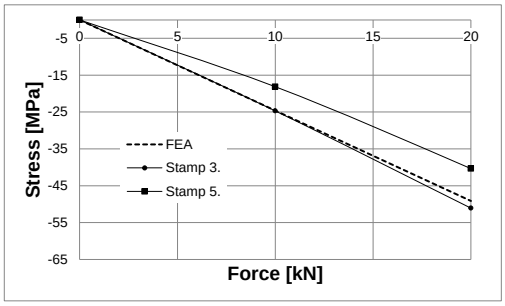

Figure 6: Comparison of the test and the FEA

2. Industrial case study for fitness for service analysis of component operates on elevated temperature

The case study is a preliminary investigation before the actual measure of creep. The reactor blows off around the perimeter and this phenomenon causes problems in the operation. The product of the reactor is NH3 so it is hazardous and can cause impair in the environment.

2.1. Parameters of the simulation

The inside pressure of the reactor pressure vessel (RPV) is 11.57 bar(a) and at the top of the RPV the temperature is 455 °C. The material of the shell, the heads, the manholes, the nozzles and the flanges are steel grade X6CrNiTi18-10. The critical part of the RPV is the upper flange, so the examination is focused for the compliance of the parts of the flange at elevated temperature. The fasteners of the flange are made of steel grade 21CrMoV 5-7+QT. The part assembly of the flange is shown in Figure 7.

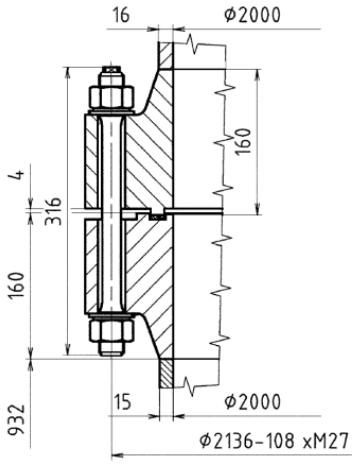

Figure 7: Geometry of the flange

2.1. Parameters of the simulation

The inside pressure of the reactor pressure vessel (RPV) is 11.57 bar(a) and at the top of the RPV the temperature is 455 °C. The material of the shell, the heads, the manholes, the nozzles and the flanges are steel grade X6CrNiTi18-10. The critical part of the RPV is the upper flange, so the examination is focused for the compliance of the parts of the flange at elevated temperature. The fasteners of the flange are made of steel grade 21CrMoV 5-7+QT. The part assembly of the flange is shown in Figure 7.

2.2. Calculation of the bolt load for gasket seating condition

The ASME BPVC III.Div.1.App. XI.was used to check the seating condition of the gasket and the bolt loads [4]. The bolt load is also a useful input parameter for the FE model. The applied gasket is a grooved gasket. Gasket parameters from Table XI-3221.1-1 of the ASME code were used for the calculations. The gasket factor m = 4.25, and the minimal seating stress y = 70 MPa (11,100 psi). From the calculations the required bolt load is F_{bolt} = 4262986.53 N (~4262.9 kN). The load distributes between the bolts equally. The flange contains 108 pieces of M27 bolts. So in the model the pre-tension force of a bolt is F_{1_bolt} = 39472.0975 N (~39.5kN).The strength calculations show that the number of bolts and the material of the gasket are sufficient and the seating condition is also suitable.

2.3. Modelling

For the simulation MSC.Marc&Mentat 2012 FE code was used. The geometry is cyclic symmetric; hence only a thin slice of the whole structure has to be modelled. Boundary conditions and the FE mesh of the flange are shown in Figure 8. The whole model is interpreted in cylindrical coordinate system. Two loadcases are set in the model. In the first loadcase the pre-tension of the bolt is computed.

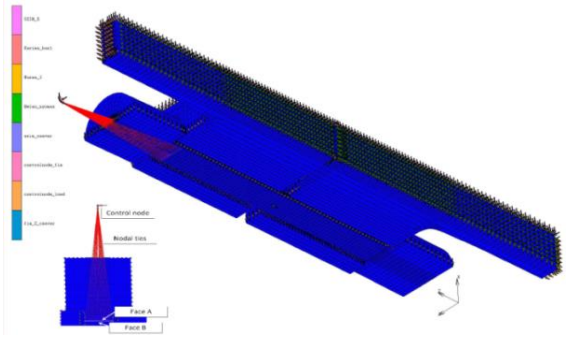

Figure 8: Boundary conditions and the FE mesh of the flange

The pre-tension was modelled according to [3]. The nodes on the new faces (Face A and Face B) are linked to the control node. The pre-tension force is transmitted by this node. The control node only moves upside (direction Z). In the first loadcase the pre-tension force of the bolt is applied to the control node. In the second loadcase the inner pressure is applied, and in the third loadcase the creep is done. The creep is considered by an exponential creep law. The total number of elements is 29696, each of them is 4-node quadrilateral element. Table 1 contains the number of elements and nodes for each part.

Table 1

Properties of FE mesh

	Number of elements	**Number of nodes**
Bolt	10784	12865
Upper part of flange	9464	11961
Lower part of the flange	9384	11844
Gasket	64	135

In the second load case the inner pressure is added. From the inner pressure originated a tensile force on the surface of the section plane of the flanges. The value of this force can be calculated by the (1). Figure 9 shows a schematic figure about the mechanical background of this relationship.

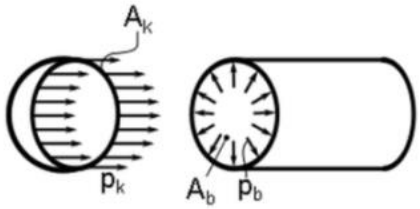

Figure 9: Illustration for the determination of the tensile force around the perimeter

$$p_k = p_b \cdot \frac{A_b}{A_k}. \tag{1}$$

2.4. Determination of the applied material properties

The material properties of the flanges and the gasket are from material database. The material properties depend on the temperature; the applied values are interpolated from the data (Figure 10–11). The material properties of the bolt are measured values. 6 specimens were tested by uni-axial tensile testing. The test temperatures are the following: 20 °C, 270 °C and 455 °C (Figure 12–13).

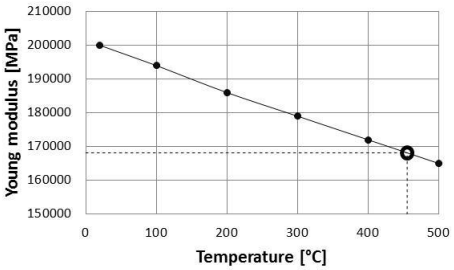

Figure 10: Temperature dependant Young modulus of X6CrNiTi18-10

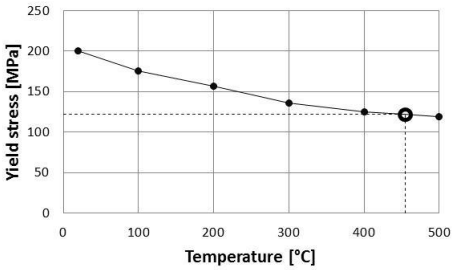

Figure 11: Temperature dependant yield stress of X6CrNiTi18-10

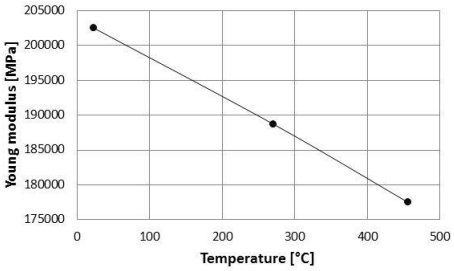

Figure 12: Temperature dependant Young modulus of 21CrMoV5-7+QT

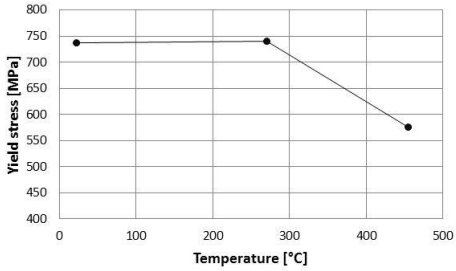

Figure 13: Temperature dependant yield stress of 21CrMoV5-7+QT

2.5. Results of the simulation

The results of the simulation show that the stress state of the bolt is high. The stress distribution at elevated temperature of the structure is shown in Figure 14. The assumption is that this stress is higher than the creep limit of the bolts. Creep data only available in literature. The creep properties of the bolt material are in Table 2. The values at 455 °C are interpolated data.

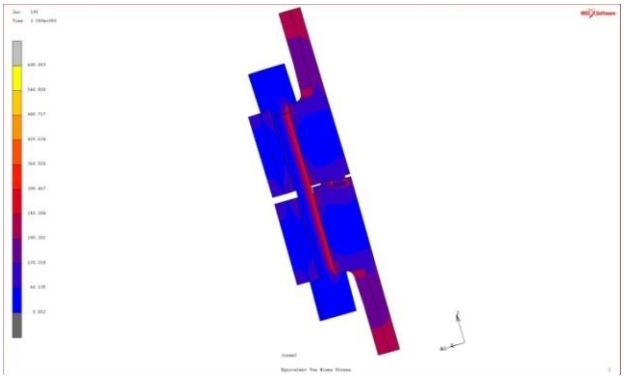

Figure 14: Equivalent Von Mises stress distribution

Table 2

Creep properties of the bolt material

Temperature [°C]	**$R_{p1/10,000}$ [MPa]**	**Temperature [°C]**	**$R_{p1/100,000}$ [MPa]**
420	429	420	365
430	407	430	340
440	385	440	315
450	363	450	288
460	339	460	262
470	314	470	235
455	349.948	455	274.805

The maximum stress of the bolt is 296.772 MPa at 455 °C. This value is higher than the Rp1/100,000. The conclusion is that the bolt is creeping and the calculation with the Larsen-Miller parameter has also supported this assumption. The determination of the creep rate needs further investigation.

3. Conclusion

The preliminary calculations and tests demonstrate that the system works. The bolts of the flanges are creeping concluded from the FE calculations. The OLMOST-HT system will be installed to the bolt, so measured values are expected later. Having proper online global and local displacement and deformation data comparison can be done between the estimated and real data and decision can be made in the frame of the OLMOST system. In case of unexpected differences between the predicted and measured response further investigation can be supported.

Acknowledgement

This research was carried out as part of the OLMOST (On-Line Monitoring of Structures and Fatigue) EUREKA_HU_08-1-2010-0021 project in the framework of the New Széchenyi Plan with support by the European Union, co-financed by the European Social Fund.

References

[1] Creep and Creep Failures. David N. French, Sc. D, President of David N. French, Inc., Metallurgists, Northborough, MA July 1991.
[2] Mukhopadhyay, N. K.–Dutta, B. K.–Kushwaha, H. S.: On-line fatigue – creep monitoring system for high-temperature components of power plants. International Journal of Fatigue, 23 (2001), 549–560.
[3] MSC.Marc&Mentat – User's guide
[4] ASME BPVC III. Div. 1.App. XI.

Design of Machines and Structures, Vol. 4, No. 1 (2014), pp. 87–98.

DEVELOPMENT OF CALCULATING PROCESS FOR ELASTO-HYDRODYNAMIC SPOT CONTACT BY P-FEM

SZABOLCS SZÁVAI–SÁNDOR KOVÁCS
Bay Zoltán Nonprofit Ltd. for Applied Research
Institute for Logistics and Production Engineering (BAY-LOGI)
3519 Miskolctapolca, Iglói út 2.
szabolcs.szavai@bayzoltan.hu
sandor.kovacs@bayzoltan.hu

Rolling-sliding machines such as gears, cams and followers, and bearings, which are often subjected to high loads, high speeds and high slip conditions when not only the pressure distribution in the lubricant and variation of the viscosity due to pressure is a question but the surface deformation to calculate the sub-surface stress field. To analyse the tribological conditions of the contact surfaces, after Osborne Reynolds (1886) [1], who presented the theory of hydrodynamic lubrication and the governing partial differential equation for the pressure field, the generalized Reynolds equation was developed by Dowson (1962) [7]. Although several methods have been already developed for solving EHD problems, the solution of the highly nonlinear problem is still quite challenging. Unfortunately, only few solutions were published based on FEM despite it permits the using of polynomial approximation for powerful calculation of the generalized Reynolds equation without smooth mesh. However, applying rough mesh, the end of the contact can locate far from the boundaries of the elements. This fact makes to be important to manage the cavitation inside elements. So the development of a p-version FEM model for calculating the film shape, the pressure and temperature distribution and its implementation to commercial software seems to be timely. For this reason, special lubricant film element can be developed for such problems where pressure and film thickness can be handled as independent element variables in the generalized Reynolds equation and determined incrementally by fully coupling the hydrodynamic and the solid mechanic problem.

1. Basic equations and boundary conditions for the description of the EHD phenomenon of lubrication theory

The generalized case of surface pairs contacting along a spot in the status of liquid friction is illustrated in Figure 1.The gap between the bodies is filled with lubricant due to the relative motion of the bodies and hydrodynamic pressure develops due to the movement of the lubricant. The movement of the lubricant is caused by the tangential (shear) stress generated in the lubricant as the result of the relative motion of the surfaces. At the particular kinematic condition of the contacting bodies and with a given gap geometry the pressure distribution acting on the surfaces is able to maintain balance with the force pressing the surfaces to each other and prevent a direct body-to-body contact thereby. It can be seen, therefore, that if the circumstances of contact developing under thermal elasto-hydrodynamic conditions of lubrication are wished to be modelled then hydrodynamic, thermodynamic and strength problems – forming highly non-linear systems even by themselves but also because of the status-dependence of the properties of the various continuums – have to be solved at the same time and in combination.

Lubrication analysis began looking into the finite element formulation in the sixties by Reddi (1969) [2], the seventies by Rohde and Oh (1975) [3], and they found the method promising and reliable. Freund and Tieu (1993) [4] used h-FEM for solving the generalized

Reynolds equation. In these investigations, the traditional h-version finite element method (h-FEM) had been used in the formulation of lubrication problems till 1991 when Nguyen [5] reported an analysis with using p-version finite element method but the geometry and the oil properties were assumed to be constant. However the p-approximation concept was introduced by Babuska and Szabó. (1979) [6], but most p-version formulation appear in the literature deal with problems in solid mechanics and heat transfers.

In this work the application possibility of p-FEM for EHD problem is presented with the necessary developments. For FEM governing equation the weak form of the weighted-residual integral form of the Reynolds has been applied. Lagrange functions have been used for the polynomial approximation of the unknown pressure distribution. The p-FEM based solution of EHD problems; the polynomial approximation makes the opportunity of replacement of the smooth mesh with a rough one. In order to have the compatible formulation to the well-known FEM solutions, the film shape has been calculated as a superposition of the discretized original geometry, the displacement of a rigid surface and the discretized deformation of the surface under pressure.

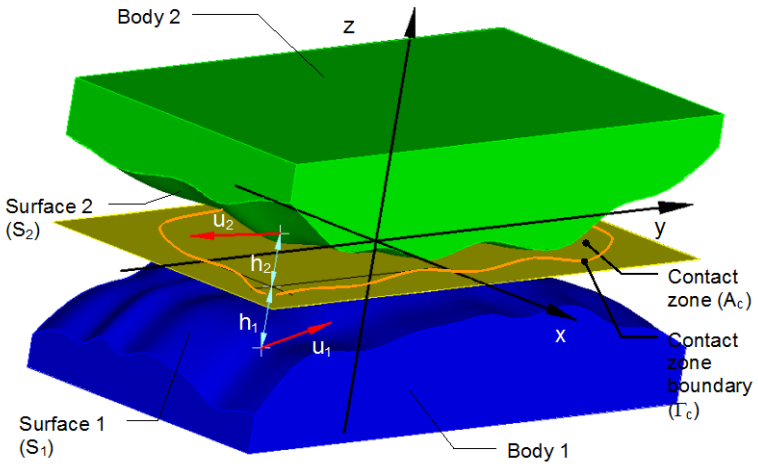

Figure 1: Contacting bodies

2. Hydrodynamic problem

For calculating the contact pressure due to fluid film lubrication the generalized Reynolds equation was developed by Dowson (1961) [7] as a partial differential equation take account the changes the viscosity across the film thickness. Based on the concepts of it, the weak integral form of the generalized Reynolds equation is:

$$\int_{A_C} \nabla_{x,y} w \cdot \Phi \cdot \nabla_{x,y} p \cdot dA - \int_{A_C} \nabla_{x,y} w \cdot \Psi \cdot dA - \int_{A_C} w \cdot \Omega \cdot dA + \oint_{\Gamma_C} w \cdot q_S \cdot ds = 0 \qquad (1)$$

where:

w: a weight function,

q: lubricant in or outlet.

$$\Phi = \mathrm{F}_2 + \mathrm{G}_1 \tag{2}$$

$$\begin{aligned}\boldsymbol{\Psi} = {} & h_2 \cdot \rho\big|_{z=h_2} \cdot \mathbf{u_{xy}}\Big|_{z=h_2} + h_1 \cdot \rho\big|_{z=h_1} \cdot \mathbf{u_{xy}}\Big|_{z=-h_1} - \\ & - \frac{F_3 + G_2}{F_0} \cdot \left(\mathbf{u_{xy}}\Big|_{z=h_2} - \mathbf{u_{xy}}\Big|_{z=-h_1} - \mathbf{K}_{0xy} \right) - G_3 \cdot \mathbf{u_{xy}}\Big|_{z=-h_1} - \mathbf{K}_{1xy} - \mathbf{K}_{2xy}\end{aligned} \tag{3}$$

$$\Omega = \rho\big|_{z=h_2} \cdot \mathbf{u_{xy}}\Big|_{z=h_2} \cdot \nabla_{x,y} h_2 + \rho\big|_{z=-h_1} \cdot u_z\big|_{z=-h_1} - \rho\big|_{z=h_2} \cdot u_z\big|_{z=h_2} - \int_{-h_1}^{h_2} \frac{\partial \rho}{\partial t} \cdot dz \tag{4}$$

Employing the customary decomposition:

$$u_z\big|_{z=-h_1} = -\mathbf{u_{xy}}\Big|_{z=-h_1} \left(\nabla_{xy} h_1 \right) + W_1(t,x,y) \tag{5}$$

$$u_z\big|_{z=h_2} = \mathbf{u_{xy}}\Big|_{z=h_2} \left(\nabla_{xy} h_2 \right) + W_2(t,x,y)$$

for the components in gap thickness direction of surface velocities Ω will take the following form:

$$\Omega = \rho\big|_{z=-h_1} \cdot W_1 - \rho\big|_{z=h_2} \cdot W_2 - \int_{-h_1}^{h_2} \frac{\partial \rho}{\partial t} \cdot dz \tag{6}$$

$\mathbf{u}_{\mathrm{xy}}{}^{\mathrm{T}} = [u_x, u_y]$: the velocity in the contact plane, u_z: the velocity in the z direction,

$\nabla_{\mathrm{x,y}} = [\partial/\partial \mathrm{x}, \partial/\partial \mathrm{y}]$

F_i,G_i, $\mathbf{K}_{\mathrm{i_{xy}}}$: viscosity-density functions:

$$F_0 = \int_{-h_1}^{h_2} \frac{F(\tau_{eq})}{\tau_{eq}} dz \qquad F_1 = \int_{-h_1}^{h_2} \frac{F(\tau_{eq})}{\tau_{eq}} z dz \qquad F_2 = \int_{-h_1}^{h_2} \rho \frac{F(\tau_e)}{\tau_e} z^2 dz - \frac{F_1 F_3}{F_0}; \quad F_3 = \int_{-h_1}^{h_2} \rho \frac{F(\tau_e)}{\tau_e} z dz$$

$$G_1 = \int_{-h_1}^{h_2} z \frac{\partial \rho}{\partial z} \left(\int_{-h_1}^{z} \frac{F(\tau_e)}{\tau_e} \hat{z} d\hat{z} - \frac{F_1}{F_0} \int_{-h_1}^{z} \frac{F(\tau_e)}{\tau_e} d\hat{z} \right) dz; \qquad G_2 = \int_{-h_1}^{h_2} z \frac{\partial \rho}{\partial z} \left(\int_{-h_1}^{z} \frac{F(\tau_e)}{\tau_e} d\hat{z} \right) dz; \; G_3 = \int_{-h_1}^{h_2} z \frac{\partial \rho}{\partial z} dz$$

$$\mathbf{K}_{0xy} = \int_{-h_1}^{h_2} A \frac{d\bar{\sigma}'_z}{dt} dz = \begin{bmatrix} \int_{-h_1}^{h_2} \frac{A d\tau_{xz}}{dt} dz \\ \int_{-h_1}^{h_2} \frac{A d\tau_{yz}}{dt} dz \end{bmatrix} \quad \mathbf{K}_{1xy} = \int_{-h_1}^{h_2} z \rho A \frac{d\bar{\sigma}'_z}{dt} dz \quad \mathbf{K}_{2xy} = \int_{-h_1}^{h_2} z \frac{\partial \rho}{\partial z} \left(\int_{-h_1}^{z} A \frac{d\bar{\sigma}'_z}{dt} d\hat{z} \right) dz$$

In case of steady-state rolling-sliding contacts $\Omega = 0$ and $\mathbf{K}_{\mathrm{i_{xy}}} = 0$ furthermore G_i negligible.

For simple model, the film shape can be calculated as a superposition of the original geometry, the displacement of a rigid surface and the deformation of a half-space under pressure.

After deformation, the film shape:

$$h = h_1 + h_2 = h_{g_1} + \Delta_{rigid\,1} + \delta_{1_1} + h_{g\,2} + \Delta_{rigid\,2} + \delta_2 = h_g + \Delta_{rigid} + \delta \tag{7}$$

where Δ_{rigid} is the displacement as a rigid surface, h_g is the undeformed gap size, the δ deformation of the surfaces. Usually it can be assumed that $h_1=0$, $h_2=h$.

The integral of the pressure over the contact area should be equal with the load.

$$F_W = \int_{A_c} p \cdot dA \tag{8}$$

F_W is the normal load of the surfaces. Loadcase can be satisfied if the Δ_{rigid} is a variable.

3. Finite Element Formulation

For the discretized governing equations, the weak form of the weighted-residual integral form of the Reynolds equation has been applied. Lagrange functions [6] have been used for the polynomial approximation of the un-known pressure and surface deformation.

In the case of variation methods, the integral forms of the differential equations are used and in the course of this, rationally, certain quantities have to be integrated over the region investigated. The integration range has to be divided into shapes characteristic of a particular element type for the use of the finite element method and then derived into a unified shape by means of conform transformation for numerical integration.

The edges and sides of the elements along the gap are parallel with coordinate axis z and thus the unit vector $\boldsymbol{e}_z$ of the global coordinate system connected to the contact surface and unit vector $\boldsymbol{e}_\zeta$ of the coordinate system connected to the element coincide. Consequently x and y coordinates, the gap size and the pressure are not the functions of ζ:

$$x^e(\xi,\eta,t) = \sum\nolimits_i X_i^e(t) N_{x\,i}^e(\xi,\eta) = \mathbf{N}_x^{eT}(\xi,\eta)\mathbf{X}^e(t) \tag{9}$$

$$y^e(\xi,\eta,t) = \sum\nolimits_j Y_j^e(t) N_{y\,j}^e(\xi,\eta) = \mathbf{N}_y^{eT}(\xi,\eta)\mathbf{Y}^e(t) \tag{10}$$

$$h_{g_i}^e(\xi,\eta,t) = \sum\nolimits_j H_{g_i\,j}^e(t) N_{h\,j}^e(\xi,\eta) = \mathbf{N}_h^{eT}(\xi,\eta)\mathbf{H}_{g_i}^e(t) \tag{11}$$

$$\delta_i^e(\xi,\eta,t) = \sum\nolimits_j H_{\delta_i\,j}^e(t) N_{h\,j}^e(\xi,\eta) = \mathbf{N}_h^{eT}(\xi,\eta)\mathbf{H}_{\delta_i}^e(t) \tag{12}$$

$$h_i^e = \left[\mathbf{N}_h^{eT}, 1\right] \begin{bmatrix} \mathbf{H}_{g\,i}^e + \mathbf{H}_{\delta i}^e \\ \Delta_{rigid\,i} \end{bmatrix} = \left[\mathbf{N}_h^{eT}, 1\right] \begin{bmatrix} \mathbf{H}_i^e \\ \Delta_{rigid\,i} \end{bmatrix} \tag{13}$$

$$p^e(\xi,\eta,t) = \sum\nolimits_j P_j^e(t) N_{p\,j}^e(\xi,\eta) = \mathbf{N}_p^{eT}(\xi,\eta)\mathbf{P}^e(t) \tag{14}$$

The approximation of coordinate z is necessary as well because of the thermodynamical problem. Since z is linear in ζ:

$$z^e = -h_1^e\left(\frac{1-\zeta}{2}\right) + h_2^e\left(\frac{1+\zeta}{2}\right) = -\left(\frac{1-\zeta}{2}\right)\mathbf{N}_h^{eT}\mathbf{H}_1^e + \left(\frac{1+\zeta}{2}\right)\mathbf{N}_h^{eT}\mathbf{H}_2^e \tag{15}$$

Since the Rayleigh-Ritz finite element model was developed, $w = \mathbf{N}_p^e$ and the following nonlinear equation system was given per elements:

$$\begin{aligned}&\mathbf{K}^{\mathbf{e}}\left(\eta(p,\vartheta),\rho(p,\vartheta),h(p)\right)\cdot\mathbf{P}^e = \\ &= \mathbf{f}_a^e\left(\eta(p,\vartheta),\rho(p,\vartheta),h(p)\right) + \mathbf{f}_b^e\left(\eta(p,\vartheta),\rho(p,\vartheta),h(p)\right) - \mathbf{Q}^e\end{aligned} \tag{16}$$

where:

$$\mathbf{K}^e = \int_{A^e}\Phi^e\cdot\left[\mathbf{B}_p^e\circ\mathbf{B}_p^e\right]\cdot dA^e\ ,\ \mathbf{B}_p^e = \nabla_{xy}\mathbf{N}_p^{eT} \tag{17}$$

$$\mathbf{f}_a^e = \int_{A^e}\partial\mathbf{N}_p^e\cdot\mathbf{\Psi}^e\cdot dA^e\ ,\mathbf{f}_b^e = \int_{A^e}\mathbf{N}_p^e\cdot\Omega^e\cdot dA^e\ ,\ \tilde{\mathbf{Q}}^e = \oint_{\Gamma^e}q_h^{n_\Gamma^e}\mathbf{N}_p^e d\Gamma \tag{18}$$

4. Penalty cavitation algorithm

For p-FEM, it is important to manage the cavitation inside elements instead of deactivating the elements where the cavitation occurs.

The connection between the viscosity and pressure has been applied according to Kumar and Booker [8][9] for further investigation as the equation (19) shows.

$$\frac{\eta}{\eta_L} = \frac{\rho}{\rho_L} \qquad \rho \le \rho_c \tag{19}$$

However the density change as a function of the pressure in the cavitation zone let be approximated by a high gradient slope under the cavitation pressure. The difference from the original Kumar and Booker model can be seen in the Figure 2. The gradient of the slope should depend on a parameter that can be called penalty parameter. The higher value of the penalty parameter is the higher gradient of the density in the cavitation zone. It should be taken into consideration as well that the density should be higher than zero everywhere.

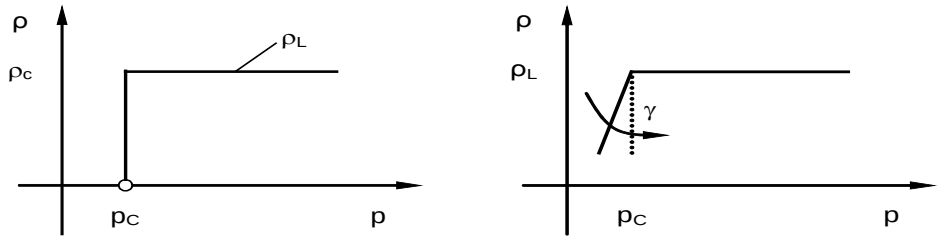

Figure 2: Penalty parameter approximation of the density

The above described criteria can be satisfied with the following density function:

$$\rho^{*} = \frac{\rho_L(p,\vartheta)}{\gamma(p)\cdot(p_c - p)+1} \tag{20}$$

where γ(p) is the penalty function which is:

$$\gamma(p) = \begin{cases} 0 & if \quad p > p_c \\ c & if \quad p \le p_c \end{cases} \tag{21}$$

The ρ* is valid in the lubrication region and the cavitation zone as well, and the volume fraction can be written as:

$$\theta(p) = \frac{\rho^{*}}{\rho_L} = \frac{1}{\gamma(p)(p_c - p)+1} \tag{22}$$

Applying the linear correlation between the density and the viscosity according to Kumar and Booker the viscosity can be written as follows:

$$\eta^{*} = \eta_L(p,\vartheta)\frac{\rho^{*}}{\rho_L(p,\vartheta)} = \theta(p)\eta_L(p,\vartheta) \tag{23}$$

All the parameters needed for the EHD analysis can be written as a function of the pressure in the cavitation zone, too.

5. Linearization of the discretized Reynolds equation

The difficulty of reaching a solution in the subject matter investigated is caused primarily by the strongly nonlinear nature of the Reynolds equation. The solutions of strongly nonlinear equations are based in the vast majority of cases on the Newtonian or gradient methods.

Consequently, the discretized Reynolds equation system has to be linearized in order to enable the determination of the pressure distribution and the associated gap size. Let us observe the equation as:

$$\mathbf{R} = \mathbf{R}\left(\mathbf{P}, \rho, \dot{\rho}, h, \vec{r}, t, \eta, \tau_{eq}, \vartheta, \theta, \vec{u}_1, \vec{u}_2 .....\right) \tag{24}$$

The linearized form of this at an arbitrary point $\mathbf{P}=\mathbf{P}^{j}$:

$${}^{i}\mathbf{R}\left(\mathbf{P}^{j}, {}^{i-1}\mathbf{R}\right) + \left(\frac{\partial^{i}\mathbf{R}}{\partial \mathbf{P}} + \frac{\partial^{i}\mathbf{R}}{\partial \rho}\frac{\partial \rho}{\partial p}\mathbf{N}_p + \frac{\partial^{i}\mathbf{R}}{\partial \eta}\frac{\partial \eta}{\partial p}\mathbf{N}_p + \frac{\partial^{i}\mathbf{R}}{\partial h}\mathbf{N}_h\mathbf{D}_p + ... \right)\Bigg|_{\mathbf{P}=\mathbf{P}^{j}} \Delta\mathbf{P} + O = 0 \tag{25}$$

The solution of ${}^{i}\mathbf{P}^{*}$ at residual ${}^{i}\mathbf{R} = 0$ is approximated with a series of solutions for $\Delta\mathbf{P}^{j}$ in this equation as shown below:

$$\mathbf{P}^{j+1} = \mathbf{P}^{j} + \alpha \cdot \Delta\mathbf{P}^{j} \qquad \alpha = [0..1] \tag{26}$$

As the initial system of equations is highly nonlinear in the case of EHD problems, it is very difficult to find an initial state where the instability of the solution can be avoided. For this reason, a properly chosen α is required. For this reason, it is expedient to determine the optimum damping rate in such a way that it should result in the largest possible reduction of the residual value. This can be ensured, obviously, only by some properly chosen methods.

6. Implementation to FEM software

The Comsol Multiphysics software was used for calculating EHD problems. The Comsol Multiphysics use the finite element formulation with Lagrange test functions as it was shown above to solve numerical problems.

It has got modules which are useful to build up an EHD model. The weak formulation of the hydrodynamic problem described by (1) equation can be created in the Mathematics module and model can be freely modified. The elastic deformation of the surface and the rigid displacement of the surfaces can be calculated in the Structural Mechanics module which uses the common structural finite element methods. The Comsol Multiphysics also provides an opportunity to incorporate function of penalty cavitation described by (20)–(23) equations.

The EHD as it was mentioned above is a highly nonlinear problem. The Comsol Multiphysics use the damping Newton-Raphson method described by (24)–(26) equation for the nonlinear problems. The method of determining the damping rate is the following:

- Firstly, the method calculate an **E** relative error value with the (27) equation

$$f'(\mathbf{P}^j)\mathbf{E} = -f(\mathbf{P}^{j+1}) \tag{27}$$

- If the relative error value is higher or equal to the **E** obtained from previous iteration step, then the value of the damping rate is reduced
- This process is repeated until the relative error value is lower than the value obtained from the previous iteration step or the minimum attenuation rate is achieved

After the determining the damping rate, the Newton-Raphson method calculate the value of the $\Delta\mathbf{P}^{j+1}$. The iteration continues until the special error norms do not achieve the value of relative tolerance.

The relative tolerance, the maximal iteration step number and the minimum damping rate can be manually given. The smaller the value of relative tolerance, the more accurate result but we risk that the iteration does not converge due to numerical errors.

7. Solved cases

The next three cases were evaluated with our calculating method introduced above:

Hydrodynamic lubrication between two plain surfaces:

- The geometrical parameters of the gap: $h_0 = 10$ μm; $h_1/h_0 = 1.25$; $l = 25$ mm as can be seen on Figure 3. Width of the plain surfaces:100 mm
- The difference of the velocity of the plains: $U = u_x = 25$ m/s; $V = u_y = 0$ m/s
- At the edges of the gap, the pressure is 0 MPa
- Viscosity of the lubricant: $\eta = 5 \cdot 10^{-2}$ Pa·s

- The upper surface is rigid and the lower surface is linear elastic: E = 109.9 GPa
- External load: W_{ext} = 0.1 MN

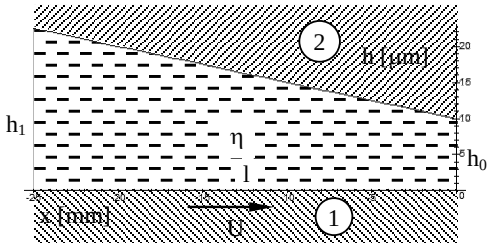

Figure 3: Initial gap geometry between two plain surfaces

Results:

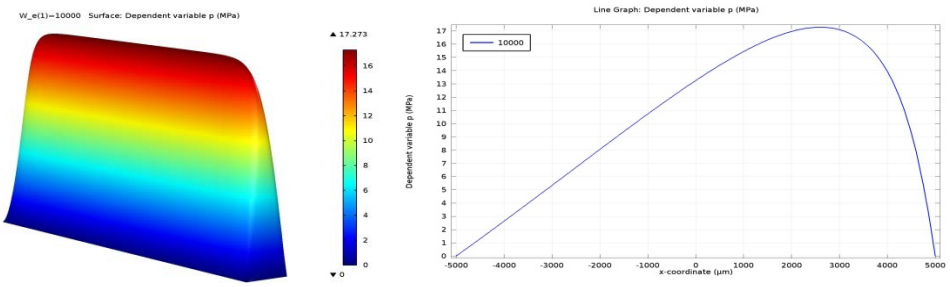

Figure 4: The pressure distribution in the gap between two plain surfaces and in the middle cross-section

Hydrodynamic lubrication between double parabolic and plain surface taking into account the cavitation

- Length of a gap: l = 76.2 mm as can be seen on Figure 5.
- Length of a bearing: l_b = 38.1 mm
- Minimal gap height: h_0 = 25,4 μm
- Maximal gap height: h_1 = 50,8 μm
- Velocity to the x direction of the bearings: U = 4,57 m/s
- Viscosity of the lubricant: η = 0,039 Pa·s
- The penalty parameter of the cavitation: $c = 1{,}9 \cdot 10^{-5}$.

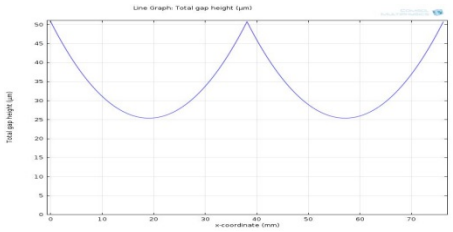

Figure 5: Total gap height between double parabolic and plain surface

Results:

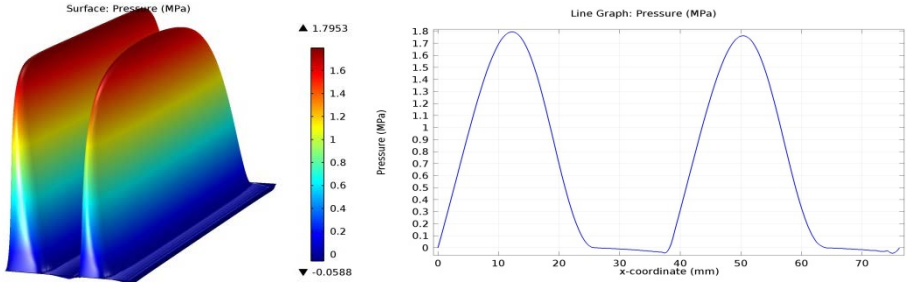

Figure 6: The pressure distribution in the gap between double parabolic and plain surface and in the middle cross-section

Elastohydrodynamic lubrication of roller-bearing

- The reduced geometrical parameters of the gap:
  - initial minimum gap height: $h_0 = 0.228127$ µm
  - radius of the roller-bearing: r = 30.031035 mm
  - width of the plain surface of the roller: 30 mm

  Schematic figure of the gap can be seen on Figure 10.
- The difference of the velocity of the surfaces: $U = u_x = 1.58853$ m/s; $V = u_y = 0$ m/s
- At the edges of the gap, the pressure is 0 MPa
- The upper surface is rigid and the lower surface is linear elastic: E = 109.9 GPa
- Viscosity of the lubricant described by Barus model: $\eta = 1.539 \cdot 10^{-2} \cdot e^{\alpha p}$ Pa·s, where $\alpha = 5000 / E$
- External load: $W_{ext} = 500$ N
- The penalty function of the cavitation: $c = 1{,}9 \cdot 10^{-5}$

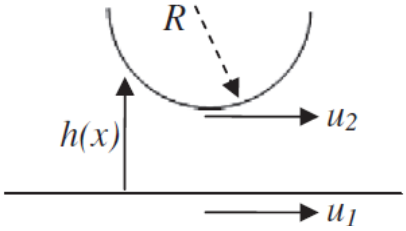

Figure 7: The reduced gap geometry of roller-bearing

Results:

This test case was solved in two steps. At first the problem was solved as a line contact. The result can be seen on the Figure 8: The pressure distribution in the gap of roller-bearing in case of line contact.. The results are in good agreement with the literature. Secondly it was solved as a finite length contact. Unfortunately the solution could not converge due to numerical instability at the side of the roller. The results of the last converged step can be seen on *Figure 10* and *Figure 12*.

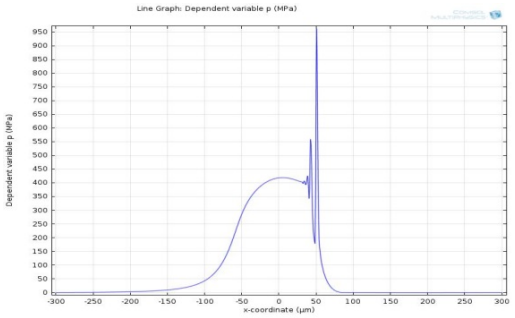

Figure 8: The pressure distribution in the gap of roller-bearing in case of line contact.

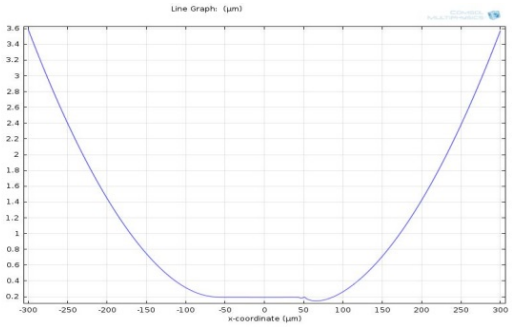

Figure 9: The gap size in the gap of roller-bearing in case of line contact

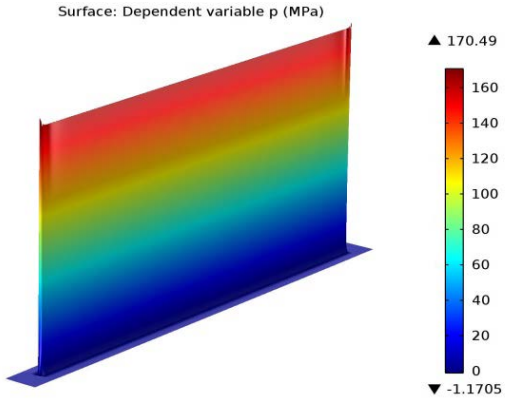

Figure 10: The pressure distribution in the gap of roller-bearing

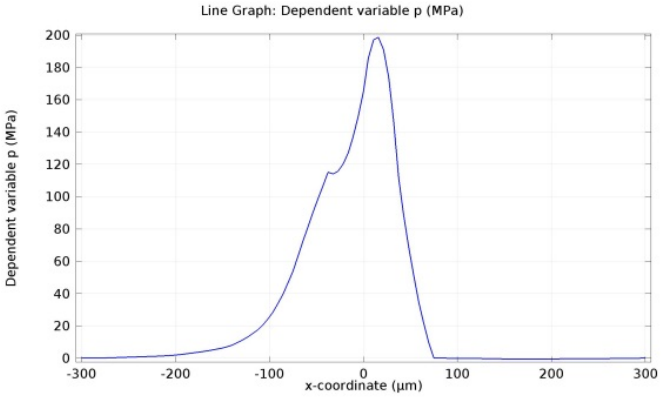

Figure 11: The pressure distribution in the middle cross-section of the gap of roller-bearing

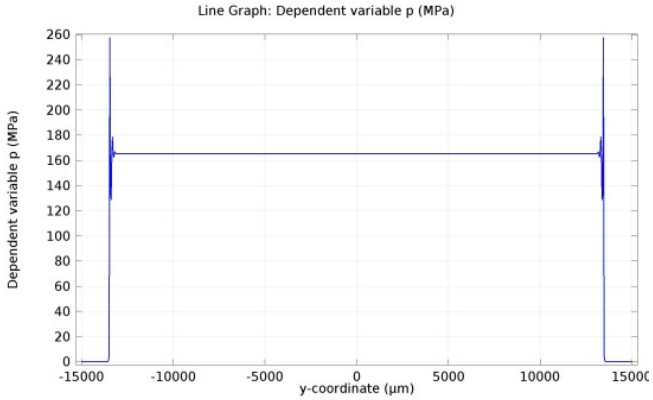

Figure 12: The pressure distribution along the length of roller

8. Conclusion

For the three-dimensional contact problem of lubrication, a two-dimensional lubrication fluid film finite element was developed and implemented to a commercial code. Presented penalty parameter method for viscosity is applicable for the advanced numerical methods, such as for the p-version finite element method. Summarising the results of the calculations we can state that the p-FEM method introduced above is a good and stable process to solve the EHD lubrication problems. It reduce the model size by decreasing the number of elements and it can be implemented for other problem types as well, such as rough surfaces, dynamically loaded bearings. However further effort is needed to handle the numerical instability in case of finite length contact.

Acknowledgement

The research work of Szabolcs Szávai was supported by the European Union and the State of Hungary, co-financed by the European Social Fund in the framework of TÁMOP-4.2.4.A/ 2-11/1-2012-0001 'National Excellence Program'.

The research work of Sándor Kovács presented in this paper was carried out as part of the TÁMOP-4.2.2.A-11/1/KONV-2012-0029 project in the framework of the New Széchenyi Plan. The realization of this project is supported by the European Union, and co-financed by the European Social Fund.

References

[1] Reynolds, O.: On the Theory of Lubrication and Its Applications to Mr. Beauchamp Tower's Experiments Including an Experimental Determination of the Viscosity of Olive Oil. Phi. Trans. Vol. 177(I), 1886, pp. 157–234.
[2] Reddi, M. M.: Finite Element Solution of the Incompressible Lubrication Problem. ASME Journal of Lubrication Technology, Vol. 91, No. 3, 1969, pp. 524–533.
[3] Rohde, S. M.–Oh, K. P.: A Unified Treatment of Thick and Thin Film Elastohydrodynamic Problems by Using Higher Order Element Methods. Proc. Royal Soc., Series A (London), Vol. 343, 1975, pp. 325–331.
[4] Freund, N. O.–Tieu, A. K.: A Thermal Elasto-Hydrodynamic Study of Journal Bearing with Controlled Deflection. ASME Journal of Tribology, Vol. 115, 1993, pp. 550–556.
[5] Nguyen, S. H.: p-Version Incompressible Lubrication Finite Element Analysis of Large Width Bearing. ASME Journal of Tribology, Vol. 113, No. 1, 1991, pp. 116–119.
[6] Páczelt I.: A végeselem-módszer lineáris sík, lemez, héj és térbeli elemei. Miskolci Egyetemi Kiadó, Miskolc, 1994.
[7] Dowson D.: A Generalized Reynolds Equation for Fluid-Film lubrication. Int. J. Mech. Sci., Vol. 4, 1961, pp. 159–170.
[8] Kumar, A.–Booker, J. F.: A Finite Element Cavitation Algorithm: Application/Validation. ASME Journal of Tribology, Vol. 113, No. 2, 1991, pp. 255–261.
[9] Kumar, A.–Booker, J. F.: "A Finite Element Cavitation Algorithm". ASME Journal of Tribology, Vol. 113, No. 2, 1991, pp. 276–286.

Design of Machines and Structures, Vol. 4, No. 1 (2014), pp. 99–104.

GREEN PRINCIPLES

ÁGNES TAKÁCS
University of Miskolc, Institute of Machine and Product Design
3515, Miskolc-Egyetemváros
takacs.agnes@uni-miskolc.hu

The paper deals with the interrelationship of the machine-human-environment cycle. It analysis what the designer should keep in front of the '*green*' eye during the conceptual design process. According to the environmentally friendly and ergonomics guidelines the paper offers a suggestion for collecting tips of conceptual design process, including *green tips*, that are of course in connection with the eco-design, and are suitable for a software that is written for helping the designers work during the conceptual design process.

1. Environmentally friendly design

It is not easy to shortly define environmentally friendly design. According to the several components it has, it is quite a complex process. According to Zilahy [1] environmentally friendly design systematically concentrates to the environmentally impacts that are potentially coming in the fore during the whole life-cycle of products and services, and to reduce or eliminate these expectable impacts still in the design process.

Orbán [2] defines DFE as a design, that minimalizes the undesired impacts for the nature (DFE = design for environment). DFE is the necessity of the developed product causes the less harmful impact on the environment that is an ever-growing claim of today.

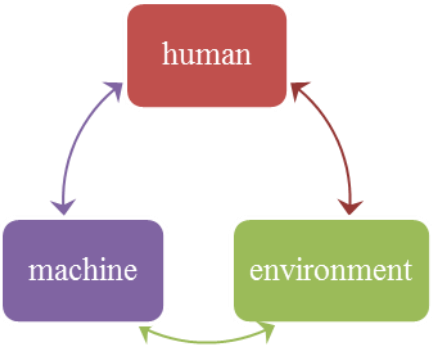

Figure 1: Machine-human-environment cycle

Due to the literature of the field *environmentally friendly design* or *DFE* or *Green design* or *eco design* mean only the protection of the nature do not pay any attention to the protection of the human that is a component of the green environment, only indirectly referring to it. It is essential to notice that the man only as a designer but also as the part of the green environment appears in the machine-human-environment cycle. The elements of the cycle are interrelationship continuously, as Figure 1 shows. So the human designs for

itself and for the environment as well. Machine has the effect for the human and for the environment too. The environment also has the impact for the human and for the machine. So environment means not only the nature over the office, the factory, but the direct environment of the human where it works, so the workplace. As for the further researches it would be practical to mention and analyse ergonomics as the element of the environmentally friendly design.

2. The tools of DFE

2.1. DFE elements

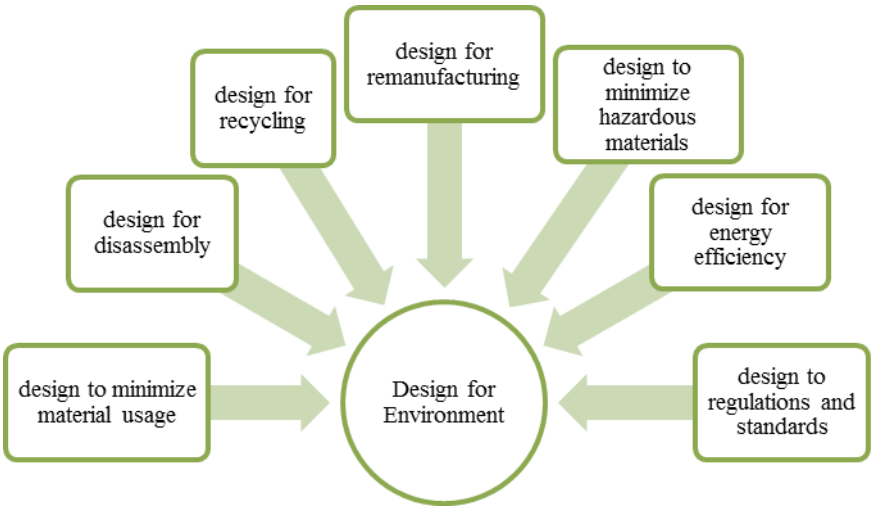

Figure 2: Design for the Environment [4]

Dfx, or design according to a given viewpoint [5] can be any formal period of the design process, or any important aspect that can be followed during the whole design activity as the main principle. Dfx is an enormous set of design principles that is really hard to describe, because this set is increasing day-by-day. Scientists define more and more principles, and for those principles methods are also created. These methods denote or can denote the adaption of Dfx techniques to computer. DfE, that is Design for the Environment is collecting the aspects of environmentally friendly design. As it is shown in Figure 2 it consists of seven essential areas. According to different aspects these can be divided into other different principles. This figure also confirms why it is so complicated to collect all the Dfx techniques and to group them.

2.2. 3R, 4R and 6R philosophies

3R philosophy means nothing else but not accumulating used or consumed materials as waste, but recycling them to the product-market. Reduce means to lower the quantity of the waste, reuse means using again the waste, recycling means using waste for creating new raw material. This cycle is shown in Figure 3.

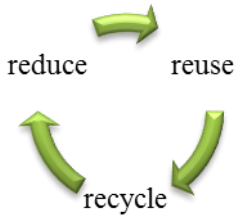

Figure 3: 3R philosophy

There are several versions for 4R. Usually recover, rethink and replace are mentioned as the 4th R. Elements of 6R are introduced in Figure 4 by a pyramid. Colures of the figure refer to the green factor of the given notion.

Figure 4: The 6R philosophy

Rethinking a product can lead to an absolute green product, for instance using biodegradable materials. Of course it determines and might lower the life-time of the product (e.g.: plant-a-tree box, as a packaging carton box, patent no.: US20080046277A1). But this way the effect on the environment can be reduced the most. *Reducing* the waste cannot be the best solution, as even though making the quantity of the waste less, it still has the impact on the environment. During *redesign* certain assemblies can be changed by less harmful ones. *Repairing* a product that is out of order its lifetime gets longer, so less new product is needed. It is sure that this possibility is not proper for the manufacturers. *Reusing* a product is significant for the environment. Due to recycling less natural raw materials have to be extracted. The recycled raw material has no impact on the environment as waste, but the recycling procedure might be dangerous for the environment. It does not mean to be worst than extracting the natural materials.

2.3. Valdez or CERES principles

There are several principles that were defined to make the industry understand and deal with the effects of producing for the environment. For example Valdez principles that were published in the Financial Times 27th March 1991. These principles later had been renamed for CERES principles. Coalition for Environmentally Responsible Economies had been established by Joan Bavaria in 1989 that is the abbreviation for CERES, who was the Roman goddess for fertility and agriculture. After the Exxon Valdez oil spill in the same year of establishing, CERES determined its 10 point principles. These help factories producing with the highest environmentally efficiency. Many industries keep CERES principles in front of the eye nowadays, General Motors among others. Principles are the following:

- Protecting the biosphere.
- Sustainable use of natural resources.
- Reducing and disposing waste.
- Wise use of energy.
- Risk reduction.
- Marketing of safe (green) products and services.
- Damage compensation.
- Disclosure.
- Environmental directors and managers.
- Assessment and audit.

2.4. Ten Golden Rules

Ten golden rules were carried out by Luttropp and Lagerstedt [3]. The rules are the summary of those principles that are used by different industries, and suggested by hand books. Ten golden rules are quite general; each industry should carry out product and industry specific rules. Golden rules are the following without any importance order:

- Limit the use of hazardous substances and arrange closed loops if necessary.
- Minimize energy and resource consumption in production and transport through housekeeping.
- Minimize energy and resource consumption in the usage phase especially for products with most significant aspects in the usage phase.
- Promote repair and upgrading especially for long lasting and system dependent products.
- Assist long lifetime for products especially for those ones that have significant effect on the environment out of usage phase.
- Use structural features and high quality materials to minimize weight (e.g.: metal foam [8]) if not interfering with necessary flexibility, impact strength or functional properties.
- Use better materials, surface treatments or structural arrangements to protect products for dirt, corrosion and wear.
- Prepare for upgrading, maintenance and recycling through information, labelling, modularization and accessibility.

- Prepare for upgrading, maintenance and recycling, by using few, simple, recycled, not blended materials and avoid alloys.
- Use as few joining elements as it is possible and promote intelligent geometric solutions.

3. Ergonomics

MacLeod [6, 7] defined twelve principles that can help the designer's work during the design process to create a machine, tool, equipment or product that ensures comfortable work for the user. These principles are general, but give significant help during design. MacLeod's principles are the following:

- Work in neutral postures!
- Reduce excessive force!
- Keep everything close!
- Work at proper heights!
- Reduce excessive motions!
- Reduce fatigue and static load!
- Reduce pressure points!
- Ensure free motions!
- Move, exercise, strength!
- Secure comfortable environment!
- Controls and displays should be clear!
- Improve work organisation!

David Ridyard determined five main territories within he declared several design principles for neutral postures. The aim is to ensure these normal positions. These main territories are the following:

- General work station
- Repetitive hand and wrist work
- Hand tool use and selection
- Lifting and lowering
- Carrying tasks

4. Summary

Principles were introduced above are the tools of the environmentally friendly design. Ergonomics is mentioned as an independent field of science by the literature, but as for the environment human should not be forgotten, as it is a component of the nature. So during environmentally friendly design designers should pay attention to human and due to its comfort to health. This way ergonomics is also practical to be mentioned among the tools of green design.

Above mentioned principles have to be examined, how designers can take them into consideration during conceptual design phase, this very early stage of the whole design process. Further task is to create a list on the basis of the introduced principles that gives 'green' tips for the designers during the conceptual design. Adapting this tip-list to computer is another task. This computer adapted tip-list would give tips while defining functional subassemblies while using an already existing concept generator software.

Acknowledgement

This research was supported by the European Union and the State of Hungary, co-financed by the European Social Fund in the framework of TÁMOP-4.2.4.A/2-11/1-2012-0001 'National Excellence Program'.

References

[1] Zilahy Gy.: Tisztább termelés, Budapesti Corvinus Egyetem, HEFOP-3.3.1., előadásfóliák.
[2] Orbán F.: Környezetszempontú tervezés. Budapesti Műszaki és Gazdasági Egyetem, HEFOP-3.3.1., előadásfóliák.
[3] Luttropp, C.–Lagerstedt, J.: EcoDesign and The Ten Golden Rules: generic advice for merging environmental aspects into product development, Journal of Cleaner Production, Elsevier, 2006.
[4] Otto, K.–Wood, K.: Product Design – Techniques in Reverse Engineering and New Product Development, Prentice Hall, 2008.
[5] Pahl, G.–Beitz, W.: Engineering Design – A Systematic Approach. Springer Verlag, London, 2005.
[6] MacLeod, D.: The Ergonomics Kit for General Industry, ebook, CRC Press, 2006.
[7] MacLeod, D.: The Rules of Work – A Practical Engineering Guide to Ergonomics, ebook, CRC Press, 2000.
[8] Sarka, F.–Döbröczöni, Á.: Using metal foams in gear-drives to reduce the emitted noise, Design of Machines and Structures, Vol. 4, Nr. 1, Miskolc, 2014, pp. 65–75.

Design of Machines and Structures, Vol.4, No. 1 (2014), pp. 105–115.

LIFETIME ANALYSIS OF ROLLING ELEMENT BEARINGS

DÁNIEL TÓTH–ATTILA SZILÁGYI–GYÖRGY TAKÁCS
University of Miskolc, Department of Machine Tools
3515, Miskolc-Egyetemváros
toth.daniel@uni-miskolc.hu; szilagyi.attila@uni-miskolc.hu;
takacs.gyorgy@uni-miskolc.hu

In several cases a rolling element bearing lifetime is under its intended limit. That may be caused by the insufficient lubrication, the higher loading (than the predefined value), the improper handling or something else. The following paper presents the vibrational analysis of a rolling element bearing.

1. Introduction

Rolling element bearings are one the most widely used machine parts and are critical to almost all forms of rotary machinery, such as machine tools, electric motors, generators, etc. Most defects of these machineries are deriving from the damage of the built-in rolling element bearings. Bearing failures may cause breakdown and might even lead to catastrophic failure or even human injuries [1]. In order to prevent unexpected bearing failures should be detected as early as possible.

When the appraisal of a rolling element bearing is performed by vibration analysis, many signal processing techniques can be considered. These methods can be performed within either the frequency or the time ranges. Perhaps the most commonly used process is the spectral analysis.

2. Bearing test machine

Rolling bearings condition monitoring can be accomplished with using test instrument. Such a device is located at University of Miskolc, Department of Machine Tools. This equipment is used to perform the bearing fatigue and measurement investigations. The main engineering parts of the bearing test device illustrated in Figure 1. During the bearing fatigue tests the 7F shaft works at the given rotational speed, while the 6 hydraulic cylinder exerts artificial load for the 4F bearing. After the fixed-term fatigue cycles, the bearing is put over to the 7M measuring axis. During the measurement investigations the 7M shaft works at the given rotational speed, while the 6 hydraulic cylinder exerts artificial load for the 4M bearing.

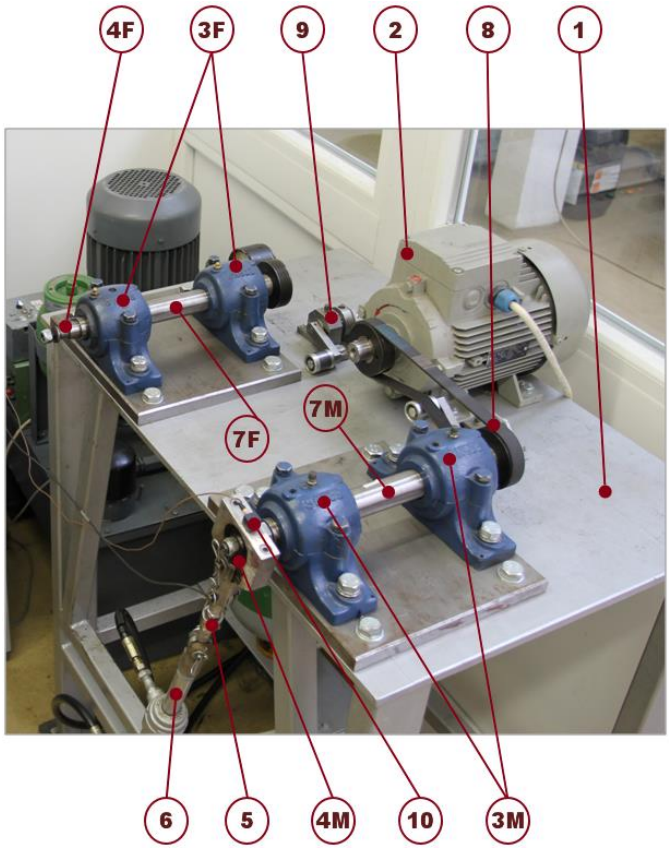

Figure 1: The main engineering parts of the bearing test device in measuring position

The individual symbols have the following meanings:

1	rigid table
2	three-phase motor
3F	supporting bearings of fatigue side
3M	special supporting plain bearings of measurement side
4F	fatigued bearing position
4M	measured bearing
5	load cell, the adjustment of hydraulic load
6	double-acting hydraulic cylinder
7F	fatigue test shaft
7M	measurement test shaft
8	length ribbed belt
9	belt tensioner
10	piezoelectric vibration accelerometer.

The measuring chain which used at vibration tests is shown in Figure 2.

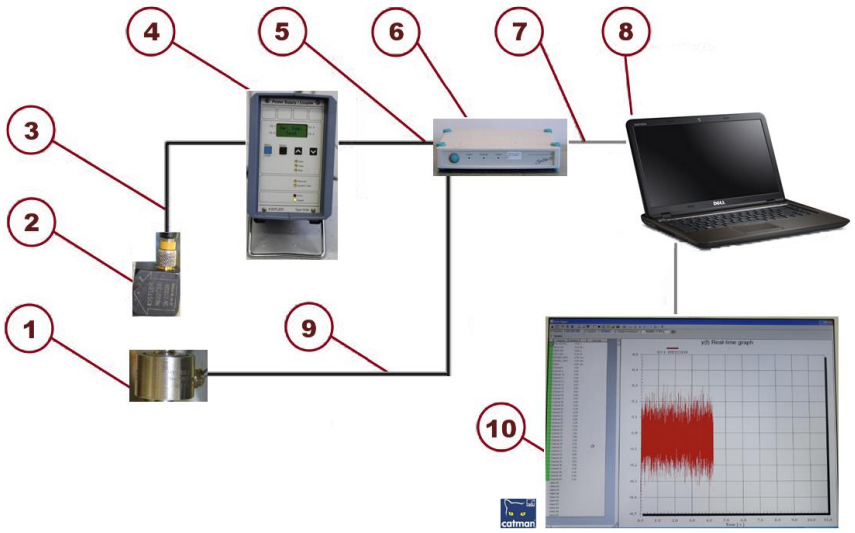

Figure 2: The measuring chain

The measuring chain elements are given in Table 1.

Table 1

The elements of the measuring chain

Code	Element of chain	Type
1	Load cell	HBM U9B
2	Piezoelectric vibration accelerometer	Kistler 8632C50
3	Connecting cable to the power supply coupler	176B cable
4	Power supply coupler	Kistler 5134
5	Connecting cable to the measuring amplifier	BNC-15PIN cable
6	Measuring amplifier	HBM Spider8
7	Connecting cable to the PC	USB cable
8	Visualization and analysis equipment	Dell Inspiron laptop
9	Connecting cable to the measuring amplifier	15PIN cable
10	Evaluation software	HBM Catman 4.0

3. The test bearing

The above-described bearing investigation device is used up to analyse an FAG 6303-2RSR, single row, deep groove ball bearing. The said bearing with some important dimensions are given in Figure 3, all the values are in mm.

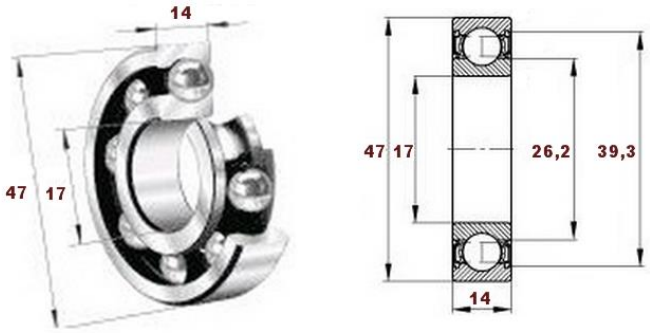

Figure 3: FAG 6303-2RSR ball bearing

Rolling bearing lifetime is finite, unfortunately one or more typical bearing failure sooner or later occurs. The finite life-time of rolling bearings may be associated with some factors, such as rotational speed, lubrication condition, load, and temperature. The length of time, until the first signs of material fatigue appear, depends on the magnitude of the load and bearing speed.

If the rotational speed is constant, the basic rating life can be expressed in operating hours, using the equation [4]:

$$L_{10h} = \frac{10^6}{60n}\left(\frac{C}{P}\right)^p \tag{1}$$

where:

L_{10h} basic bearing life in operating hours [h],

n rotational speed [min^{-1}],

C basic dynamic load [N],

P equivalent dynamic bearing load [N],

p life equation exponent (p = 3 for ball bearings).

During the experiments, the equivalent dynamic bearing load is 6000 N and always set on 1500 min^{-1} rotational speed. The 6303-2RSR ball bearing basic dynamic load is 14400 N [3].

Using these parameters, the bearing life is as follows:

$$L_{10h} = \frac{10^6}{60n}\left(\frac{C}{P}\right) = \frac{10^6}{60 * 1500\left[\text{min}^{-1}\right]} * \left(\frac{14400[N]}{6000[N]}\right)^3 = 153,6\,[h] \tag{2}$$

Accordingly, the examined FAG 6303-2RSR ball bearing – with the set values – will have circa 154 hours lifetime.

4. Bearing investigations with spectral analysis

Spectral analysis plays an important role in the detection and diagnosis of machine faults. We can use effectively in order to identify the location and the relative size of the bearing defects. Each bearing element has a characteristic rotational frequency. With a defect on a particular bearing element, an increase in vibrational energy at this element's rotational frequency may occur.

As we have already discussed the explorations concentrate on the 6303-2RSR ball bearing. The ball bearing frequencies [3] with the used settings are given in Table 2. The tested ball bearing's rotational frequency is 22,85 Hz [3].

Table 2

6303-2RSR ball bearing frequencies on 1500 min^{-1} rotational speed

Frequency name	**Abbreviation**	**Special abbreviation**	**Value [Hz]**	**Divided by the rotational frequency [–]**
Ball Pass Frequency of Inner ring	BPFI	I	101,1	4,425
Ball Spin Frequency	BSF	G	40,21	1,76
Fundamental Train Frequency	FTF	K	8,4	0,368
Ball Pass Frequency of Outer ring	BPFO	O	58,84	2,575

After the fixed-term fatigue cycles we take vibration specimens from the test bearing. Fast Fourier Transform is used to illustrate the recorded spectral specimens as spectrum. The program code, which runs in Maple software, is seen in Figure 4. The measurement cycles are always perform at 9600 Hz sampling frequency. We generally take five vibration samples and 16,384-element samples within each measurement cycle.

```
with (Matlab)
a := readdata("1.txt")
V := convert (a, list)
num := 16384
Time := [ seq( 1/9600 (h), h = 1..num ) ]
ft := Matlab [ fft](V)
setvar ("FT", ft)
setvar ("n" num)
```

$$evalM(\text{“}result = \text{FT}.*\text{conj(FT)} / n\text{”})$$

$$pwr := getvar(\text{“result”})$$

$$pwrlist := convert\left(\frac{pwr}{num}, list\right);$$

$$pwrlist1 := \left[seq\left(2 \cdot \sqrt{pwrlist_w}, w = 1..num\right)\right]$$

$$pwr\_points := \left[seq\left(\left[\frac{h-1}{Time_{num}}, pwrlist1_h\right], h = 1..\frac{num}{2}\right)\right]$$

$$plots\left[pointplot\right](pwr\_points, style = line, view = [0..4500, 0..0.05])$$

Figure 4: The FFT program code in Maple software

Figure 5 shows the nature of vibrations after 23 operating hours. During this period, the bearing was running safely.

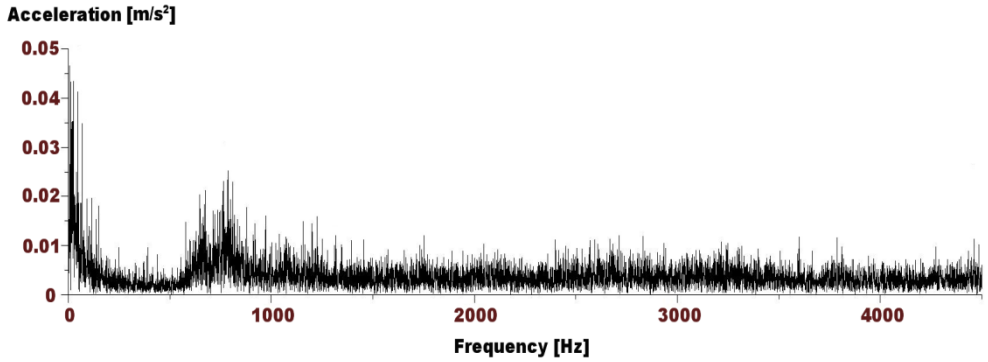

Figure 5: Vibrations spectrum at 23 operating hours

Figure 6 shows the nature of vibrations after 70 operating hours. It is conspicuous that the acceleration values have increased substantially at this bearing lifetime period.

Most of the typical machine errors belong to the rotation frequency or its integer multiples. A widespread method is to scale the frequency axis into rotational speed units. In this case, the horizontal spectrum frequency axis is divided by the bearing rotational frequency. Consequently dimensionless frequency value is received, where “1” corresponds to the rotational frequency. Some literature [2] also called this to order-number. The typical bearings failure frequencies linear depend on the rotational speed.

Some bearing frequencies appeared after 36 operating hours, which illustrated in Figure 7. The marking of the frequency codes are realized according to the abbreviations of Table 2.

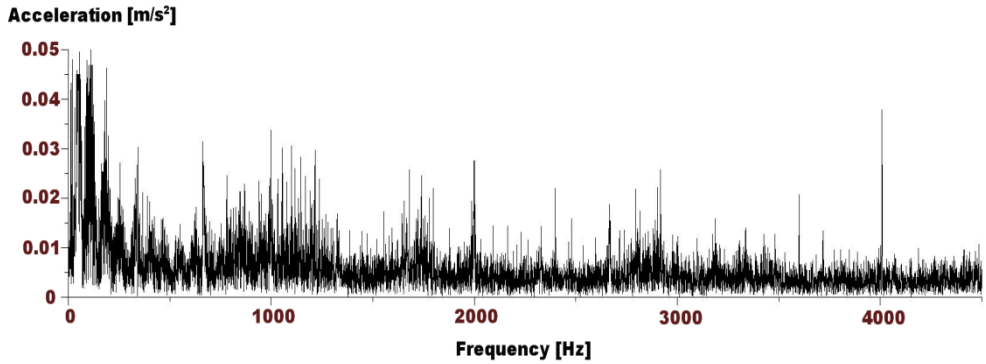

Figure 6: Vibrations spectrum at 70 operating hours

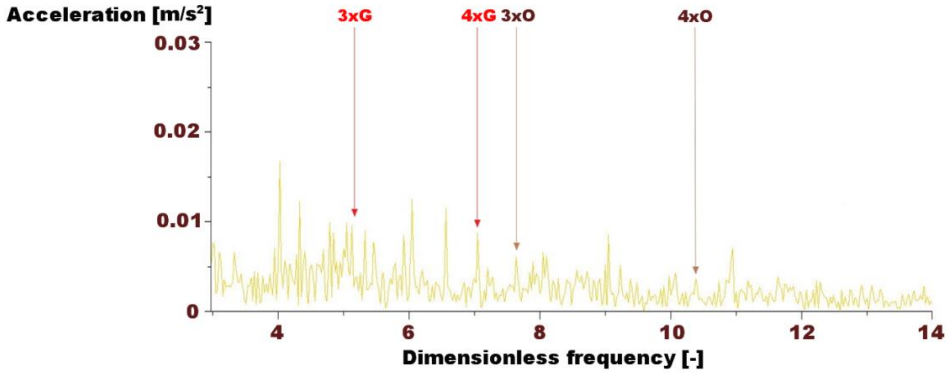

Figure 7: Vibrations spectrum with bearing failures at 36 operating hours

Figure 8 shows some bearing failures grew after 60 operating hours.

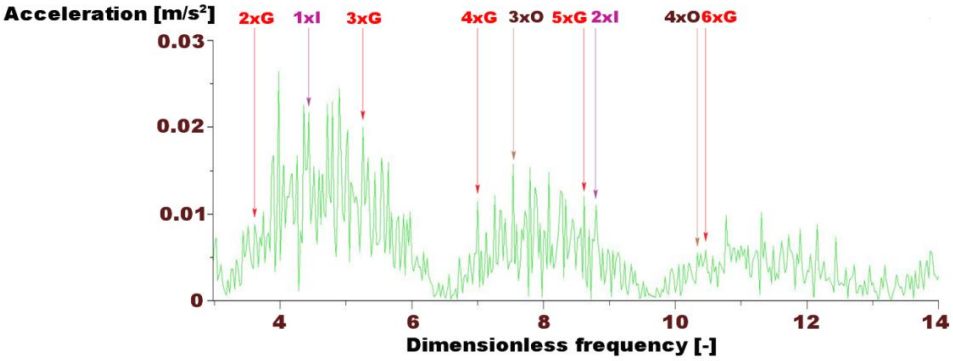

Figure 8: Vibrations spectrum with bearing failures at 60 operating hours

It is conspicuous that the passage of time the acceleration values grew materially. It is also apparent, that more and higher upper harmonic frequencies appeared as the time progressed.

The evaluation of the experiments, it was concluded that the Ball Spin Frequency and the Fundamental Train Frequency (frequency of the cage) give the most striking change. The following figures (Figure 9 and Figure 10) show the change of these frequencies and upper harmonic frequencies parallel with the operating hours.

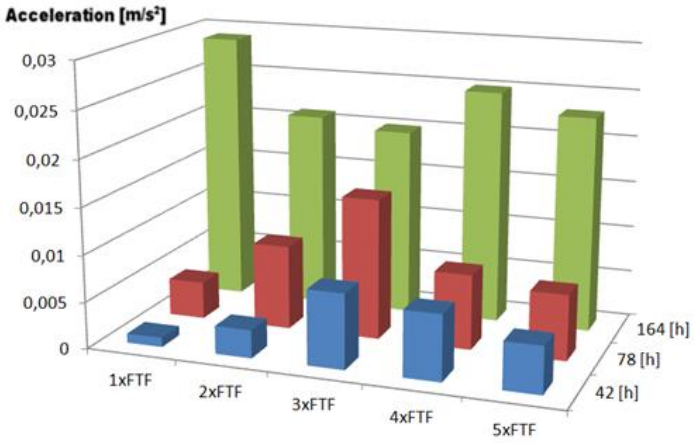

Figure 9: Cage frequency changes parallel the operating hours

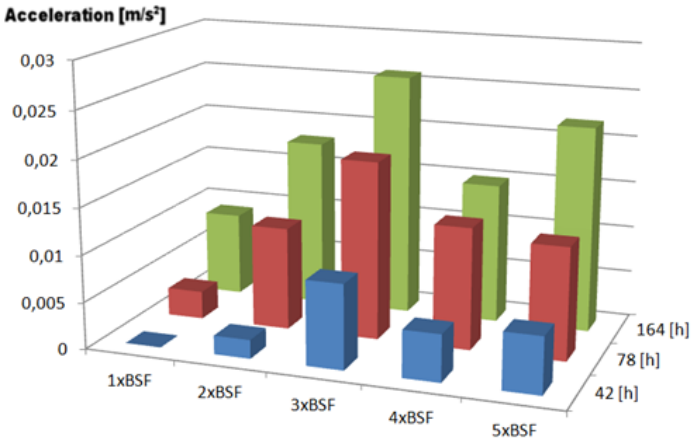

Figure 10: Ball Spin Frequency changes parallel the operating time

The bearing failure frequency peaks became well separable at the boundary of the basic bearing life.

5. Bearing damages

When the bearing noise had increased and the bearing had exceeded its nominal lifetime, the bearing was disassembled by cutting its outer ring and cage using professional angle grinder. The disassembled ball bearing – together with all elements of it – is given in Figure 11.

Figure 11: The disassembled ball bearing

As predicted the results of the spectral analysis so the bearing failure's main reasons were the damage of the cage structure and the rolling elements impairments. The broken cage structure is illustrated in Figure 12.

Figure 12. Cage structure defects

At the deterioration of the bearing, the ball rolling elements were not able to properly roll off on the inner and outer ring's surfaces. Many small damage trail visible on the rolling element (see Figure 13), so it is subjected to microscopic studies.

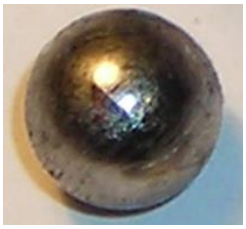

Figure 13: Damaged ball rolling element

Figure 14 shows the microscopic photo of the ball rolling element.

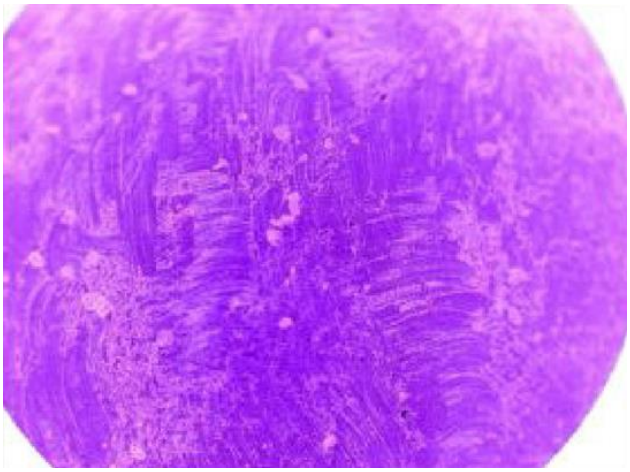

Figure 14: Ball rolling element defects (30 times magnification)

The microscopic photo clearly shows the tiny (10–55 μm) indentations, which probably caused by the metal particles, that came off from the bearing elements.

6. Conclusion

In the present paper, the authors analysed the lifecycle of an FAG 6303-2RSR single row, deep groove ball bearing. University of Miskolc, Department of Machine Tools has a bearing test device, which is used to perform the fatigue and the measurement investigations. After fatigue cycles the rolling bearing spectrum photos were presented and analyzed. When the bearing noise had increased and the bearing had exceeded its nominal lifetime, the bearing was disassembled to pieces. Having disclosed the failures of the bearing, we could realise the distraction anticipated by the previous measurements and also the efficiency of spectrum analysis.

Acknowledgement

This research was carried out as part of the TÁMOP-4.2.1.B-10/2/KONV-2010-0001 project with support by the European Union, co-financed by the European Social Fund.

References

[1] Bejzelman R. D.–Cipkin, B. V.: Gördülőcsapágyak kézikönyv. Nehézipari Könyv- és Folyóirat-kiadó Vállalat, Budapest, 1953.
[2] Dömötör F.: Rezgésdiagnosztika I. Dunaújváros, 2008.
[3] FAG 6303-2RSR technical data: http://medias.schaeffler.de/medias/en!hp.ec.br.pr/63..-2RSR*6303-2RSR.
[4] Molnár L.–Varga L.: Gördülőcsapágyazások tervezése. Műszaki Könyvkiadó, Budapest, 1976.

REVIEWING COMMITTEE

Á. DÖBRÖCZÖNI	Institute of Machine- and Product Design University of Miskolc H-3515 Miskolc-Egyetemváros, Hungary machda@uni-miskolc.hu
M. GERGELY	Acceleration Bt. mihaly_gergely@freemail.hu
K. JÁRMAI	Department of Materials Handling and Logistics University of Miskolc H-3515 Miskolc-Egyetemváros, Hungary altjar@uni-miskolc.hu
I. KEREKES	Institute of Mechanics University of Miskolc, H-3515 Miskolc-Egyetemváros, Hungary mechker@uni-miskolc.hu
F. J. SZABÓ	Institute of Machine- and Product Design University of Miskolc H-3515 Miskolc-Egyetemváros, Hungary machszf@uni-miskolc.hu
A. SZILÁGYI	Institute of Machine Tools and Mechatronics Universityof Miskolc H-3515 Miskolc-Egyetemváros, Hungary szilagyi.attila@uni-miskolc.hu
J. PÉTER	Institute of Machine and Product Design Universyti of Miskolc H-3515 Miskolc-Egyetemváros, Hungary machpj@uni-miskolc.hu

University of Miskolc Secretariat of the Vice-Rector for Research and International Relations
Responsible for publication: Prof. Dr. Tamás Kékesi
Miskolc-Egyetemváros
Published by the Miskolc University Press under leadership of Erzsébet Burmeister
Editor: Dr. Ágnes Takács
Number of copies printed:
Put to Press in 2014
Number of permission: TNRT – 2014 – 199 – ME HU ISSN 1785-6892

DESIGN OF MACHINES AND STRUCTURES

Volume 4, Number 1 (2014)

PUBLICATION OF THE UNIVERSITY OF MISKOLC – A SHORT HISTORY

The University of Miskolc (Hungary) was founded by the Empress Maria Teresia in Selmecbánya in 1735. After the first World War the university moved to Sopron, where in 1929, it started the series of university publications with the title Publications of the Mining and Metallurgical Division of the Hungarian Academy of Mining and Forestry Engineering (Volumes I–VI). From 1934 to 1947 the Institution became the Faculty of Mining, Metallurgical and Forestry Engineering of the József Nádor University of Technology and Economical Sciences at Sopron. The publications got the title Publications of the Mining and Metallurgical Engineering Division (Volumes VII–XVI). For the last volume before 1950 – due to a further change in the name of the Institution – Technical University, Faculties of Mining, Metallurgical and Forestry Engineering, Publications of the Mining and Metallurgical Division was the title. For some years after 1950 the Publications were temporarily suspended. After the foundation of the Mechanical Engineering Faculty in Miskolc in 1949 and the movement of the Sopron Mining and Metallurgical Faculties to Miskolc the Publications restarted with the general title Publications of the Technical University of Heavy Industry in 1955. Four new series – Series A (Mining), Series B (Metallurgy), Series C (Machinery) and Series D (Natural Sciences) – were founded in 1976. These came out both in foreign languages (English, German and Russian) and in Hungarian. In 1990, right after the foundation of some new faculties, the university was renamed to University of Miskolc. At the same time the structure of the Publications was reorganized so that it could follow the faculty structure. Accordingly three new series were established: Series E (Legal Sciences), Series F (Economical Sciences) and Series G (Humanities and Social Sciences). The latest series, the Series H (European Integration Studies) was founded in 2002. Design of Machines and Structures (HU ISSN 1785-6892) first published in 2003 as a part of the Series C.